CHEMICAL REVIEWS

Review

Cite This: *Chem. Rev.* 2018, 118, 3722–3751

pubs.acs.org/CR

Gold Nanofilms at Liquid–Liquid Interfaces: An Emerging Platform for Redox Electrocatalysis, Nanoplasmonic Sensors, and Electrovariable Optics

Micheál D. Scanlon,*[,†] Evgeny Smirnov,[‡] T. Jane Stockmann,[§] and Pekka Peljo*[,‡]

[†]The Bernal Institute and Department of Chemical Sciences, School of Natural Sciences, University of Limerick (UL), Limerick V94 T9PX, Ireland

[‡]Laboratoire d'Electrochimie Physique et Analytique (LEPA), École Polytechnique Fédérale de Lausanne (EPFL), Rue de l'Industrie 17, CH-1951 Sion, Switzerland

[§]Interfaces, Traitements, Organisation et Dynamique des Systèmes, CNRS-UMR 7086, Sorbonne Paris Cité, Paris Diderot University, 15 Rue J.A. Baïf, 75013 Paris, France

ABSTRACT: The functionality of liquid–liquid interfaces formed between two immiscible electrolyte solutions (ITIES) can be markedly enhanced by modification with supramolecular assemblies or solid nanomaterials. The focus of this Review is recent progress involving ITIES modified with floating assemblies of gold nanoparticles or "nanofilms". Experimental methods to controllably modify liquid–liquid interfaces with gold nanofilms are detailed. Also, we outline an array of techniques to characterize these gold nanofilms in terms of their physiochemical properties (such as reflectivity, conductivity, catalytic activity, or plasmonic properties) and physical interfacial properties (for example, interparticle spacing and immersion depth at the interface). The ability of floating gold nanofilms to impact a diverse range of fields is demonstrated: in particular, redox electrocatalysis, surface-enhanced Raman spectroscopy (SERS) or surface plasmon resonance (SPR) based sensors, and electrovariable optical devices. Finally, perspectives on applications beyond the state-of-the-art are provided.

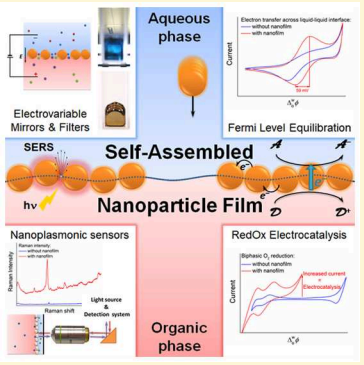

CONTENTS

1. Introduction 3722
2. Interface between Two Immiscible Electrolyte Solutions 3723
3. Functionalization of Liquid–Liquid Interfaces with Floating Gold Nanofilms 3725
   3.1. Thermodynamics of Nanoparticles at the Liquid–Liquid Interface 3725
   3.2. Experimental Strategies 3726
   3.3. Electrovariable Nanofilms 3728
   3.4. Critical Influences of Interfacial AuNP Immersion Depth and Interparticle Spacing 3728
4. Experimental Techniques to Characterize Floating Gold Nanofilms 3729
   4.1. Surface Tension, Capacitance, and Optical Techniques 3729
   4.2. Physical Position and Three-Phase Contact Angle of the Nanoparticles 3731
   4.3. X-ray Reflectivity and Scattering 3731
   4.4. Optical Reflectivity and Scattering 3731
   4.5. Electrochemical Techniques 3732
   4.6. Summary 3734
5. Applications of Floating Gold Nanofilms 3735
   5.1. Redox Electrocatalysis 3735
   5.2. Nanoplasmonics 3736
   5.3. Optical Applications 3739
   5.4. Plasmonic Photocatalysis 3739
6. Perspective Applications of Floating Gold Nanofilms at the ITIES 3740
   6.1. Surface-Enhanced Raman Spectroscopy 3740
   6.2. Electrovariable Optics 3741
7. Conclusions and Outlook 3742
Author Information 3742
   Corresponding Authors 3742
   ORCID 3742
   Notes 3742
   Biographies 3742
Acknowledgments 3743
Abbreviations 3743
References 3744

1. INTRODUCTION

Liquid–liquid interfaces are emerging as powerful, transparent, defect-free platforms for bottom-up self-assembly of ordered two-dimensional (2D) and three-dimensional (3D) nanoparticle (NP) arrays.[1−6] The fluidic nature of these interfaces allows them to self-heal, permitting the preparation of robust gold nanofilms of remarkable uniformity at room temperature,

Received: September 27, 2017
Published: January 30, 2018

DOI: 10.1021/acs.chemrev.7b00595
Chem. Rev. 2018, 118, 3722–3751

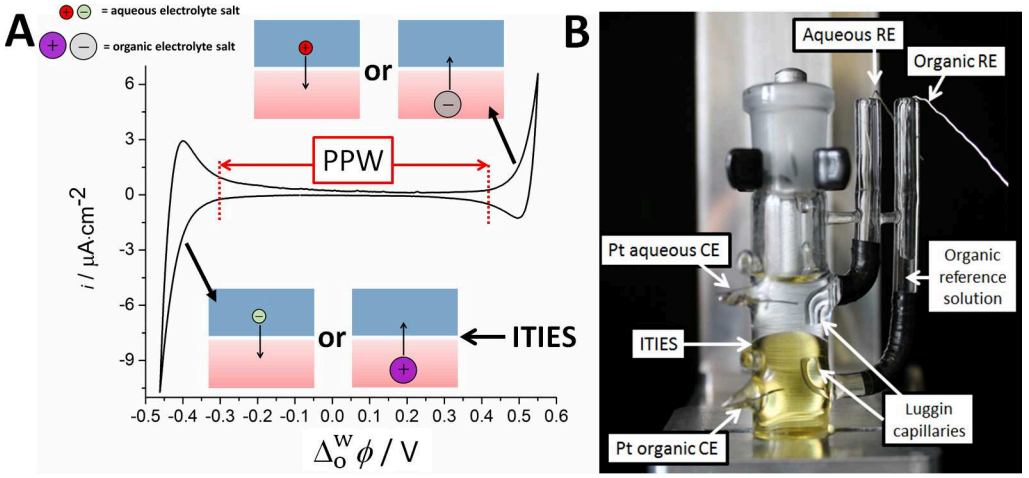

Figure 1. Electrochemistry at the interface between two immiscible electrolyte solutions (ITIES). Note that the water phase is blue and the oil phase is red in this scheme. (A) Typical cyclic voltammogram (CV) obtained by external polarization of an ITIES using a potentiostat. At high positive potentials the polarizable potential window (PPW) is limited by aqueous cation transfer (e.g., Li^+, Na^+, or Mg^{2+}), while at negative potentials the aqueous anion limits (e.g., Cl^- or SO_4^{2-}). In theory, the PPW may be limited by transfer of organic cations and anions at positive and negative polarizations, respectively. This is indeed the case if moderately hydrophobic salts such as tetrabutylammonium tetraphenylborate (TBATPB) are dissolved in the oil phase. However, an extremely hydrophobic salt, such as bis(triphenylphosphoranylidene) ammonium tetrakis-(pentafluorophenyl)borate (BATB), dissolved in the oil phase contributes minimally. (B) Photo representing a typical 4-electrode electrochemical cell used to polarize an ITIES externally with two platinum (Pt) counter electrodes (CEs), one in each phase, and two Ag/AgCl reference electrodes (REs), one in the aqueous phase and one in the organic reference solution (see the reviews listed in the text for more details on this solution). The dense halogenated solvent, in this case *α,α,α*-trifluorotoluene (TFT), is on the bottom and yellow-colored because ferrocene is dissolved in it to clarify the position of the ITIES in the image.

extending over large geometric areas (at least cm^2), without the use of specialized equipment.[7] The utilization of liquid interfaces dates back to the beginning of the 20th century. Initially Ramsden,[8] and shortly afterward Pickering,[9] discovered the stabilization of emulsions, i.e., interfaces between either two liquids or air and liquid, by particles. Those particles underwent assembly processes at liquid−liquid interfaces and, thus, stabilized emulsions in a similar manner to surfactants. Subsequently, such emulsions were called "Pickering emulsions". However, the utility of this discovery remained dormant for several decades and was only revitalized upon the development of analytical methods capable of investigating the emulsions mechanisms of formation and intrinsic properties.

Since the turn of the 21st century, the spontaneous adsorption of micro- and nanoparticles at either liquid−liquid or air−liquid interfaces[1,10−12] and the invention of practical methods of self-assembly[13−15] have been the subject of much scrutiny. Numerous industrial products and processes involve particles immobilized at soft interfaces such as antifoam formulations, crude oil emulsions, aerated foodstuffs, and flotation. The immobilized particles act in many ways like traditional surfactant molecules, but they also offer distinct advantages. This research area is now very versatile and multidisciplinary, combining fundamental science with large-scale industrial applications. The topic of colloidal particles at fluid−fluid interfaces has recently been comprehensively reviewed by Binks.[16]

Nanofilms consisting of conductive NPs, for example, gold nanoparticles (AuNPs), are of significant interest both in terms of fundamental and applied research as they possess unique optical, conductive, and catalytic properties. The manipulation of the physical positions[17,18] and electrochemical activity[19−21] of the AuNPs within the nanofilm is possible by controllably applying an electric field across an interface formed between two immiscible electrolyte solutions (ITIES).[17,22] An ITIES may be formed between either aqueous−organic solvent,[23,24] aqueous−superhydrophobic ionic liquid,[25] or organic solvent−ionic liquid phases.[26] As ionic liquid-based ITIES have yet to be modified with gold nanofilms, this Review will focus exclusively on aqueous−organic solvent ITIES.

In addition to floating nanofilms, it is well-known that NPs can be assembled on solid supports as superlattices or superstructures.[27] This field has attracted tremendous interest over the past few decades, as highlighted by several recent reviews covering the synthesis, optical properties, etc. of these superlattices.[28−36] In the present Review, we give a broad overview of the challenges inherent to self-assembling NPs at liquid−liquid interfaces, in particular with regard to AuNPs. We comprehensively summarize the methods currently available to study the physiochemical properties of nanofilms both in situ at the liquid−liquid interface and ex situ after transfer of the nanofilms to solid substrates. We also compare the two approaches to nanofilm formation (liquid−liquid and solid−liquid) in order to help the reader understand the enormous breadth of this research field. However, the primary focus of this Review is toward nanofilm-functionalized liquid−liquid interfaces, and the Review will not cover nanofilms at solid−liquid interfaces in depth.

2. INTERFACE BETWEEN TWO IMMISCIBLE ELECTROLYTE SOLUTIONS

The meaning of the word "immiscible" in the abbreviation of ITIES is multifaceted. The ITIES is first immiscible in terms of the solvent molecules, resulting in a molecularly sharp interface but with a dynamic microscopic roughness as "fingers" of the aqueous phase protrude into the organic solvent and vice versa.[37] Second, the ITIES is immiscible in terms of partition of the electrolyte ions between the two phases within a certain range of applied potentials across the interface, known as the

DOI: 10.1021/acs.chemrev.7b00595
Chem. Rev. 2018, 118, 3722−3751

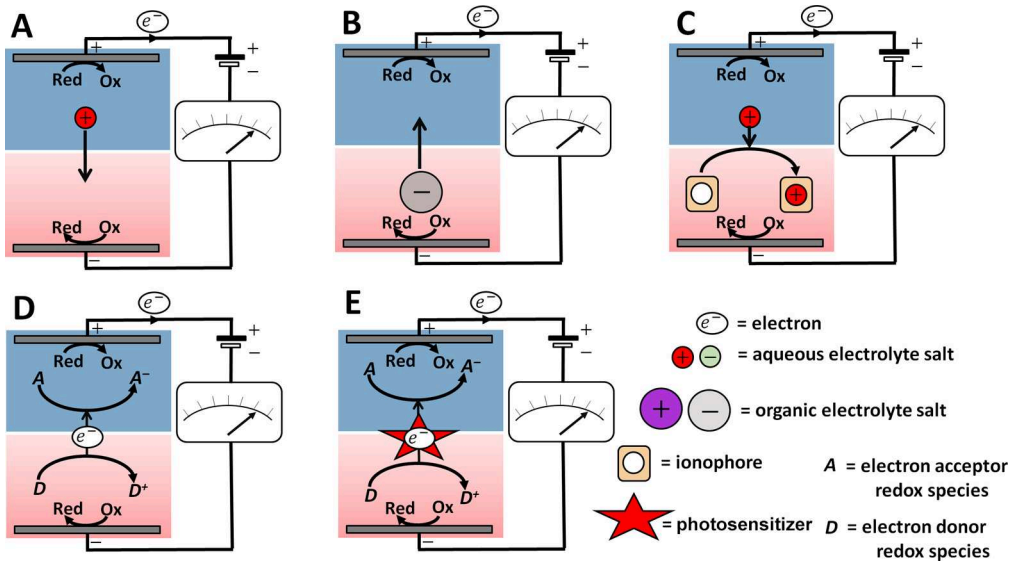

Figure 2. Versatility of electrochemistry at the ITIES. In each of the schemes, the ITIES is polarized positively by a potentiostat. Positive polarization of the ITIES can lead to ion transfer (IT) with the polarizable potential window (PPW) of (A) cations from the oil phase (red) to the water phase (blue) or (B) anions from oil to water. (C) For very hydrophilic cations, facilitated ion transfer (FIT) is achieved in the presence of a suitable ionophore species in the oil phase. Ionophores are complexing agents that shift the apparent solvation energy and are typically used to facilitate the transfer of very hydrophilic species from water to oil within the PPW. Positive polarization of the ITIES can provide (D) a thermodynamic driving force for interfacial electron transfer (IET) from a hydrophobic electron donor redox couple, *D*, to a hydrophilic electron acceptor redox couple, *A*. In some instances, more driving force is required to achieve electron transfer across the ITIES, and this can be provided by (E) harvesting solar energy using photosensitizers immobilized at the ITIES (e.g., porphyrins or semiconductors) in a process known as photoinduced interfacial electron transfer (PIET). Negative polarization of the ITIES may impede or reverse the direction of the described charge-transfer events. The reactions at the electrodes (marked as Ox to Red and Red to Ox), typically decomposition of the solvent or the supporting electrolytes, are not of importance as long as the potentiostat can supply enough compliance voltage to support the current flow. As the counter electrodes are sufficiently far away from the interface, the reaction products are not affecting the reactions taking place at ITIES within the timescale of typical experiments.

polarizable potential window (PPW). In truth most of the solvents are slightly miscible, e.g., the water concentration in 1,2-dichloroethane can be up to 110 mM.[38] Experiments are typically performed with mutually saturated solutions.

As the acronym ITIES suggests, both phases contain dissolved supporting electrolyte salts in either phase, enabling electrical conductivity. At a liquid−liquid interface the maximum upper and lower potentials are limited by the transfer of the supporting electrolyte ions. Thus, to obtain a wide PPW, highly hydrophilic inorganic salts (e.g., Li_2SO_4, KCl, $MgSO_4$, etc.) are used in the aqueous phase and highly hydrophobic salts, typically composed of bulky organic ions such as bis(triphenylphosphoranylidene)ammonium cations (BA^+) and tetrakis(pentafluorophenyl)borate anions (TB^-), are employed in the organic phase. This means that at high positive potentials the PPW is limited by aqueous cation transfer, while at negative potentials the aqueous anion limits the potential window (see Figure 1), whereas the organic-phase electrolytes BA^+ and TB^- contribute minimally.[39−41] Of course, supporting electrolyte of the organic phase can be chosen so that the ion transfer from the organic phase limits the potential window from one or both ends. For example, the replacement of TB^- with tetraphenylborate (TPB^-) results in the positive end of the PPW being limited by transfer of TPB^- from organic to aqueous phase. A sufficiently polar organic solvent, typically 1,2-dichloroethane (DCE),[41] 1,2-dichlorobenzene (DCB),[42,43] or α,α,α-trifluorotoluene (TFT)[44] having relative permittivities (ε) of 10.4, 10.1, or 9.2,[45] respectively, is often required to facilitate dissociation of the organic electrolyte salt as well as to support the flow of current. However, even chloroform[46,47] or toluene,[48] which have low values of ε (4.8 and 2.4, respectively), can be used at microinterfaces, where the low conductivity of the organic solvent is not a significant issue. More-polar water-immiscible organic solvents have also been used, such as nitrobenzene (ε = 34.8).[49] Other highly polar organic solvents such as acetonitrile (ε = 36.6)[50,51] or propylene carbonate (ε = 66.1)[52] become immiscible with water if a heavy loading of supporting electrolyte is employed to force a phase separation. However, use of the latter two approaches results in a reduction in the overall size of the PPW. This is due to the fact that the solvation of ions is similar in both phases because the transfer energy of even highly hydrophilic and hydrophobic ions between phases is too close to 0 kJ mol^{-1} to allow separation of the waves. As a result, neither is suitable to form an ITIES with a usable PPW. This discussion is not an exhaustive account of all organic solvents used to form ITIES. For more options, see the Introduction of the article by Kasuno et al.[48]

The ITIES can be controllably polarized, or electrified, by application of a potential, either externally through the use of electrodes immersed in both phases or through a common ion dissolved in the organic and aqueous phases. The potential drop spans the interface and is termed the Galvani potential difference ($\phi_w - \phi_o = \Delta_o^w\phi$); it can be manipulated to provide a PPW as wide as ∼1.0 V.[23,24] The width of the PPW is limited by the discussed factors (choice of supporting electrolyte, solvent, etc.). A typical 4-electrode electrochemical cell used to polarize an ITIES externally is shown in Figure 1B.

According to molecular dynamics simulations and experiments, the liquid−liquid interface is molecularly sharp but rough, with fluctuation in the pico-second time scale of the thickness of ca. 1 nm for a water−DCE interface.[53−56] If the

DOI: 10.1021/acs.chemrev.7b00595
Chem. Rev. 2018, 118, 3722−3751

majority of the potential drop takes place across this thin 1 nm interface, very strong electric fields can be achieved (ca. 10^9 V/m) for modest applied Galvani potential differences. However, the potential distribution within the interfacial layer is still poorly understood. Molecular dynamics simulations and X-ray reflectivity measurements indicate that both the liquid−liquid interface and the potential drop are almost molecularly sharp. For example, the electron density profile obtained from X-ray reflectivity shows a sharp change over a 0.2 nm distance,[57] and the electric potential difference from molecular dynamics simulations of a slab of water−DCE−water shows a similar sharp decrease.[58] Girault and co-workers have estimated that ca. 30% of the potential drop is within the inner layer,[59] while Niu and co-workers[60] argued (based on earlier work by Schmickler[61]) that the potential drop at the interface is mostly at the electric double layer of the organic phase. However, Samec argued that this assumption is unjustified, as the potential drop is located at the nanoscopic interface.[62] The structure of the liquid−liquid interface has been discussed by Dryfe.[63]

A major distinguishing factor of electrochemistry at the ITIES is its sheer versatility in comparison with using solid electrodes, encompassing ion transfer (IT; Figure 2A and B), facilitated ion transfer (FIT; Figure 2C), interfacial electron transfer (IET; Figure 2D), and photoinduced interfacial electron transfer (PIET; Figure 2E) processes. In-depth discussions of the theoretical background and plethora of possible applications of electrochemistry at the ITIES beyond the scope of this Review are available in a series of recent reviews.[23,24,64−68]

3. FUNCTIONALIZATION OF LIQUID−LIQUID INTERFACES WITH FLOATING GOLD NANOFILMS

In this section, we discuss experimental strategies to induce the adsorption of preformed colloidal spherical AuNPs at planar 2D liquid−liquid interfaces. A comprehensive review of the adsorption of other nanomaterials at liquid−liquid interfaces (beyond the scope of this Review), including both nonspherical nanomaterials, e.g., 1D nanorods or 2D sheets, and Janus NPs was recently provided by Booth and Dryfe.[69] Additionally, the electrodeposition of AuNPs at the ITIES has been reviewed by Dryfe et al.[70] The latter approach "decorates" the ITIES with AuNPs, although not to the extent that gold nanofilms of densely packed assemblies of uniformly arranged AuNPs are formed. Another topical review by Poltorak et al. comprehensively detailed both in situ and ex situ functionalization of soft interfaces with molecules, nano-objects, and nanopore arrays.[71] Very recently, both Lee et al.[72] and Binks[16] provided thorough reviews on the applications of NPs adsorbed in 3D configurations at liquid−liquid interfaces (also beyond the scope of this Review), forming either "liquid marbles" or colloidosomes. Liquid marbles are macroscopic 3D particle encapsulated liquid droplets with diameters in the millimeter to centimeter range.[10,72,73] Colloidosomes are >1000-fold smaller than liquid marbles, forming micrometer-sized particle stabilized Pickering emulsions.[72,74] On the other hand, the formation of superlattices at solid−liquid interfaces has been thoroughly reviewed in recent years by a number of different authors.[28−35,75,76]

3.1. Thermodynamics of Nanoparticles at the Liquid−Liquid Interface

Several key studies have outlined in detail the various forces at play that dictate the adsorption of NPs at a liquid−liquid interface.[13,14,77−80] In this regard, Flatté et al.[80] provided a particularly useful numerical model consisting of analytical equations that describe several key contributions to the total free energy of the biphasic system upon adsorption of NPs at the liquid−liquid interface. The key energies identified were (i) the energy of capillary forces, (ii) the energy devoted to changing the solvation sphere as the NP moves from an aqueous to an organic environment, (iii) the line tension, and (iv) the presence of an external electric field (applicable only for NPs adsorbed at an ITIES). Recently, Smirnov et al.[52] created a very assessable calculator using the equations of Flatté et al. (available online in the Supporting Information of their article). The calculator describes the balance of the interfacial energies at a nonpolarized liquid−liquid interface for NP adsorption as a function of NP size, dielectric constant of the organic solvent, surface charge of the NP, and three-phase contact angle of the NP (θ_0).

The main driving force entrapping an NP at a liquid−liquid interface is the capillary energy, i.e., the energy a system gains if an NP occupies a portion of the interface. Primarily, the capillary energy is dictated by the interfacial tension ($\gamma_{w/o}$) and θ_0 (see Figure 3A for a graphical representation of the precise meaning of θ_0). On the other hand, the solvation energy acts as a barrier to NP adsorption. As a charged NP transfers from a more-polar to less-polar medium (so from water to oil), the contribution of the solvation energy to the overall energetic balance increases significantly, especially once the NP pierces the organic side of the interface. The line tension contains all kinds of interactions pushing NPs away from the interface, whereas an external electric field at an ITIES can be applied to forcibly entrap NPs at the interface (discussed vide infra).

A typical energetic profile of NP adsorption at a water−DCE interface is demonstrated in Figure 3B(i). On the aqueous side of the interface, approach of the NPs to the liquid−liquid interface is impeded by an energy barrier. As the NPs cannot reach the potential well that exists at the interface, no interfacial assembly of adsorbed NPs takes place. However, if $\gamma_{w/o}$ or θ_0 are tuned (for example, by changing the organic solvent from DCE to propylene carbonate, as shown in Figure 3B(ii)), adsorption of NPs is facilitated. The latter is possible as the barrier on the aqueous side of the interface has decreased, increasing the likelihood of the NPs falling into the potential well at the interface and becoming trapped.[7,52,81]

Once two or more AuNPs assemble at the liquid−liquid interface, Coulombic repulsive and van der Waals attractive forces exert influence on the adsorbed AuNPs. Thus, the surface charge density (σ) of adsorbed AuNPs critically influences their tendency to adsorb and their equilibrium interfacial surface coverage.[13,14,77,79] In the case of large particles (typically >1 μm), their weight and associated additional capillary forces need to be considered (not discussed herein).

Thus, all-in-all, three main strategies have been developed to induce AuNP adsorption at the interface by reducing the total free energy of the biphasic system through manipulating either (i) electrostatics (i.e., minimizing Coulombic repulsion between interfacially adsorbed AuNPs by reducing screening effects, decreasing σ, or applying an electric field at the ITIES), (ii) hydrophobicities of adsorbed AuNPs (i.e., affecting $\gamma_{NP/w}$,

DOI: 10.1021/acs.chemrev.7b00595
Chem. Rev. 2018, 118, 3722−3751

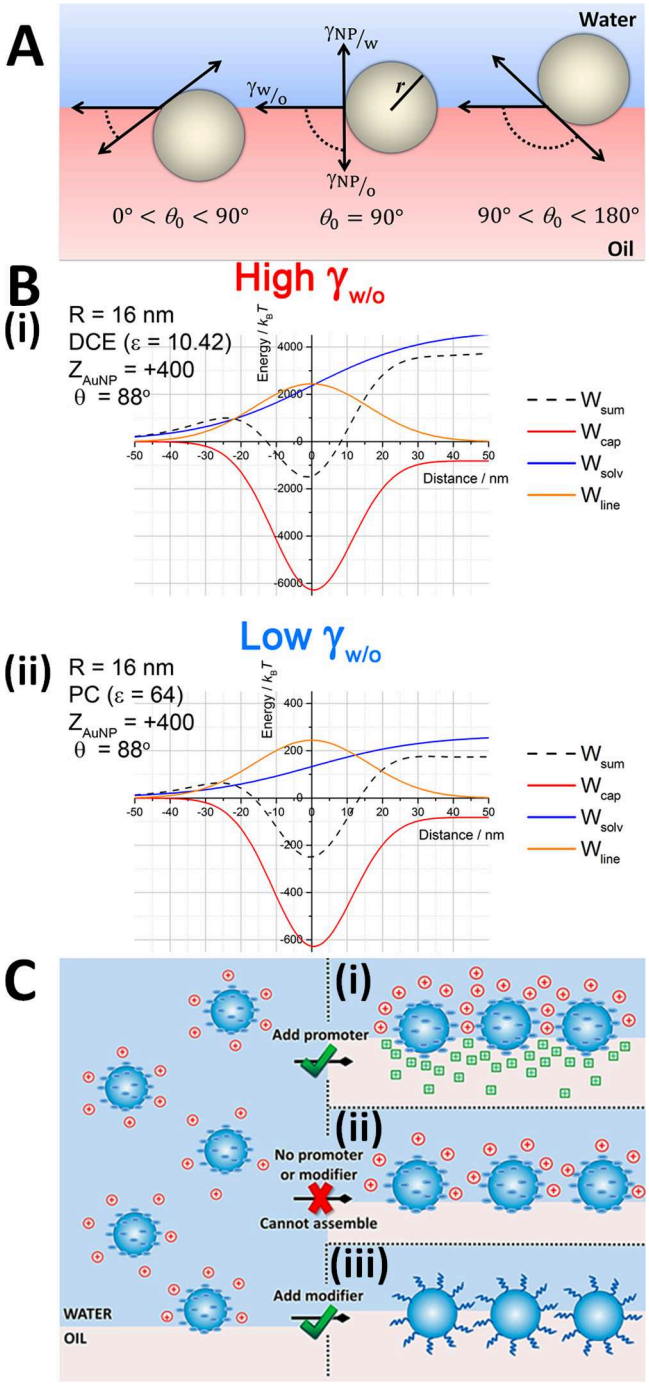

Figure 3. Functionalization of liquid−liquid interfaces with nanoparticles. (A) Schematic representation of the position of a AuNP at a liquid−liquid interface for a three-phase contact angle (θ_0) with the interface <90° (left), equal to 90° (center), and >90° (right). θ_0 is defined as the angle between the water−oil interface and the NP−oil side of the tangent plane at the line of contact. $\gamma_{NP/w}$, $\gamma_{NP/o}$, and $\gamma_{w/o}$ are the interfacial energies of the NP−aqueous phase interface, NP−organic solvent interface, and water−organic solvent interface, respectively. The effective radius of the AuNP is *r*. (B) Contribution of the components of capillary forces (W_{cap}, red line), solvation energy (W_{solv}, blue line), and line tension (W_{line}, orange line) to the overall energy profile (W_{sum}, dashed black line) for a AuNP adsorbed at (i) a water−DCE interface ($\gamma_{w/o} \approx 30$ mN/m) and (ii) a water−propylene carbonate (PC) interface ($\gamma_{w/o} \approx 3$ mN/m). The excess of charge on the AuNP (Z_{AuNP}) was set to +400, and θ_0 was set to 88°. These calculations were carried out using Mathematica software, and the CDF file is available in the Supporting Information of ref 52. Adapted with permission from ref 52. Copyright 2017 The Royal Society of Chemistry. (C) On contact between an aqueous colloidal solution of AuNPs and an immiscible oil phase, a few AuNPs are driven to the interface by the reduction of interfacial energy. However, the strong potential barrier on the aqueous side of the interface (seen at a distance of ∼ −20 nm from the interface for the experimental conditions, modeled with the dashed line for sum in (B(i))) keeps most AuNPs dispersed in the aqueous phase. Thus, as shown in C(ii), self-assembly of the AuNPs into a gold nanofilm under these conditions is not possible. On the contrary, the addition of promoters C(i) or modifiers C(iii) significantly reduces this potential barrier by providing charge screening, changing the AuNPs' surface charge density (σ), or synergistically modifying the AuNPs hydrophobicity (i.e., affecting θ_0). Adapted with permission from ref 82. Copyright 2016 American Chemical Society.

$\gamma_{NP/o}$, and θ_0; see Figure 3A), or (iii) interfacial tension (i.e., decreasing $\gamma_{w/o}$). Also, simultaneously achieving a synergistic mix of more than one effect is common (e.g., decreasing σ and bringing θ_0 closer to 90° with one strategy). Finally, as the adsorption of AuNPs is typically a kinetically controlled process dictated by the AuNP's Brownian motion,[82] many of the strategies discussed involve emulsification or vigorous shaking of the biphasic systems to accelerate AuNP adsorption.

3.2. Experimental Strategies

Bell and co-workers[2,82,83] have classified a series of chemically diverse molecules (e.g., tetrabutylammonium nitrate and 4-tertbutylcalix[4]arene tetraethylester (Na^+) complex) that when introduced to a biphasic system act as electrostatic "promotors" of AuNP adsorption. A promotor must (i) contain a hydrophobic ion of opposite charge to the AuNP, (ii) not directly adsorb onto the AuNP (i.e., displace the original stabilizing ligand), and (iii) induce adsorption when present at low concentrations. Promoters induce adsorption by condensation of the hydrophobic ions on the organic side of the interface, thereby screening Coulombic repulsion acting on the portions of each AuNP submerged into the organic solvent,[2,82,83] as shown in Figure 3C(i). The latter, combined with the attractive van der Waals forces, determines the interparticle separation distances at the interface. Both hydrophilic salts present at low (ppm) concentrations and amphiphilic salts with hydrophobic ions of identical charge to the AuNP reduce Coulombic repulsion only in the aqueous phase. Thus, neither can act as promoters. Nevertheless, Turek et al. demonstrated that, by increasing the ionic strength in the aqueous phase by addition of salt, the reduction in Debye length at the surface of each AuNP can be sufficient to induce adsorption upon centrifugation.[84]

A variety of methods have been introduced to reduce σ. Modification of AuNPs with stabilizing ligands that terminate in carboxylic groups (e.g., 3-mercaptopropionic acid, 4-mercaptobenzoic acid, and 16-mercaptohexadecanoic acid) allows effective modulation of σ by pH.[79,85] Indeed, such a tactic was used to reversibly adsorb/desorb AuNPs < 10 nm in size from the interface.[85] Another approach is to introduce "modifiers" to the biphasic system. As defined by Bell and co-workers,[2,82] a modifier tunes σ but also synergistically modifies the surface hydrophobicity of the AuNPs (i.e., affecting θ_0). Unlike promoters, modifiers may coordinate with the initial ligand on the AuNP or substitute the ligand

DOI: 10.1021/acs.chemrev.7b00595
Chem. Rev. 2018, 118, 3722−3751

completely in situ; see Figure 3C(iii). Examples of modifiers include 1-dodecanethiol,[5,6] mercaptosuccinic acid in combination with tetraoctylammonium bromide,[4] 2,2′-dithiobis[1-(2-bromo-2-methyl-propionyloxy)ethane] (DTBE),[78] poly-*N*-isopropylacrylamide (PNIPAM),[86] and tetrathiafulvalene.[81]

Arguably, the most widely used method of inducing interfacial AuNP adsorption is to introduce an alcohol, such as ethanol or methanol, to the biphasic system that simultaneously reduces σ and $\gamma_{w/o}$, ultimately allowing θ_0 to approach the optimal 90°.[5−7,17,19,20,77−79,87−91] Alcohols may first reduce σ by competitive displacement of citrate ligands (i.e., acting as modifiers).[77,79] Additionally, water-miscible alcohols will lower the dielectric constant of the aqueous phase as a function of alcohol content, thereby gradually decreasing σ.[6] Experimental evidence[92] and molecular dynamics (MD) simulations[93] indicate that the presence of a mutually miscible alcohol across both phases reduces $\gamma_{w/o}$. Indeed, gold nanofilms have also been successfully formed at pure aqueous−pentanol interfaces.[94] Also, the ITIES was modified using a minimum amount of methanol by initially suspending the citrate-stabilized AuNPs in a methanol solution and then injecting this alcoholic colloidal solution directly at the ITIES using a microsyringe;[17,19,20,95] see Figure 4. Such an approach was beneficial to prevent artifacts in ensuing electrochemical studies.

Intensive mixing of immiscible biphasic systems of extremely low $\gamma_{w/o}$, such as the aqueous−propylene carbonate system ($\gamma_{w/o}$ = ca. 3 mN·m^{-1}), can directly lead to gold nanofilm formation.[95] The disadvantage of using propylene carbonate, however, is its inability to form an electrified ITIES with a wide PPW, thereby limiting its potential utility.

For solid−liquid interfaces, superlattice formation is governed by size, ligand effects,[96] and chain length of the ligand.[29] A narrow size distribution is essential for increasing the degree of ordering in NP superlattices,[28] and this requires specialized synthetic methods such as digestive ripening.[97] The latter process is essentially a thermochemical step where a ligand-exchange reaction induces the redistribution of atoms from polydisperse NPs, leading to a very narrow size distribution.[97] This method has been widely used for a long time, but the theoretical description of the process based on statistical thermodynamics was only developed recently.[98] The detailed understanding of superlattice formation at solid−liquid interfaces has yet to be replicated for the formation of nanofilms at liquid−liquid interfaces, where, for example, higher flexibility of the interface makes the film more tolerant to defects.

Different strategies may be implemented to prepare nanocrystal superlattices at solid−liquid interfaces. One approach is to increase the concentration of nanocrystals by evaporating off the solvent.[99−101] At a critical nanocrystal concentration, this leads to an entropy-driven self-assembly phase transition to form an ordered superlattice known as the Kirkwood−Alder transition.[102−104] Alternatively, the solvent composition may be altered to induce aggregation or self-assembly by decreasing the solubility of the nanocrystals.[105] The self-assembly of nanocrystals may be influenced by applying external stimuli such as electric, magnetic, or electromagnetic fields.[106−108] This can lead to a tilting of the orientation of anisotropic NPs.[106−108] However, only recently have Yu et al. demonstrated the first use of an external stimulus, an electric field, to reversibly drive nanocrystal superlattice self-assembly.[109]

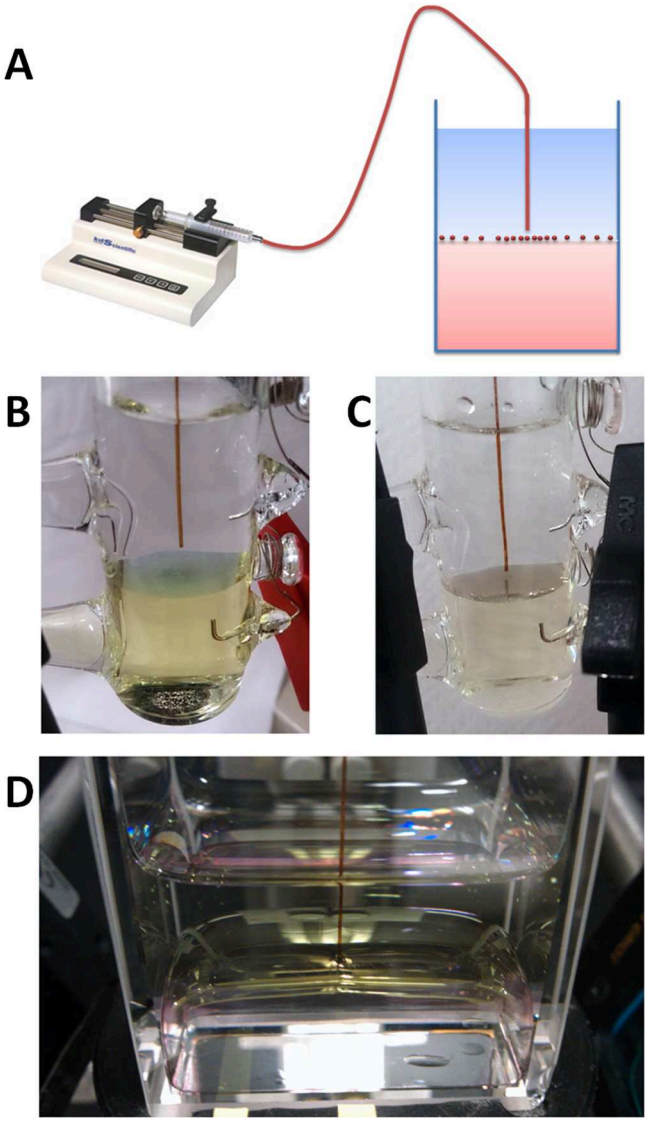

Figure 4. Functionalization of liquid−liquid interfaces with floating gold nanofilms by precise injection of AuNPs suspended in methanol at the interface. (A) Schematic of the capillary and syringe-pump setup used to settle AuNPs directly at the ITIES, allowing precise control over the AuNP surface coverage. Examples of gold nanofilms prepared at flat water−TFT interfaces in 4-electrode electrochemical cells using AuNPs with mean diameters of (B) 12 nm and (C) 38 nm. Flat liquid−liquid interfaces were achieved by partial silanization of the bottom half of the electrochemical cell glass walls. (D) Gold nanofilms were also prepared on larger curved soft interfaces using a 2 × 4 cm quartz cell. Adapted with permission from ref 20. Copyright 2015 American Chemical Society.

Another interesting approach is the combination of liquid−liquid and solid−liquid methods for nanofilm formation. For example, the "drain to deposit" method, where NPs assembled at a liquid−liquid interface are drained to deposit the film on a solid substrate, allows tunable formation of large-area NP films on solid substrates.[95,110,111] Other examples include NP monolayer assembly by the Langmuir−Schaefer method[112] and by the three-phase self-assembly method.[113] Additionally, bubbles (liquid−gas interfaces) can be employed for nanocrystal formation.[114]

DOI: 10.1021/acs.chemrev.7b00595
Chem. Rev. 2018, 118, 3722−3751

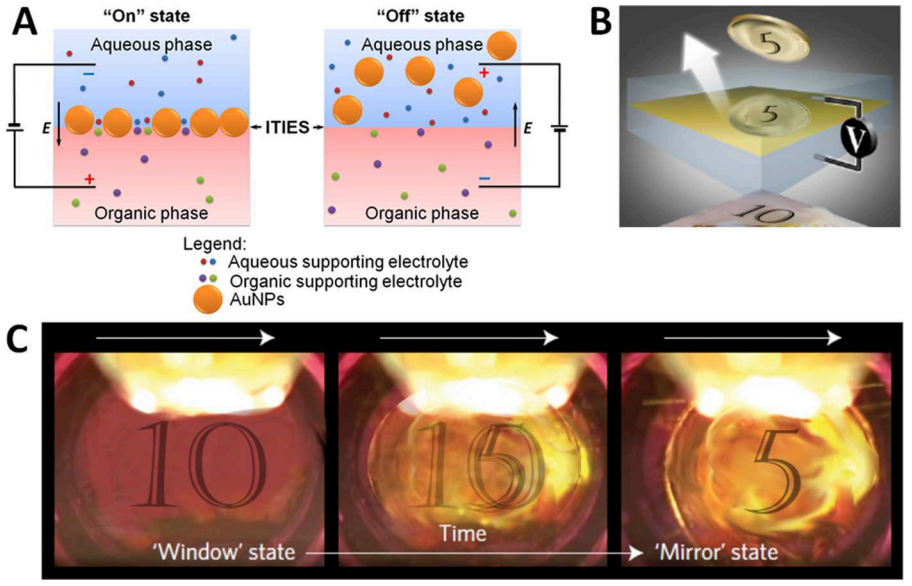

Figure 5. Electrovariable gold nanofilm formation by polarization of the ITIES. (A) (Left panel) On application of a negative potential at the ITIES, the negatively charged AuNPs are electrostatically pushed to the ITIES and form a gold nanofilm. (Right panel) On application of a positive potential at the ITIES, the AuNPs are electrostatically repelled from the ITIES and the gold nanofilm disassembles. (B) Schematic of a demonstration device illustrating an electrovariable gold nanofilm in action by using a setup with a coin facing the liquid mirror and a currency note at the back of the mirror. Modified with permission from Macmillan Publishers Ltd.: Nature Materials, ref 22. Copyright 2017. (C) Modified images observed during the transition between a transmissive "window" state (when no NPs are at the interface) to a reflective "mirror" state (when NPs assemble densely at the interface). MDDA-functionalized gold NPs with 16 nm diameter were used, and the ITIES consisted of an aqueous phase containing 10 mM NaCl and a DCE organic phase containing 10 mM TBATPB electrolyte salt. Modified with permission to avoid copyright issues regarding the use of coins and bank notes from Macmillan Publishers Ltd.: Nature Materials, ref 22. Copyright 2017. The real images featuring a £10 note and a coin are available in ref 22.

3.3. Electrovariable Nanofilms

Uniquely, an ITIES provides the additional ability to externally tune the electric field felt by AuNPs in close proximity to the interface. Thus, for negatively charged colloidal AuNPs in the aqueous phase, polarization of the ITIES negatively (i.e., the aqueous phase is negatively charged with respect to the organic phase) will push the AuNPs toward the interface and potentially induce gold nanofilm formation (see Figure 5A, left panel). On the contrary, positive polarization will repel the AuNPs from the interface, electrostatically dragging them back into the bulk aqueous phase and disassembling any formed gold nanofilm (see Figure 5B, right panel).

The voltage-induced reversible adsorption and desorption of NPs is dependent on their size and σ and has been demonstrated for AuNPs < 2 nm in size[18,115] and core−shell gold−silver NPs ca. 16−20 nm in size (but with a 4-fold increase in σ in comparison to pure AuNPs).[116] However, AuNPs < 2 nm in size do not form lustrous gold nanofilms. Very recently, Montelongo et al.[22] have shown that relatively large NPs can be assembled by the electric field at a water−DCE interface. In their study, AuNPs (16 nm in diameter) were functionalized with 12-mercaptododecanoic acid (MDDA) in order to protect them from aggregation by NaCl and TBATPB used as supporting electrolytes for the aqueous and organic phases, respectively. Nevertheless, it takes hours to induce assembly of such AuNPs into a lustrous film, although desorption of AuNPs from the interface can be performed in several minutes. Reversible electric-field driven formation of silver superlattices on solid electrodes has also been demonstrated recently,[109] so similar approaches can also be extended to solid−liquid interfaces.

In comparison, lateral movement of larger AuNPs on the fluidic interface may be much more accessible. Bera et al. showed that the interparticle distance of interfacial adsorbed 2 nm AuNPs can be varied by as much as 1 nm by tuning $\Delta_o^w\phi$.[18] Gschwend et al. demonstrated that changes in $\gamma_{w/o}$ in the presence of a surfactant as a function of $\Delta_o^w\phi$ can induce rapid lateral movement of relatively large 12 nm AuNPs from one position on the ITIES to another, thereby behaving as "electrovariable Marangoni shutters" (discussed in section 6.2).[17]

3.4. Critical Influences of Interfacial AuNP Immersion Depth and Interparticle Spacing

The immersion depth at the interface (i.e., θ_0 values) may influence a AuNPs catalytic activity as an interfacial bipolar electrode (discussed in section 5.1) by altering the ratio of surface area available for electron-transfer reactions between the water and organic sides of the interface.[20] Additionally, the potential drop across the ITIES is not uniformly spread between the aqueous and organic back-to-back diffuse layers, although the exact potential distribution is not fully understood, as discussed in section 2. Thus, the rate of electrochemical reactions taking place on the aqueous side of the interface may benefit from a greater proportion of the potential drop taking place there.

Charge transport along a gold nanofilm is achieved by multiple electron tunneling events (i.e., electrons hopping between conductive AuNPs separated by a dielectric medium). The tunneling probability falls off exponentially with distance.[117] The latter was demonstrated by Wuelfing et al.,[118] who observed an exponential decay of conductivity as a function of the thickness of an alkanethiol matrix separating gold monolayer-protected cluster (MPC) cores cast onto

DOI: 10.1021/acs.chemrev.7b00595
Chem. Rev. 2018, 118, 3722−3751

interdigitated array electrodes (Figure 6A). The MPC core separation distances in the film were easily varied by choice of the alkanethiol monolayer chain length.[118] Thus, the extreme sensitivity of the tunneling probability to MPC core separation distances clearly highlights the need to precisely tune interparticle spacing to achieve truly conductive interfacial gold nanofilms. The latter would permit a massively increased cross-sectional area of reaction to facilitate IET by providing a continuous conductive interfacial route for electrons to travel from donor to acceptor molecules on either side of the interface. Thus, electrons injected anywhere on the gold nanofilm can be discharged at any point of contact on the opposite side of the interface. Support for the latter mechanism is evident from the significant increases in the rates of reaction for biphasic H_2 evolution and O_2 reduction due to redox electrocatalysis by interfacially adsorbed conductive bare or catalytic NP decorated carbon materials (e.g., graphene or carbon nanotubes (CNTs)).[119−124] The mechanism of redox electrocatalysis for these conductive carbon materials is explained in detail in a recent review[125] and incorporates most of the elements of redox electrocatalysis by gold nanofilms described vide infra in section 5.1.

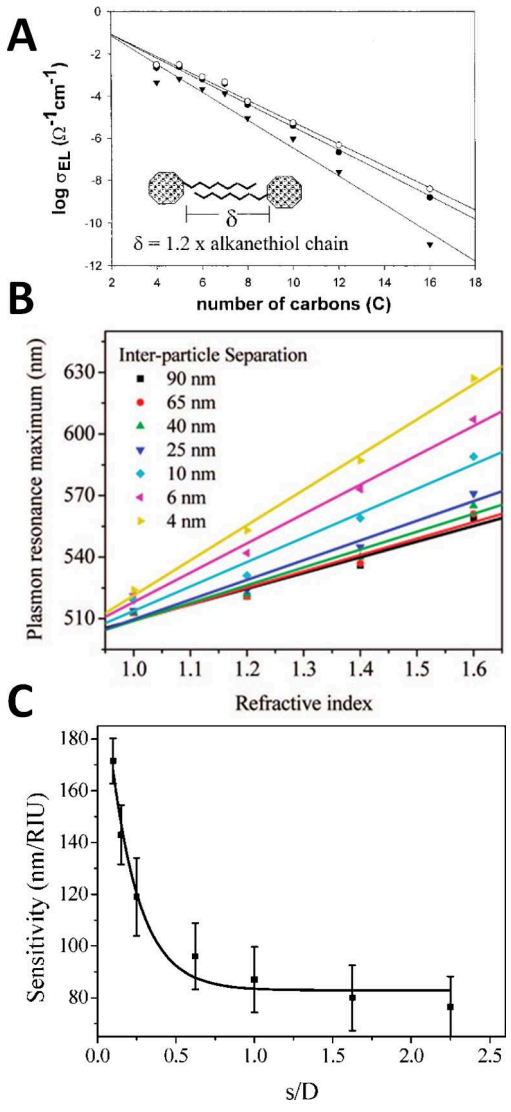

Figure 6. Properties of nanofilms related to the interparticle gap. (A) Conductivity of gold monolayer protected cluster (MPC, specifically of $Au_{309}(C_n)_{92}$) solid-state films cast onto an interdigitated electrode surface decays exponentially as a function of the numbers of carbons in the alkanethiolate chain. The temperature of the measurements was either 70 (solid circle), 30 (hollow circle), or 60 °C (inverted solid triangle). The inset schematically presents the interdigitation of monolayer chains in the solid-state MPC films. Adapted with permission from ref 118. Copyright 2000 American Chemical Society. (B) The LSPR maximum of a NP dimer (for polarization along dimer axis) increases linearly with increasing refractive index, similar to that for an isolated NP. However, the increase has a much higher slope for dimers with a smaller inter-NP gap. Adapted with permission from ref 127. Copyright 2008 American Chemical Society. (C) A plot of the SPR sensitivity (i.e., the slopes of the data plotted in (B)) versus the inter-NP gap (*s*, normalized by the NP diameter, *D*) clearly highlights that the SPR sensitivity to the medium increases almost exponentially with decreasing interparticle gap. Adapted with permission from ref 127. Copyright 2008 American Chemical Society.

Critically, for the performance of interfacial gold nanofilms as nanoplasmonic sensors, the strength of plasmon coupling, as well as associated hot-spots for SERS sensing, is dependent on the distance between the AuNPs.[126] Furthermore, Jain and El-Sayed[127,128] demonstrated that, as the interparticle gap decreases, the strengthening electric field causes a near-exponential increase in the sensitivity of the SPR frequency shift to the medium refractive index (Figure 6B and C).

With regard to electrovariable optics, theoretical[129−134] and experimental[7,90,135] studies have indicated that resonant light reflection, allowing gold nanofilms to act as nanoplasmonic mirrors, depends on the material of the NPs, their size, and their interfacial surface coverage (i.e., average interparticle spacing should be substantially less than half the AuNP size[1]). In this case, the immersion depth plays a minor role in determination of optical responses from a nanofilm. However, this parameter is crucial to facilitate electrovariable on/off behavior of nanoplasmonic mirrors. As discussed in section 3.1, the deeper an NP is immersed at the liquid−liquid interface, the higher is the energy needed to remove that NP from the interface.

Unfortunately, key factors that are beneficial for reflective interfacial gold mirror formation are diametrically opposed to facilitate electrovariable on/off behavior. On the one hand, the AuNPs must be >25 nm in size and suitably functionalized to have as low a σ as possible in order to achieve very dense packing at the interface. On the other hand, such large AuNPs are typically irreversibly trapped in a potential well at the liquid−liquid interface upon adsorption (considered in section 3.1). An obvious approach is to increase σ, causing an increase in the electrostatic driving force for desorption to overcome the trapping potential well. However, an increase in σ will also likely negate the formation of a dense gold nanofilm in the first instance. This problem has recently been partially solved by Montelongo et al.[22] through using MDDA-functionalized AuNPs (high σ) and salt at moderate concentrations (screens Columbic repulsions between NPs in the film). Nevertheless, the assembly process took a long time and, thus, imaginative approaches to find the correct balance of opposing factors are still required to achieve rapid on/off electrovariable optics.

4. EXPERIMENTAL TECHNIQUES TO CHARACTERIZE FLOATING GOLD NANOFILMS

4.1. Surface Tension, Capacitance, and Optical Techniques

Techniques that monitor the adsorption of AuNPs in situ are extremely useful, in particular when multiplexed with a 4-

DOI: 10.1021/acs.chemrev.7b00595
Chem. Rev. 2018, 118, 3722−3751

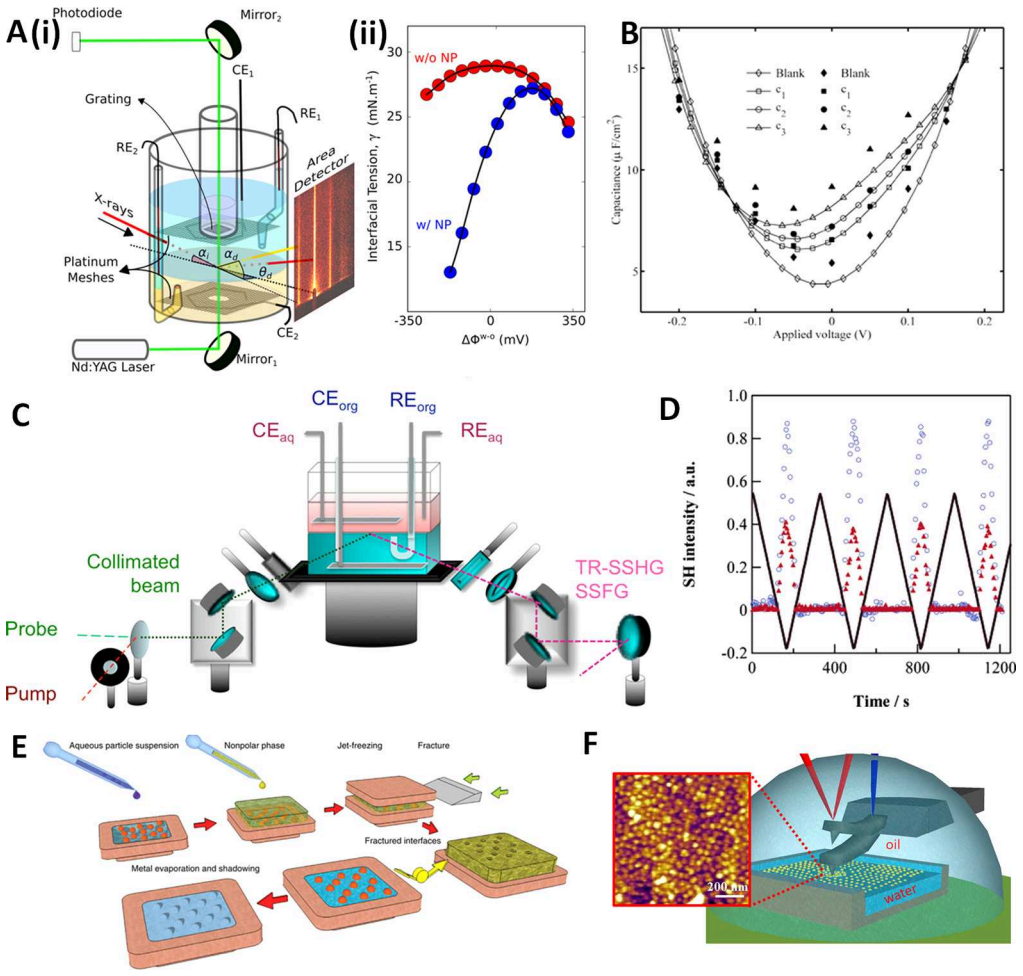

Figure 7. Variety of methods to locate nanoparticles at the liquid−liquid interface. (A) (i) Schematic of a 4-electrode electrochemical cell configured for either X-ray surface-scattering measurements or quasi-elastic light-scattering (QELS) interfacial tension measurements (CE_1 and CE_2 are made of Pt mesh; RE_1 and RE_2 are Ag/AgCl reference electrodes). (ii) Electrocapillary curves generated using QELS, i.e., plots of interfacial tension measurements of the water−oil interface as a function of the Galvani potential difference ($\Delta_o^w\phi$) with AuNPs (blue) and without AuNPs (red). Adapted with permission from ref 18. Copyright 2014 American Chemical Society. (B) Calculated specific capacitance curves (lines) are compared to the data measured (symbols; from ref 88) for various concentrations of AuNPs in the bulk aqueous electrolyte: c_1 = 0.42 nM, c_2 = 0.67 nM, and c_3 = 1.26 nM. "Blank" refers to the unpopulated interface. Adapted from ref 143 with permission from the Royal Society of Chemistry. Copyright 2012. (C) Schematic of the electrochemical time-resolved surface second harmonic generation (TR-SSHG) experimental setup (CE = counter electrode, RE = reference electrode, Aq = aqueous phase, and Org = organic phase). Adapted with permission from ref 144. Copyright 2014 American Chemical Society. (D) SSHG intensity (symbols) and Galvani potential difference (solid black line) as a function of time at the water−DCE interface for (triangles) $Au_{0.9}Ag_{0.1}$ NPs and (circles) $Au_{0.6}Ag_{0.4}$ NPs. Adapted with permission from ref 116. Copyright 2007 American Chemical Society. (E) Schematics of the sample preparation for freeze-fracture shadow casting (FreSCa) cryo-SEM imaging. Reprinted by permission from Macmillan Publishers Ltd.: Nature Communications, ref 150. Copyright 2011. (F) Operational scheme of amplitude-modulation AFM at a water−heptane interface and images of the NP monolayers. The depth of the water layer confined by a mica container is kept <100 μm, and the cantilever is excited by photothermal actuation (blue laser) inside the heptane drop. Adapted with permission from ref 152. Copyright 2016 American Chemical Society.

electrode electrochemical cell to track adsorption as a function of applied $\Delta_o^w\phi$. The voltage-induced reversible adsorption and desorption of AuNPs < 2 nm in size, noted earlier, was monitored by quasi-elastic light scattering (QELS);[18,115] see Figure 7A(i) for a scheme of the experimental setup. QELS monitors the frequencies of capillary waves of a selected wavelength at the liquid−liquid interface spontaneously generated by thermal fluctuations. The resulting plots of $\gamma_{w/o}$ vs $\Delta_o^w\phi$ are known as electrocapillary curves (Figure 7A(ii)). In the presence of AuNPs, the shape of an electrocapillary curve changes significantly, as shown in Figure 7A(ii), reflecting changes in the number density of AuNPs at the interface.

An alternative experimental approach to measure electrocapillary curves is pendant drop tensiometry.[136−138] This technique has yet to be applied to monitor the adsorption of AuNPs as a function of $\Delta_o^w\phi$. Nevertheless, measurements of $\gamma_{w/o}$ for nonpolarized water−decane interfaces in the presence of various adsorbed AuNPs clearly highlight the technique's suitability for future studies.[139−141] Also, Hua et al.[142] studied the adsorption of 5 nm AuNPs at the toluene−water interface using this method. The particles were functionalized with ion-pair ligands that promote adsorption to, and desorption from, the interface.

Electrochemical capacitance measurements at the ITIES have highlighted an increased capacitance at negative potentials in the presence of either citrate-stabilized 16 nm AuNPs[88] or mercaptosuccinic acid-stabilized <2 nm AuNPs.[115] Because of their negatively charged stabilizing ligands, the AuNPs are

DOI: 10.1021/acs.chemrev.7b00595
Chem. Rev. 2018, 118, 3722−3751

induced to adsorb at a negatively polarized ITIES and excess charge density builds at the interfacial boundary. Additionally, excess charge density may be attributable to interfacial corrugation in the presence of adsorbed AuNPs. Marinescu et al.[143] developed a theoretical model to facilitate further development of such capacitance-based characterization of interfacial AuNP adsorption as a function of $\Delta_o^w\phi$, with experimental data closely matching the theory (Figure 7B). The nonlinear optical technique surface second harmonic generation (SSHG) is a powerful surface-specific technique that may be applied to the study of molecular species or solid nanomaterials adsorbed at the liquid−liquid interface;[144] see Figure 7C for a scheme of the experimental setup. SSHG is ideal for monitoring voltage-induced reversible adsorption and desorption, as exemplified for core−shell gold−silver NPs ca. 16−20 nm in size (Figure 7D).[116] The surface specificity of SSHG arises from the vanishing of the second-order nonlinear susceptibility in centrosymmetric media within the electric dipole approximation.[145]

4.2. Physical Position and Three-Phase Contact Angle of the Nanoparticles

To understand the measured conductive, catalytic, or plasmonic activity of a gold nanofilm, the physical positions of individual AuNPs within the nanofilm need to be determined with nanometer accuracy in terms of interparticle spacing and θ_0 values. The characterization of AuNPs on solid supports is dominated by electron and scanning probe microscopy techniques (i.e., scanning/transmission electron microscopy (SEM/TEM) and scanning probe microscopy (SPM), such as atomic force microscopy (AFM) and scanning tunneling microscopy (STM)). However, the motion of AuNPs on a fluidic interface makes such in situ analysis at liquid−liquid interfaces exceptionally difficult. Ex situ analysis, for example, by SEM/TEM, via transferring the gold nanofilms to solid supports may cause alteration of the initial microstructure, leading to the formation of drying artifacts and, finally, to incorrect interpretation of the obtained data.

Recent reviews have provided an overview of common techniques applied to determine θ_0 values of various nanomaterials at fluidic interfaces.[146,147] Techniques such as capillary rise methods, surface-pressure isotherms, or drop-shape analysis measure macroscale interfacial properties related to θ_0 through theory and therefore are indirect. The drawback of these techniques is an inability to analyze the distribution of θ_0 values. Only a single average θ_0 value can be extracted, and it relies on assumptions that tend to break down at the nanoscale. However, using optical microscopy to observe floating particles, Snoeyink et al.[148] obtained the distribution of θ_0 with good statistics for 1 μm polystyrene spheres at the interface of water−glycerol and water−decane.

One promising technique designed to overcome these issues is freeze-fracture shadow casting (FreSCa) cryo-SEM.[149,150] This technique was used to image ca. 100 nm AuNPs in situ at water−decane interfaces and additionally determine θ_0 values. As the name suggests, the AuNP-functionalized liquid−liquid interface is frozen in a liquid propane jet with a speed of up to 10^6 K s^{-1}, and then cracked open and imaged. The key is that the interface acts as a weak fracture plane that is preferentially exposed on fracturing; see Figure 7E. Techniques that trap AuNPs in gels, followed by analysis with SEM or AFM, have also been developed.[151] However, potential drawbacks of both FreSCa cryo-SEM and gel-trapping techniques are the deformation of the interface due to the freezing/gelling process and difficulties providing statistically significant individual data points to evaluate the distribution of θ_0 values at the interface.

Costa et al. successfully imaged SiO_2 NP monolayers self-assembled at a water−heptane interface with an unprecedented lateral resolution of <10 nm using amplitude-modulation AFM;[152] see Figure 7F for a scheme of the experimental setup. The development of such real-space in situ imaging techniques will allow in-plane structural information, such as the interparticle spacing, to be gathered on a localized area of the interface. This is in sharp contrast to reciprocal techniques, such as X-ray reflectivity (discussed vide infra), where structural information is averaged over the finite size of the radiation beam and nonperiodic isolated AuNP aggregates or defects in the nanofilm may not be easily detected.

4.3. X-ray Reflectivity and Scattering

Several techniques based on scattering of X-rays from liquid−liquid interfaces are capable of determining in situ both in-plane and out-of-plane structural information on floating gold nanofilms.[18,135,153,154] X-ray reflectivity measurements identify variations in electron density perpendicular to the liquid−liquid interface;[57,155] the experimental setup is identical to that for QELS, as shown in Figure 7A(i). Schlossman and co-workers showed that the resulting electron-density profiles allow the precise interfacial location of a monolayer of 2 nm AuNPs to be determined with subnanometer resolution as a function of $\Delta_o^w\phi$.[18] Under experimental conditions that induce very dense arrangements of AuNPs at the liquid−liquid interface, for example, upon lateral compression,[153] X-ray reflectivity measurements provide evidence for the formation of interfacial bi- or trilayers of AuNPs.

Grazing-incidence small-angle X-ray scattering (GISAXS) reveals the 2D ordering of the AuNPs within the gold nanofilm; for example, changes in the lattice spacing or interparticle separation distance as a function of $\Delta_o^w\phi$[18] or solution ionic strength[135] have been demonstrated. Typically, X-ray scattering experiments have been combined with other techniques to gain deeper insights. Schlossman and co-workers[18] combined insights from X-ray reflectivity, GISAXS, electrocapillary curves, and molecular dynamics (MD) simulations (all as a function of $\Delta_o^w\phi$) to demonstrate that hydrophobic TB^- anions in the organic phase condense onto the surface of very positively charged AuNPs coated with trimethylammonium-terminated ligands at the aqueous−organic interface. Snapshots of the MD simulations at various time periods are shown in Figure 8. This is strong experimental proof of the concept that TB^- acts as a promoter, as described by Bell and co-workers for the case of tetrabutylammonium (TBA^+) cations condensing onto the surface of very negatively charged AuNPs.[2,82] Schlossman and co-workers[18] showed that the small 2 nm AuNPs were drawn across the interface into the low-polarity organic phase by shielding their charge with hydrophobic counterions. Meanwhile, Velleman et al.[135] utilized X-ray reflectivity, grazing-incidence X-ray diffraction (GIXRD), and optical reflectance (discussed vide infra) as complementary techniques to independently verify the decrease in interparticle spacing and increase in AuNP surface coverage with increasing ionic strength in either the aqueous or organic phase.

4.4. Optical Reflectivity and Scattering

Optical reflectivity measurements have been used to investigate propagating SPR due to strong plasmon coupling in densely packed interfacial gold nanofilms.[89,91,156] Using a pseudo-

DOI: 10.1021/acs.chemrev.7b00595
Chem. Rev. 2018, 118, 3722−3751

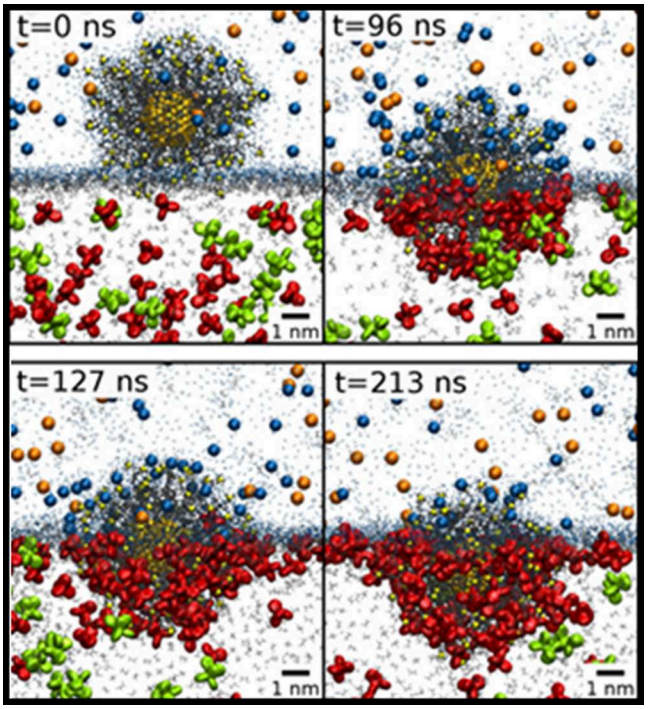

Figure 8. Molecular dynamics (MD) simulation of nanoparticles at liquid−liquid interfaces. Time-sequence snapshots of the submersion of a AuNP from an aqueous (top) to an organic (bottom) electrolyte phase accompanied by the exchange of loosely bound Cl^- ions (blue) in the aqueous phase for condensed organic TB^- ions (red) in the organic phase. Adapted with permission from ref 18. Copyright 2014 American Chemical Society.

Kretschmann configuration, Cohanoschi et al. highlighted that a 10^3 times enhancement of the interfacial fluorescence of dyes is possible at water−xylene interfaces at the surface plasmon resonance angle (θ_{SPR}) in the presence of interfacial gold nanofilms. The enhancement was attributed to the electric field enhancement in the plasmonic hot-spots and the reduction of the fluorescence lifetime of dye molecules in close vicinity to the metal surface.[156] θ_{SPR} is the angle of the incident light hitting the interfacial gold nanofilm that leads to a minimum (or dip) in reflectance at a specific wavelength. Also using a pseudo-Kretschmann configuration (see Figure 9A(i)), Hojeij et al. produced clear experimental evidence of the dip in reflectance beyond the critical angle due to SPR absorption by the interfacial gold nanofilm, closely matching theoretical calculations;[89] see Figure 9A(ii) and (iii).

SPR is also sensitive to changes in refractive index of the medium (discussed in detail in section 5.2 vide infra), measured as the change in reflected light passing through a prism and reflected off of the back of the interfacial gold nanofilm. The "back" of the interfacial gold nanofilm can refer to the oil side or water side depending on the density of the chosen oil phase. Thus, a low-density oil phase such as toluene will be on top of the water phase and, when illuminated from the bottom, water is at the back of the interfacial gold nanofilm, and vice versa for a high-density oil phase such as TFT. Therefore, SPR-based nanoplasmonic sensors based on interfacial gold nanofilms using a pseudo-Kretschmann configuration are envisioned.

Girault and co-workers developed a setup with robotic arms to change the angle of incident light hitting the interfacial gold nanofilms, shown in Figure 9B. The latter setup has been used to generate optical reflectivity data, allowing the quantification of the influence of a host of variables (AuNP size, interfacial surface coverage and light wavelength, polarization and angle of incidence, presence of surfactant, and applied $\Delta_o^w\phi$) on the effectiveness of variously prepared interfacial gold nanofilms to act as nanoplasmonic mirrors.[17,90]

Smirnov et al.[7] probed the optical extinction and reflectance of interfacial gold nanofilms that encapsulated the entirety of an oil droplet using an integration sphere (Figure 9C). Additionally, they imaged gold nanofilms in situ with μm resolution with optical microscopy revealing the formation of microscale cracks and wrinkles. Comparison of SEM and TEM images obtained with transfer of the nanofilm on a solid substrate shows similar features, confirming that the structure of the film can stay more or less intact during the transfer.[7]

Furthermore, Velleman et al.[135] used a commercial reflectivity probe positioned at 90° to the liquid−liquid interface (see Figure 9D) to monitor the red-shift in SPR reflectance maxima as a result of enhanced plasmonic coupling between AuNPs due to decreasing interparticle spacing with increasing ionic strength in either the aqueous or organic phase (allowing calibration of a so-called "plasmonic ruler").

As detailed in section 3.4, decreasing the interparticle gap in a gold nanofilm causes a near-exponential increase in the sensitivity of the responses of SPR and SERS-based nanoplasmonic sensors, as well as an exponential increase in the conductivity of the gold nanofilm. Thus, the creation of calibrated plasmonic rulers using easily accessible optical spectroscopic techniques, as described by Velleman et al.,[135] provides a precise guide to tune the interparticle gaps through addition of salt, applying an electric field, etc. in real time. The latter will be hugely beneficial to tune the strength of homogeneous plasmonic hotspots, necessary to optimize the responses of nanoplasmonic sensors using floating gold nanofilms and also as a guide to predicting the conductivity of floating gold nanofilms. Most recently, Velleman et al.[157] further demonstrated the reduction of interparticle distance between AuNPs in the nanofilm in situ at a water−DCE interface as a function of pH, which led to a 20- to 40-fold increase of Raman intensity. Moreover, these changes were monitored in real time.[157]

4.5. Electrochemical Techniques

Scanning electrochemical microscopy (SECM) at liquid−liquid interfaces can be used to probe the local conductivity or potentially characterize redox electrocatalysis reactions taking place at an interfacial gold nanofilm. The working principle of SECM involves the continuous recycling of a redox mediator, either in the aqueous or organic phase, between the tip of a biased micro- or nanoelectrode and the surface of the interfacial gold nanofilm; see Figure 10A. If a microelectrode (biased positively to oxidize the mediator) approaches an area of the interface that is nonconductive, a gradual decrease of the measured current is observed due to confinement of the semispherical diffusion field at the surface between the microelectrode and the liquid−liquid interface (Figure 10A(i)). The latter causes a depletion of the reduced species and accumulation of oxidized species, and it is called "negative feedback". A nonconductive interface can mean simply the absence of AuNPs at that local area on the interface or the presence of AuNPs with such a large interparticle spacing that charge transport cannot propagate across the interfacial gold nanofilm. The latter was shown by Fang et al., who observed negative feedback until a sufficiently large AuNP surface

DOI: 10.1021/acs.chemrev.7b00595
Chem. Rev. 2018, 118, 3722−3751

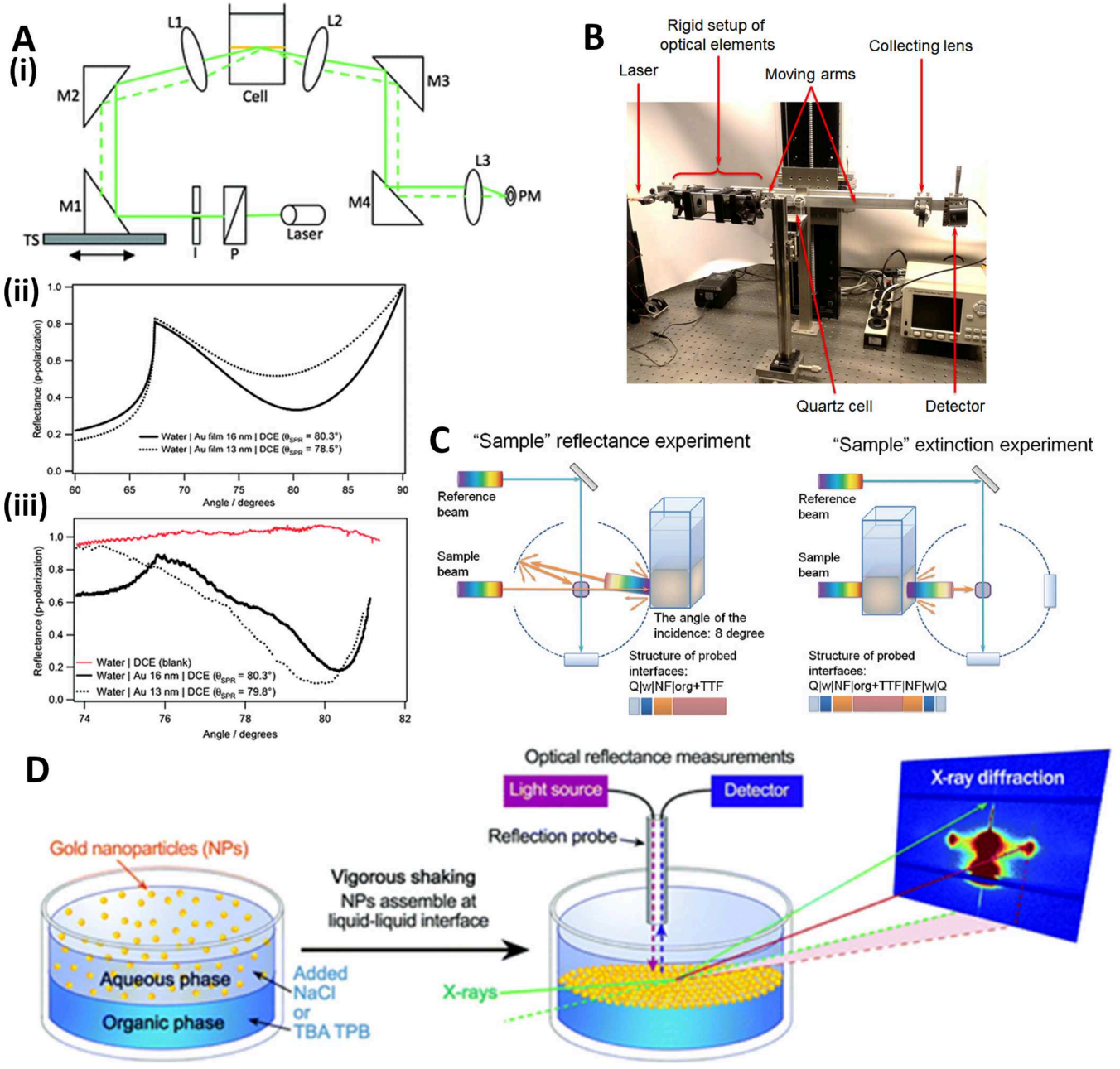

Figure 9. Reflectance measurements from a liquid−liquid interface functionalized with a nanofilm. (A)(i) Schematic of the experimental setup to measure surface plasmon resonance (SPR) at a gold nanofilm floating at a liquid−liquid interface using a pseudo-Kretschmann configuration. (A)(ii) Calculated and (A)(iii) experimental SPR curves for a gold nanofilm floating at a water−DCE interface for an excitation wavelength of 544 nm (full line, 16 nm Au film; dotted line, 13 nm Au film). Adapted from ref 89 with permission from The Royal Society of Chemistry. Copyright 2010. (B) Image of an experimental setup with robotic arms to investigate the angular dependence of the laser reflectance from interfacial gold nanofilms. The setup consists of robotic arms, a laser light source, various optical components, and a detector, all of which move simultaneously as the angle of the laser incident to the gold nanofilms is varied. Adapted from ref 17 with permission from The Royal Society of Chemistry. Copyright 2017. (C) Reflectance and extinction spectra acquisition for interfacial gold nanofilms in situ by UV−vis−NIR with a white integrating sphere. Sample (with the gold nanofilm coating the organic droplet) reflectance spectra were obtained at a single gold nanofilm interface on one side of the quartz cell. Sample extinction spectra were measured through two gold nanofilms at opposite walls of the quartz cuvette. Q, w, org, and NF are acronyms for quartz, water, organic solvent, and gold nanofilm. Adapted from ref 7 with permission from The Royal Society of Chemistry. Copyright 2016. (D) Schematic describing the self-assembly of AuNPs at a water−DCE interface when either NaCl or TBATPB was added to the aqueous or organic phase, respectively. The assembled floating gold nanofilm was analyzed by X-ray reflectivity and diffraction to obtain structural information, as well as by optical reflectance to study the plasmon coupling between the AuNPs. Adapted from ref 135 with permission from The Royal Society of Chemistry. Copyright 2016.

coverage (and therefore small interparticle distance) was reached to allow charge transport across at least μm^2-sized portions of the interfacial gold nanofilm;[90] see Figure 10B. For these conductive densely packed interfacial arrays of AuNPs, the measured current increased on approaching the interface as the oxidized species were reduced by the AuNPs (Figure 10A(ii)). The latter is called "positive feedback", and the conductive gold nanofilm is recharged by electron injection

DOI: 10.1021/acs.chemrev.7b00595
Chem. Rev. 2018, 118, 3722−3751

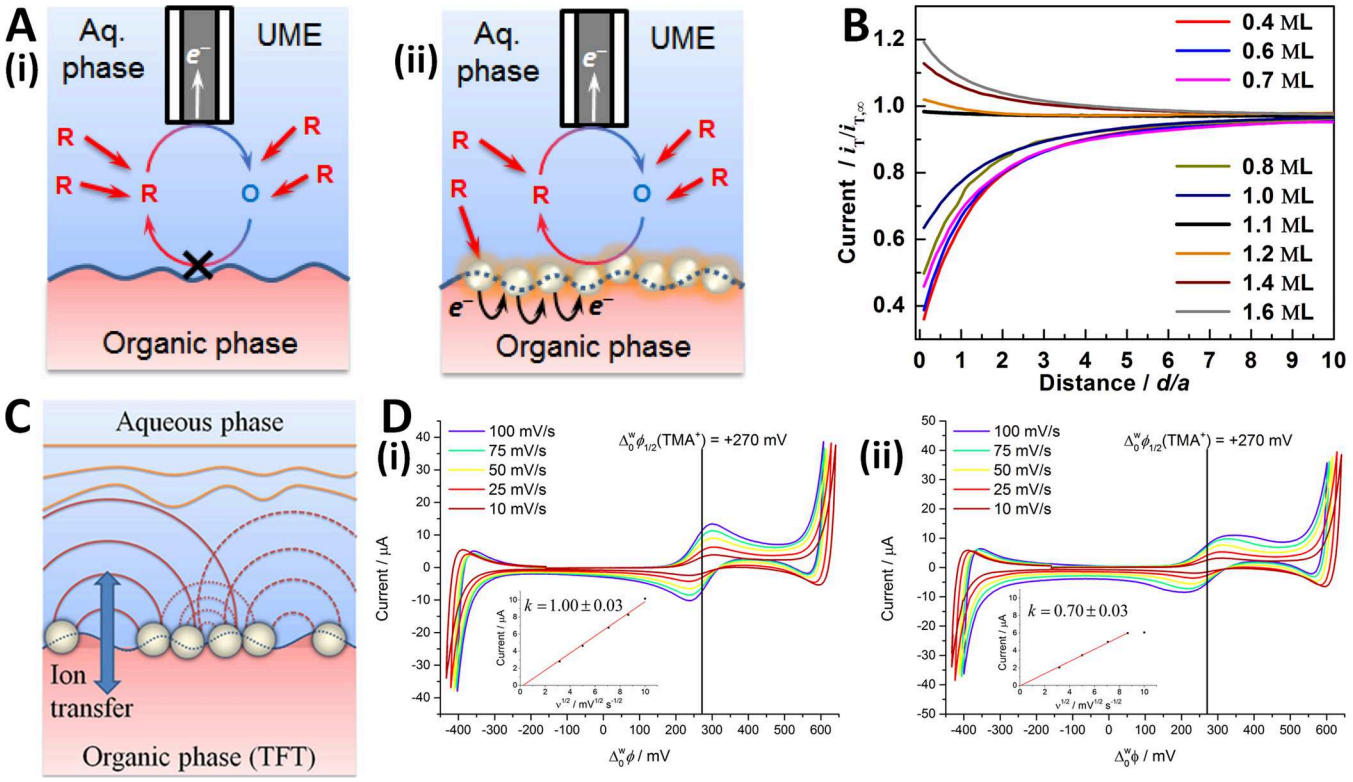

Figure 10. Electrochemical methods used to characterize nanofilms at liquid−liquid interfaces. Schemes of scanning electrochemical microscopy (SECM) experiments with (A) (i) negative feedback at a bare water−oil interface and (ii) positive feedback at a floating gold nanofilm at a water−oil interface. (B) SECM approach curves with a Pt microelectrode (radius, a = 10 μm; RG = 7) to a water−[heptane/DCE] interface in the presence of different AuNP surface coverages. The oil phase contained 2 mM DMFc and 2 mM BATB. The translation rate was 1 $\mu m \cdot s^{-1}$. Adapted with permission from ref 90. Copyright 2013 American Chemical Society. (C) Schematic representation of the cross-sectional view of the ITIES partially occupied by a gold nanofilm. The lines show the diffusion profiles of ion concentration. Adapted with permission from ref 20. Copyright 2015 American Chemical Society. (D) Ion-transfer CVs (IR compensated) of 25 μM tetramethylammonium cations (TMA^+) in the aqueous phase at a water−TFT interface (i) without a gold nanofilm and (ii) with a gold nanofilm composed of 12 nm AuNPs. The apparent standard ion-transfer constant (k^0_{app}) for TMA^+ was calculated by the method of Nicholson, allowing estimation of the interfacial AuNP surface coverage (θ). Adapted with permission from ref 20. Copyright 2015 American Chemical Society.

from another redox species in the opposite phase at any point on the gold nanofilm (i.e., at a considerable distance from where the microelectrode is positioned). Although as yet not demonstrated for redox electrocatalysis with gold nanofilms, in a related study, SECM has been used to monitor photoinduced water oxidation at ITIES functionalized with nanosized bismuth vanadate ($BiVO_4$) crystals.[158]

Ion-transfer voltammetry can also be also used to roughly estimate the surface coverage of the nanofilms. NPs adsorbed at the interface reduce the available surface area for IT, effectively blocking the surface.[20] As discussed by Amatore et al.,[159] a blocking layer at the electrode surface leads to a decreased apparent standard rate constant for the electron-transfer reaction ($k^0_{app} = k^0(1 - \theta)$, where θ is the surface coverage of the blocking porous layer). The same approach is true for the nanofilm covering the ITIES; see Figure 10C. Hence, a simple estimation of the apparent standard ion-transfer constant for the transferring ion by the method of Nicholson allows estimation of the surface coverage if the rate constant on the clean surface is known;[20] see Figure 10D. Other techniques successfully used to characterize the coverage of porous layers on solid electrodes, like chronoamperometry,[160] also could be utilized at liquid−liquid interfaces for IT reactions.

4.6. Summary

A summary of the main experimental techniques used to probe AuNP adsorption at liquid−liquid interfaces, and the resulting properties of gold nanofilms formed at liquid−liquid interfaces, is provided in Table 1.

For solid−liquid interfaces, electrochemical capacitance measurements are useful to probe the nanofilm porosity.[161] SSHG is well-known from metal island films[162] and has been utilized for designing a nonlinear plasmonic nanoruler with high sensitivity.[163] Surface probe techniques are much easier to employ for films assembled at solid−liquid interfaces, with techniques like SEM, TEM, STM, and AMF used routinely. Additionally, spectroscopic techniques have been widely utilized to characterize optical properties of superlattices. More specialized techniques such as liquid cell transmission electron microscopy (LC-TEM) have been utilized to follow NP self-assembly in situ.[164] Both grazing-incidence (GISAXS) and small-angle X-ray scattering (SAXS) have been widely used for investigation of NP superlattices. They also allow statistical determination of superlattice grain size and size distributions over larger areas than accessible with electron microscopy due to systematic mapping of the sample.[165] SAXS measurements were also used for spatial mapping of the grain size, orientation, uniformity, strain, or crystal projections and polymorphs.[165] SAXS measurements of NPs have been recently reviewed.[166]

DOI: 10.1021/acs.chemrev.7b00595
Chem. Rev. 2018, 118, 3722−3751

Table 1. Summary of Experimental Techniques Applied to the Characterization of AuNP Adsorption at Liquid−Liquid Interfaces and the Properties of the Resulting Floating Gold Nanofilms

experimental technique	information/measurement results	ref
quasi-elastic light scattering (QELS)	monitoring the adsorption of AuNPs to the ITIES as a function of applied $\Delta_o^w\phi$ (electrocapillary curve)	18, 115
pendant drop tensiometry		136−140, 142
electrochemical capacitance		88, 115, 143
surface second harmonic generation (SSHG)		116, 145
freeze-fracture shadow casting (FreSCa) cryo-SEM	in situ determination of θ_0 for AuNPs adsorbed at a liquid−liquid interface	149, 150
gel-trapping techniques followed by SEM or AFM		151
amplitude modulation atomic force microscopy (AFM)	in situ real-space determination of interparticle separation for AuNPs adsorbed at a liquid−liquid interface	152
X-ray reflectivity	in-plane in situ reciprocal-space determination of interparticle separation for AuNPs adsorbed at a liquid−liquid interface; precise determination of AuNP out-of-plane shifts as a function of $\Delta_o^w\phi$	18, 153
grazing-incidence small-angle X-ray scattering (GISAXS)		18
grazing-incidence X-ray diffraction (GIXRD)		135
molecular dynamics (MD) simulations	simulation of AuNP adsorption at a liquid−liquid interface, e.g., probing the influence of organic electrolyte counterion condensation on the surface of an AuNP during adsorption	18
reflection measurements in pseudo-Kretschmann configuration (prism) or with robotic arms	angular dependence of reflectivity from floating gold nanofilms at a liquid−liquid interface at a given wavelength; determination of θ_{SPR}	17, 89−91, 156
UV−vis−NIR spectroscopy with an integration sphere	reflectivity and extinction spectra vs coverage of the interface; monitoring red- and blue-shifts of SPR and SPC extinction bands to determine in situ the interparticle separation for AuNPs adsorbed at a liquid−liquid interface	7
commercial reflectivity fiber probe		135
scanning electrochemical microscopy (SECM)	conductivity measurements of floating gold nanofilms at the ITIES; probing catalytic properties of NPs adsorbed at the liquid−liquid interface	90, 158
ion-transfer (IT) voltammetry	ion permeability; estimation of the surface coverage of AuNPs at the ITIES	20

For example, GISAXS was utilized to follow swelling of the film in the presence of volatile organic compounds.[167]

5. APPLICATIONS OF FLOATING GOLD NANOFILMS

5.1. Redox Electrocatalysis

As described in a recent review, electrocatalysis is catalysis of electron transfer at the electrode surface (catalyzed by the electrode material itself or by a catalyst attached to the electrode surface), while redox electrocatalysis is catalysis of electron transfer between two redox couples, catalyzed by a floating conductive catalyst.[125] Electrocatalysis and redox electrocatalysis are topics of pivotal importance impacting a huge variety of fields ranging from corrosion science, fuel cell and battery research, electro-organic synthesis, and electro-analytical sensor development to wastewater purification.[125,168] To optimize the performance of NPs toward electrocatalysis, a burgeoning area of research concerns support-induced effects.[169,170] For example, the supporting material for AuNPs can deeply affect their activities, as exhibited for AuNPs supported on carbon and on titania in the CO oxidation reaction.[171]

Electrochemistry of catalytic interfacial gold nanofilms at the ITIES has several distinguishing features in comparison to electrochemical studies of AuNPs on solid electrode surfaces. Most strikingly, the electrocatalytic activity of interfacial adsorbed AuNPs can be studied in a contactless manner, free from the influence of an underlying support. Just as with solid electrodes, the ITIES allows direct measurement of the electrocatalytic impact of gold nanofilms by measurement of charge transfer across the interface corresponding to electron-transfer events. At solid electrode interfaces the rate of an electrocatalyzed reaction is controlled by varying the electrode potential and concentrations of oxidized to reduced species initially present in solution. The degree of freedom of this system is 1, as the system is fully characterized by the mass balance equation ($Ox + e^- \Leftrightarrow Red$) and the Nernst equation,

$$E = E^0 + \frac{RT}{F}\ln\left(\frac{a_{Ox}}{a_{Red}}\right) \quad (1)$$

where E is the electrode potential, E^0 is the standard redox potential of Ox/Red, a is the activity (where the activity is related to the concentration, c, by $a = \gamma c/c^0$, taking into account the activity coefficient, γ, which becomes 1 for infinite dilution, and where c^0 is the standard concentration 1 mol L^{-1}), and R, T, and F are the gas constant, temperature, and Faraday's constant, respectively. Attractively, the ITIES has in fact two degrees of freedom, as five variables are interconnected by two mass balance equations and the Nernst equation.[172] The first mass balance equation concerns Ox/Red species in the aqueous phase, and the second concerns Ox/Red species in the organic phase, resulting in $Ox_1^w + Red_2^o \Leftrightarrow Red_1^w + Ox_2^o$, where superscripts w and o refer to aqueous and organic phases, respectively. Thus, the Nernst equation for IET across the ITIES is[172]

$$\Delta_o^w\phi = \Delta_o^w\phi_{ET}^0 + \frac{RT}{F}\left(\frac{a_{Red_1}^w a_{Ox_2}^o}{a_{Ox_1}^w a_{Red_2}^o}\right) \quad (2)$$

where $\Delta_o^w\phi_{ET}^0$ is the standard redox potential for the IET reaction: $\Delta_o^w\phi_{ET}^0 = [E_{Ox_2/Red_2}^0]_{SHE}^o - [E_{Ox_1/Red_1}^0]_{SHE}^w$, where superscript 0 refers to the standard value and SHE refers to standard hydrogen electrode scale.

This IET reaction can take place also without catalysts, but a gold nanofilm deposited at the interface may be utilized to significantly enhance the reaction rate. Effectively, the AuNPs

DOI: 10.1021/acs.chemrev.7b00595
Chem. Rev. 2018, 118, 3722−3751

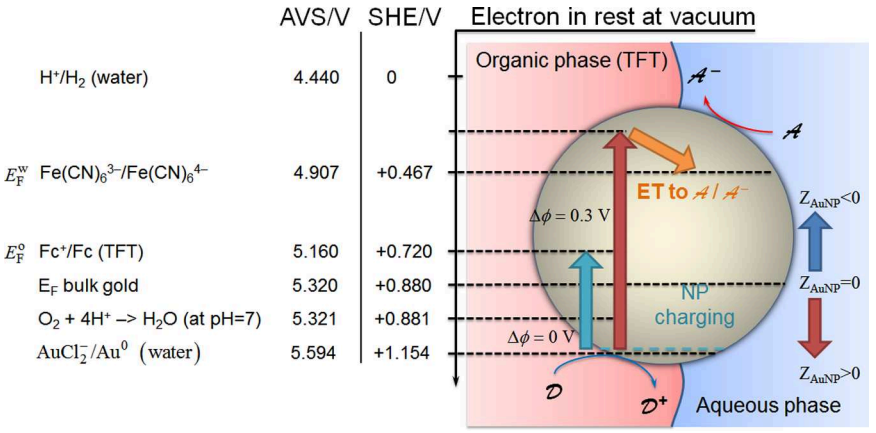

Figure 11. Mechanism of interfacial redox electrocatalysis by floating gold nanofilms. Equilibration of the Fermi level of the electrons in a single AuNP within a gold nanofilm (E_F^{NP}) adsorbed at a liquid−liquid interface with those of two redox couples in solution, a hydrophilic electron acceptor species ($\mathcal{A}$) in the aqueous phase and a hydrophobic electron donor species ($\mathcal{D}$) in the organic phase. The AuNP is charged during this process by $\mathcal{D}$, for example, ferrocene (Fc). The AuNP acts as an interfacial reservoir of electrons, and the final position of E_F^{NP} (a turquoise line for $\Delta_o^w\phi$ = 0 V and a red line for $\Delta_o^w\phi$ = 0.3 V, respectively) is determined by the kinetics of both the oxidation half-reaction on the organic side of the interfacial gold nanofilm and the reduction half-reaction on the aqueous side (for example, O_2 reduction). IET between the two redox couples via the conductive AuNP, and the provision of a catalytic surface in the specific case of O_2 reduction, significantly enhance the kinetics of IET. The standard redox potentials of all redox couples are expressed versus both the standard hydrogen electrode (SHE) and absolute vacuum scale (AVS), respectively, and the organic phase is TFT. Adapted from ref 19 with permission from Elsevier. Copyright 2016.

act as conductive bipolar electrodes facilitating catalysis via direct IET (through Fermi level equilibration)[20,173] between a lipophilic electron donor and a hydrophilic electron acceptor, or vice versa (see Figure 11). Finite-element method simulations have also been used to study this process.[174,175]

Moreover, the AuNPs provide a catalytic surface to further negate the kinetic barriers to IET at bare liquid−liquid interfaces. Additional thermodynamic driving force can then be provided by adjusting $\Delta_o^w\phi$ to establish further control over both the rate of a reaction and the direction of electron transfer across the interface. As a proof-of-concept, interfacial gold nanofilms were shown to effectively catalyze IET between a lipophilic electron donor redox couple, ferrocenium cation/ferrocene, and a hydrophilic electron acceptor redox couple, ferri-/ferrocyanide;[20] see Figure 12A. The peak-to-peak separation for IET reduced significantly from >90 mV in the absence of the gold nanofilm (Figure 12B) to between 65 and 70 mV in its presence (Figure 12C). Additionally, a clear shift of the ratio of the forward and reverse peak current toward unity was observed in the presence of the gold nanofilm. Furthermore, dissolved oxygen (O_2) in the aqueous phase was reduced to H_2O_2 and H_2O by IET from either the lipophilic electron donor redox couple decamethylferrocenium cation/decamethylferrocene,[19] as shown in Figure 12D and E, or 1,1′-dimethylferrocenium cation/1,1′-decamethylferrocene.[21] Recently, redox electrocatalysis of O_2 reduction was also utilized to study Pt NP impacts upon a microscopic liquid−liquid interface, extending the NP impact studies to collisions at liquid−liquid interfaces.[176]

Beyond gold nanofilms, redox electrocatalysis of energy-related reactions such as the biphasic O_2 reduction reaction (ORR)[38,177−205] and biphasic hydrogen evolution reaction (HER)[185,201,206−217] has also been demonstrated numerous times by immobilization of catalytic NPs ranging from inorganic nanomaterials (e.g., Pt,[185] MoS_2,[208] Mo_2C,[210] Cu_2CoSnS_4,[213] etc.) to carbon-supported nanocomposites (e.g., Cu NPs on carbon nanotubes)[215] at the ITIES. Furthermore, redox photoelectrocatalysis of the water oxidation reaction (WOR) has been achieved by immobilization of $BiVO_4$ semiconductor NPs at the ITIES.[158] These burgeoning areas of redox (photo)electrocatalysis of energy-related reactions by ITIES functionalized with nanomaterials (beyond gold nanofilms) are very exciting current avenues of research and as such have been the subject of two recent comprehensive reviews by Peljo et al.[125] and Poltorak et al.[71]

NP superlattices formed at solid−liquid interfaces can be utilized for electrocatalysis as well as for heterogeneous catalysis, as reviewed by Boles et al.[33] and by Henry.[218] For example, Au nanocrystals were found to be highly active for oxidation of CO when assembled on metal oxide surfaces,[219] most likely due to the contact electrification.[220−222] Binary superlattices containing Au−Fe_3O_4 and Pt−CeO_2 and their pairs have been employed for CO oxidation[223] and methanol decomposition,[224] respectively. Curiously, electrocatalysis utilizing superlattices has not been explored in detail. Instead, significant attention has been focused on NPs supported on carbon and on single NP electrochemistry.[225] However, recent examples demonstrated binary Pd−Pt superlattices for electrocatalytic O_2 reduction,[226] as well as AuNP superlattices for electrochemical detection of microRNA-21 utilizing toluidine blue as a hybridization indicator.[227] Additionally, polyelectrolyte/AuNP hybrid films have been utilized for NO sensing,[228] as well as similar layer-by-layer films of IrO_2 particles for O_2 evolution.[229,230] On the other hand, NP arrays have been utilized for multivariable gas and vapor sensing using a panoply of techniques ranging from impedance spectroscopy to optical methods measuring the reflected light.[231]

5.2. Nanoplasmonics

Localized surface plasmon resonance (LSPR) occurs when the incident light frequency impacting a AuNP is resonant with the collective oscillation of the conduction band electrons.[126] LSPR leads to a marked enhancement in the local (near-field) electromagnetic field at the surface of the AuNP in comparison to the incident light. Yang et al. have used a three-dimensional finite-difference time domain (3D-FDTD) method to clarify the LSPR-based optical properties of AuNPs adsorbed at the

DOI: 10.1021/acs.chemrev.7b00595
Chem. Rev. 2018, 118, 3722−3751

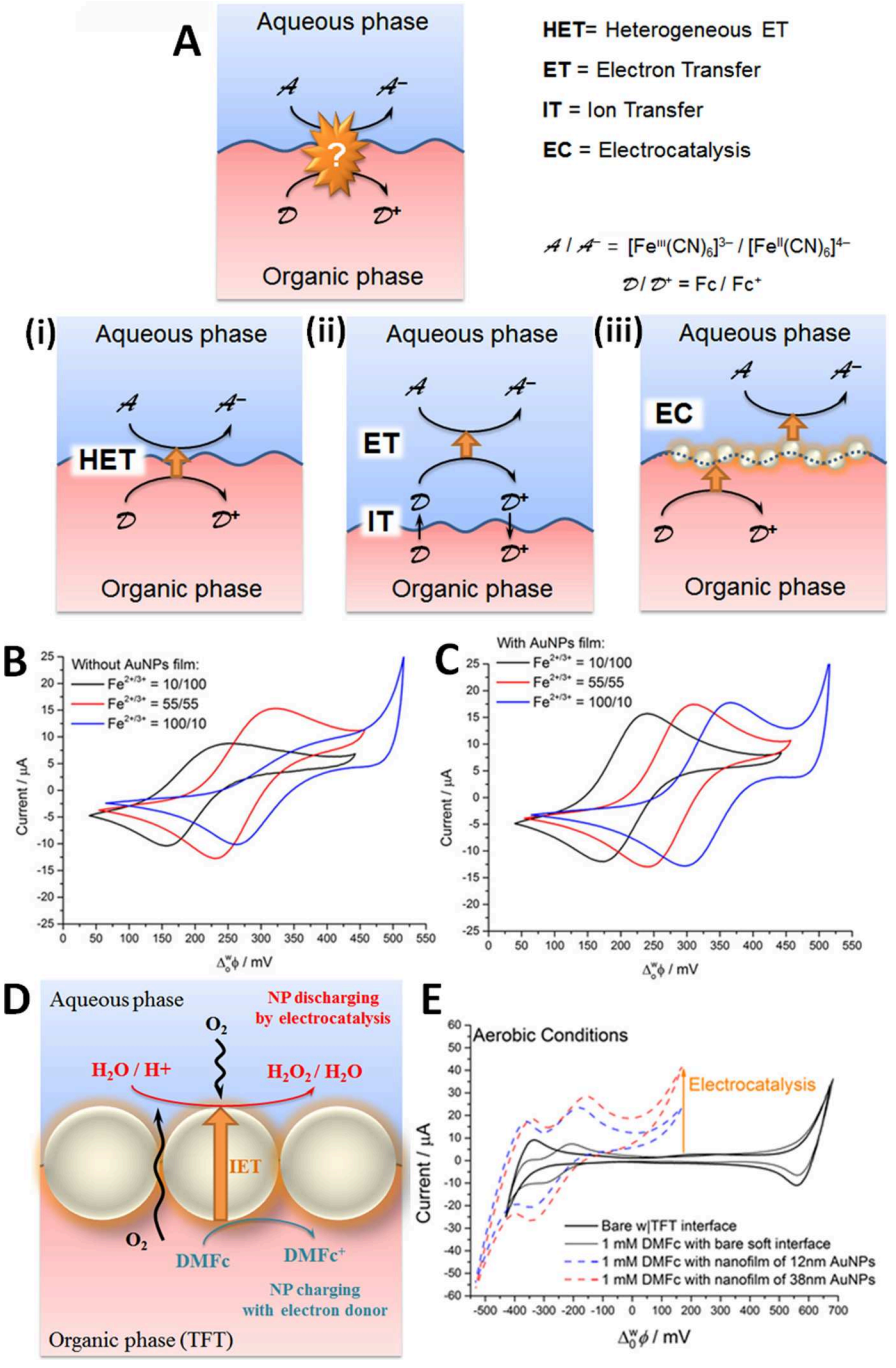

Figure 12. Experimental evidence of interfacial redox electrocatalysis by floating gold nanofilms. (A) Possible mechanisms, each leading to a measurable current across the ITIES when an electron-donor species ($\mathcal{D}$, such as the ferrocenium cation/ferrocene redox couple, Fc^+/Fc) is present in the organic phase and an electron-acceptor species ($\mathcal{A}$, such as ferri-/ferrocyanide, $[Fe^{III}(CN)_6]^{3-}/[Fe^{II}(CN)_6]^{4-}$) is present in the aqueous phase: (i) bimolecular IET, (ii) a homogeneous electron transfer−ion transfer (ET-IT) mechanism, and (iii) interfacial redox electrocatalysis with the floating gold nanofilm acting as a bipolar electrode. The orange arrow indicates the ET reaction with a rate constant, k^0. Adapted with permission from ref 20. Copyright 2015 American Chemical Society. CVs of ET between the oil-solubilized Fc^+/Fc redox couple and the aqueous $[Fe^{III}(CN)_6]^{3-}/[Fe^{II}(CN)_6]^{4-}$ redox couple, with various ratios between Fe^{2+} and Fe^{3+} investigated, both (B) in the absence and (C) in the presence of an interfacial gold nanofilm. Scan rate for all CVs was 10 mV s^{-1}, and the organic phase was TFT. Adapted with permission from ref 20. Copyright 2015 American Chemical Society. (D) Mechanism of O_2 reduction in the aqueous phase by charging a floating gold nanofilm with an electron donor (such as decamethylferrocene, DMFc) in the organic phase. The gold nanofilm acts as a barrier-free shortcut for IET to the aqueous phase. Adapted from ref 19 with permission from Elsevier. Copyright 2016. (E) CVs provide clear evidence of IET between DMFc and aqueous O_2 via the floating gold nanofilm due to the appearance of a significant current wave at $\Delta_o^w\phi$ = 50 mV under aerobic conditions only. The scan rate was 25 mV s^{-1} in all cases, and the organic phase was TFT. Adapted from ref 19 with permission from Elsevier. Copyright 2016.

water−oil interface, including near-field distribution and far-field absorption.[232] In the case of a AuNP adsorbed at a liquid−liquid interface, the presence of an underlying substrate (i.e., the oil phase) distorts the distribution of the plasmon field around the AuNP (see Figure 13(i−iv)). The latter is due to

DOI: 10.1021/acs.chemrev.7b00595
Chem. Rev. 2018, 118, 3722−3751

the change of the dielectric function at one side of the AuNP causing the LSPR to be either red- or blue-shifted.[7,232−237]

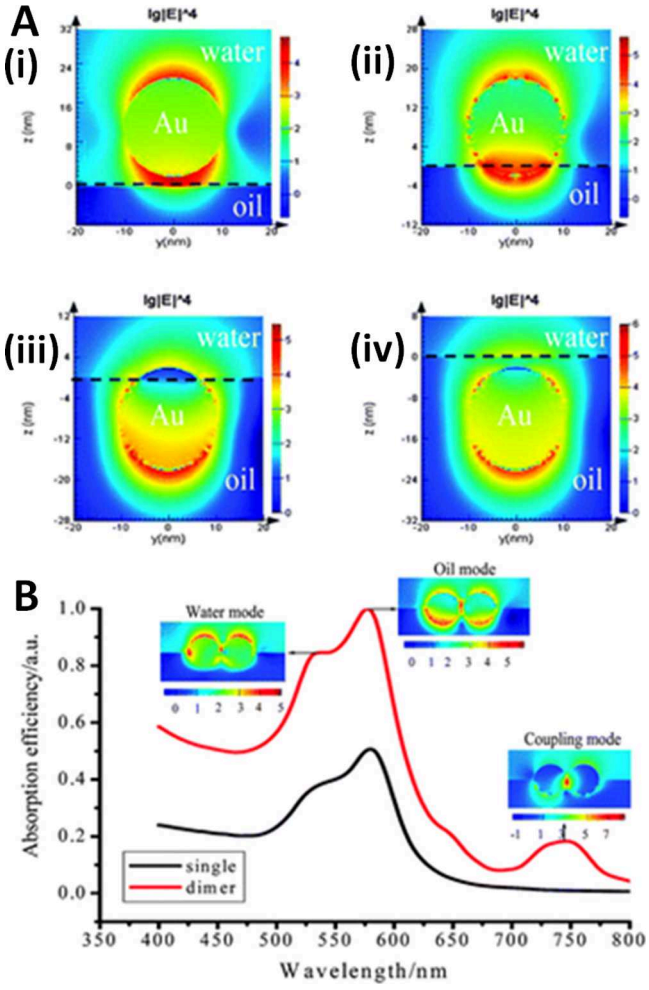

Figure 13. Distortion of the distribution of the plasmon fields around AuNPs floating at a liquid−liquid interface. (A) Finite-difference time domain (FDTD) calculated SERS electromagnetic enhancement distribution in the *yz*-plane at the frequency of LSPR for various interfacial positions of a AuNP: (i) 2 nm above the interface, (ii) 2 nm submerged into the oil, (iii) 2 nm remaining in water, and (iv) 2 nm below the interface. The dashed line represents the water−oil interface. (B) Calculated absorption spectra of AuNP dimers (red line) at the water−DCE interface and the corresponding electric-field distribution for three peaks (SPR "water mode", SPR "oil mode", and SPC "coupling mode"). Adapted from ref 232 with permission from the PCCP Owner Societies. Copyright 2013.

It is important to distinguish that "localized" in LSPR refers to the plasmonic response of separate, noninteracting AuNPs only. This is typically the case for AuNPs dispersed in a colloidal solution or for a hypothetical situation where a single AuNP adsorbs at a liquid−liquid interface, as modeled by Yang et al. in Figure 13(i−iv).[232] However, each AuNP in a gold nanofilm inevitably interacts with its neighboring AuNPs, and thereby all AuNPs in a gold nanofilm affect each other's plasmonic responses. Thus, the optical response of a film of NPs contains two plasmon peaks. The first one refers to extinction peaks of out-of-plane (transverse) AuNP plasmon oscillations for interacting AuNPs adsorbed at a water−oil interface, known simply as surface plasmon resonance (SPR) bands. The second one corresponds to in-plane (longitudinal) propagating plasmon oscillations that give rise to the appearance of additional coupling-mode extinction peaks and is called the surface plasmon coupling (SPC) band. Usually the SPC band is red-shifted in comparison to the SPR band. Figure 13B demonstrates the presence of both SPR and SPC bands in calculated absorbance spectrum for a dimer of interacting AuNPs at the water−DCE interface. Further, a series of works carried out by the group of Prof. Kornyshev revealed a high correlation between theoretically predicted[133] and experimentally obtained[135] absorbance and reflectance spectra for nanofilms at liquid−liquid interfaces. A significant number of articles focus on the plasmonics of NP superlattices at solid−liquid interfaces,[238] as highlighted in recent reviews.[31,33−35,76,239−241] The basic physics and applications are similar to those at liquid−liquid interfaces; however, nanoplasmonics at solid−liquid interfaces is a field of its own and is covered in detail, for example, by Gwo et al.[34]

The hot-spots formed between plasmonically coupled AuNPs experience hugely enhanced electromagnetic fields. Indeed, the study by Yang et al. concluded that, in hot-spots between adjacent AuNPs in an interfacial gold nanofilm, the efficiency of Raman scattering was enhanced in excess of 10^7−10^9-fold upon excitation with a laser of appropriate wavelength.[232] Such a phenomenon is known as surface-enhanced Raman spectroscopy (SERS),[242] an analytical method capable of providing molecular fingerprint information with ultrahigh surface sensitivity.

The SPR and SPC extinction bands observed for AuNPs represent both light absorption and scattering by the AuNPs. Reflection can be considered as a special case for light scattered along the specular direction. Furthermore, the AuNPs characteristic SPR wavelengths shift with changes of the medium refractive index. Thus, as the introduction of analyte molecules influences the bulk refractive index of the AuNPs environment, the resulting shifts in SPR maxima position are the basis of SPR sensors.[243] Both extinction (i.e., transmission expressed in log units) and reflectance measurements have been used to monitor shifts in the SPR maxima position on introduction of an analyte, with Kedem et al. demonstrating that reflectance measurements are more sensitive due to the dominance of absorption in transmission spectroscopy.[244]

Thus, using interfacial gold nanofilm sensors, the resulting SERS- or SPR-based nanoplasmonic sensors have the potential to facilitate the identification of single molecules attached, or located in close proximity, to the AuNP surface. The defect-free nature of the interface allows the creation of gold nanofilms with an exceptionally homogeneous distribution of hot-spots, which are difficult to achieve using either bottom-up or top-down approaches on solid substrates. This key feature maximizes the reproducibility of the resulting SERS- or SPR-based nanoplasmonic sensors. Prospective floating gold nanofilm-based SERS and SPR sensors will be discussed in more detail in section 6.1. However, superlattice formation of SERS-active NPs at solid substrates has already been demonstrated, and SERS is actually one of the main applications of AuNP nanofilms at solid−liquid interfaces.[34,113,245] Additionally, three-phase self-assembly, utilizing both solid−liquid and liquid−liquid interfaces, can also be performed for preparation of SERS substrates of high Raman enhancement factors.[113]

DOI: 10.1021/acs.chemrev.7b00595
Chem. Rev. 2018, 118, 3722−3751

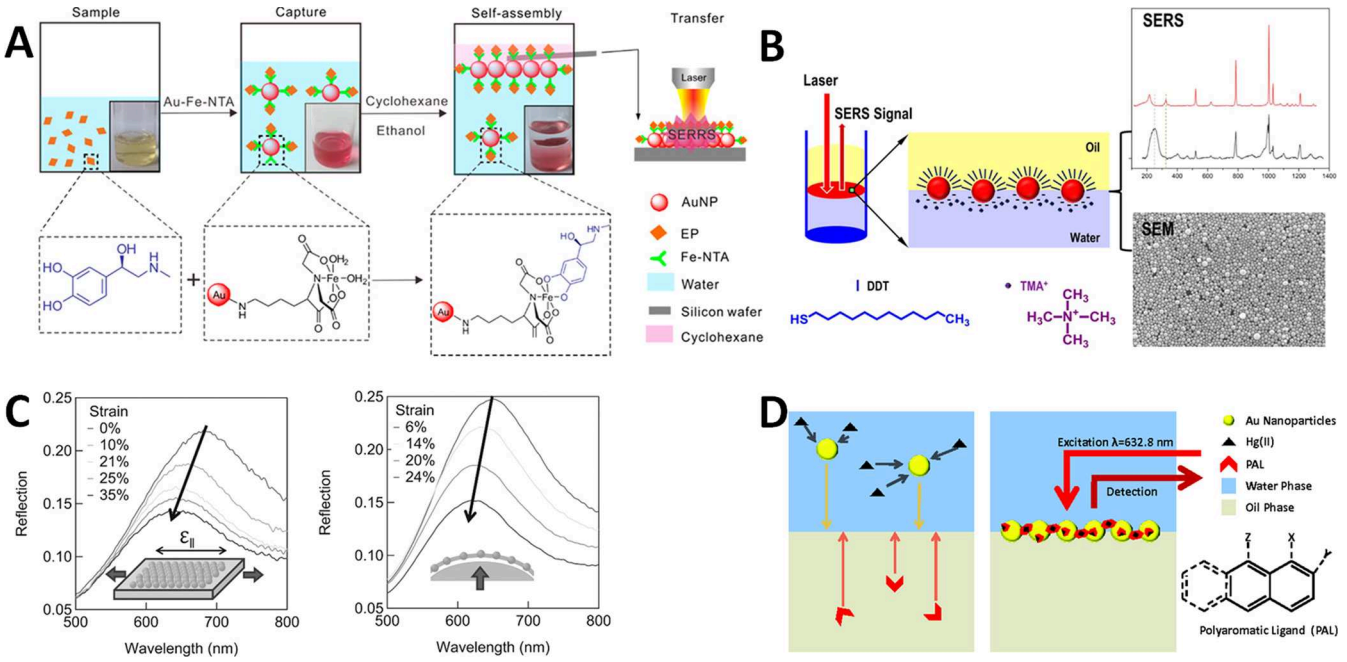

Figure 14. Current state-of-the-art surface-enhanced Raman spectroscopy (SERS) studies utilizing liquid−liquid interfaces. (A) Schematic representation of the detection process for epinephrine (EP) by a 2D surface-enhanced resonance Raman spectroscopy (SERRS) platform. The sample contains EP in serum (so an aqueous solution), to which AuNPs modified with α,β-nitriloacetic acid and $Fe(NO_3)_3$ are added. The modified AuNPs capture the EP and self-assembly (due to addition of ethanol) at the water−cyclohexane interface. The self-assembled gold nanofilms, enriched with the target EP analyte, are transferred to a silicon substrate for ex situ SERRS analysis. Adapted with permission from ref 264. Copyright 2017 American Chemical Society. (B) A gold nanofilm was formed at the water−toluene interface by addition of 1-dodecanethiol (DDT) and TMA^+ ions to the biphasic cell. In situ SERS analysis at the liquid−liquid interface demonstrated that the interfacial morphology of the gold nanofilm was closely linked to its chemical environmental (e.g., in the presence of TMA^+ alone, with varying amounts of DDT present, etc.). Adapted with permission from ref 275. Copyright 2015 American Chemical Society. (C) Reflection spectra of AuNP mats under increasing strain. The AuNP mats were prepared by transferring a floating gold nanofilm formed at a water−hexane interface to a flexible PDMS substrate. (Left) Uniaxial stretch parallel to optical polarization and (Right) biaxial uniform stretch with unpolarized light. The discrepancy in intensity is due to the curved film on the lens surface. Adapted from ref 261 with permission from AIP Publishing. Copyright 2012. (D) An aqueous phase containing AuNPs and a heavy metal ion target analyte (e.g., Hg^{2+}) are placed in contact with an oil phase containing a dissolved polyaromatic ligand (PAL). Shaking creates a biphasic emulsion, causing all aqueous and organic species present to self-assemble at the common liquid−liquid interface. After assembly, Hg^{2+} can be detected sensitively by SERS through its effects on the in situ SERS signals from the PAL molecules attached to the AuNPs surface adsorbed at the interface. Adapted with permission from ref 274. Copyright 2014 Wiley-VCH.

5.3. Optical Applications

A series of theoretical studies[129−134] have shown that coupling between localized surface plasmons of AuNPs in an interfacial gold nanofilm leads to significant reflection of light from the interface. The latter is perhaps surprising as only a monolayer of AuNPs is required to achieve this nanoplasmonic mirror effect. When incident light strikes strongly coupled interfacial AuNPs, light is scattered with phase coherence from AuNP to AuNP (in contrast to plasmonically noncoupled single AuNPs that scatter light in random directions according to Mie theory). This results in a very high reflection coefficient for an interfacial gold nanofilm, with reflection dominating over transmission and being dependent on the wavelength of the incident light.

From a practical point-of-view, Smirnov et al.[7] have shown that the size of the AuNPs is critical. Small AuNPs (<15 nm in diameter) are capable of effectively absorbing the incident light, whereas larger AuNPs (>25−30 nm) are more suited for liquid mirror applications due to efficient reflection of light (in agreement with theory).[7] The larger AuNPs absorb very little light due to being low dissipation materials that facilitate long-lived plasmons.[130] By comparison, NPs of aluminum, for example, would absorb significant amounts of light at the interface via dissipation of surface plasmons.[130] Thus, the reversible electrovariable movement of AuNPs both to and from the interface (on and off mirrors) and in-plane of the interface (shutters) as a function of $\Delta_o^w\phi$ lays the foundations for a host of potential technological applications of interfacial gold nanofilms in the realm of optics.

5.4. Plasmonic Photocatalysis

The topic of plasmon-enhanced photoreactions with floating gold nanofilms is not explored in detail in this Review. However, it is worth mentioning briefly, as conflicting reports have emerged regarding whether photocurrents at porphyrin-sensitized liquid−liquid interfaces can be significantly enhanced by devising protocols that incorporate plasmonic metallic NPs into the photoactive interfacial films.[17,91,246] Insights from such studies may potentially find applications in future artificial photosynthesis systems.[247,248] The underlying fundamental reasons for any enhanced photocurrents are as yet unresolved, with electrocatalytic and/or plasmonic factors needing to be considered. Nagatani et al.[246] and Schaming et al.[91] observed increased photocurrents that may be attributed to increased absorption due to surface plasmons and light-trapping effects, improved charge separation due to a localized intense electromagnetic field, or perhaps electron-storage effects that alter the Fermi level of the interfacial gold nanofilm. Alternatively, the photocurrents may actually decrease, as

DOI: 10.1021/acs.chemrev.7b00595
Chem. Rev. 2018, 118, 3722−3751

observed by Gschwend et al.,[17] as the surface area of the liquid−liquid interface becomes blocked with AuNPs, reducing the interfacial concentration of excited porphyrin molecules. Thus, some key questions remain unresolved. Which of the noted possible factors dominate the enhanced photoresponses seen by Nagatani et al. and Schaming et al.? Do the observations of Gschwend et al. negate all of the possible beneficial electrocatalytic or plasmonic attributes of the interfacial AuNPs? Each of the three studies to date introduced AuNPs to the electrochemical cell using very different experimental protocols, and therein likely lays the discrepancies between these preliminary studies.

6. PERSPECTIVE APPLICATIONS OF FLOATING GOLD NANOFILMS AT THE ITIES

6.1. Surface-Enhanced Raman Spectroscopy

A series of SERS-active solid electrode substrates, e.g., electrically contacted lithographic nanohole and nanopore arrays,[249,250] periodic particle arrays prepared by nanosphere lithography on transparent conductive oxides,[251,252] or colloidal silver nanoparticle (AgNP) and AuNP aggregates on conductive electrodes,[253,254] are suitable for electrochemical SERS (EC-SERS) applications. EC-SERS involves immersing these suitable SERS substrates in electrolyte solution and establishing an electrochemical double layer at the substrate/electrolyte interface, the potential drop across the layer can be controlled externally by a potentiostat.[255−257] The ultimate goal of EC-SERS is to monitor structural changes of molecules in situ as they are subjected to an electric field and in some cases undergo redox processes. The insights from such experiments have tremendous potential, for example, we may improve our understanding of how a molecule's redox activity is influenced by its immobilization chemistry.[258,259] The precipitous improvement in Raman instrumentation has now reached a point that the time resolution for spectra acquisition is comparable or even shorter than the charging time of the double layer capacitance for both reversible and irreversible electrochemical processes.[260] The significance of this milestone cannot be understated as it means structural molecular information on transient intermediate species in electrochemical reactions can be directly probed in situ, for example, during proton-coupled electron-transfer reactions. The structural information gained from EC-SERS measurements can give insights that indicate potential induced (i) adsorption or desorption of molecules, (ii) molecular reorientation of molecules, (iii) rearrangement of the electrochemical double layer, or (iv) electrochemical reduction or oxidation.[255]

To date, strategies to achieve EC-SERS at interfacial gold nanofilm functionalized ITIES are rare. Virtually all SERS studies involving liquid−liquid interfaces only take advantage of their inherent ability to facilitate defect-free self-assembly of floating gold nanofilms (with uniform distribution of plasmonic hot-spots) and not the ability to controllably apply a potential difference across the ITIES. For example, nanoplasmonic SERS sensors to detect epinephrine in serum, Cu^{2+}, Hg^{2+}, rhodamine 6G, malachite green, *p*-aminothiophenol, and *p*-nitrothiophenol have been developed by either transferring floating gold nanofilms to silicon wafer, glass, paper, or PDMS substrates (for example, see Figure 14A),[261−270] or by their in situ analysis at nonpolarized water−oil interfaces (for example, see Figure 14B).[2,271−275] The use of flexible PDMS substrates[261,262] is a particularly interesting strategy to vary the interparticle spacing using an external mechanical strain applied in a reversible manner (Figure 14C), thereby modulating the gold nanofilms plasmonic responses (e.g., toward applications in stretchable optical color filters).

The biphasic nature of SERS sensors created using floating gold nanofilms circumvents any issues regarding solubility limitations of the analyte. Both hydrophilic and hydrophobic analyte may easily come in contact with, and become preconcentrated by attaching to, interfacial AuNPs during emulsification by sonication. Thus, simultaneous multiphase analyte detection is possible.[272] Additionally, tailored detection strategies can be developed to facilitate large SERS enhancements involving oil-based hydrophobic ligands binding hydrophilic target aqueous analytes (such as heavy metal ions) at the liquid−liquid interface during emulsification.[274] Ideally, as shown in Figure 14D, interfacial metal−ligand binding and attachment of the metal−ligand complexes to the interfacial AuNPs occur simultaneously.

In this perspective section, we denote experiments that combine an external manipulation of $\Delta_o^w\phi$ with a potentiostat and simultaneous SERS measurements in situ at the ITIES as EC-SERS@ITIES. The only report to date of EC-SERS@ITIES is that by Booth et al.[276] In that study, citrate-stabilized AgNPs were reversibly adsorbed and desorbed from the ITIES for a finite number of cycles by varying $\Delta_o^w\phi$ negatively and positively, respectively. Upon AgNP adsorption at negative potentials, a sharp increase in the SERS intensity of the lipophilic organic cation BA^+ was detected. This observation corresponds very well with that by Bera et al.[18] (described vide supra) of organic counterion condensation onto highly charged AuNPs overcoming the electrostatic barrier presented by the low-permittivity organic material at the ITIES during potential-induced adsorption events. Thus, EC-SERS@ITIES can be used to sensitively detect organic ions of opposite charge to the stabilizing ligand on interfacially adsorbed plasmonic NPs.

Many other possibilities of EC-SERS@ITIES have yet to be explored. For example, certain charged species (i.e., ions) in either the aqueous or organic phase can be transferred reversibly over and back across the ITIES by varying $\Delta_o^w\phi$. Each ion will undergo IT at a signature formal ion-transfer potential ($\Delta_o^w\phi^{0\prime}$) that is a measure of the Gibbs energy of transfer for that ion expressed on the voltage scale and depends heavily on the charge and chemical structure of the ion.[23] Thus, certain ions in a mixture can be selectively transferred over and back across the ITIES by matching the applied $\Delta_o^w\phi$ with the $\Delta_o^w\phi^{0\prime}$ for that ion. Therefore, in theory, the SERS signal for the selected ion undergoing IT will be transiently enhanced as it traverses the ITIES through the hot-spots between interfacial AuNPs in the floating gold nanofilms. Indeed, Smirnov et al. have demonstrated that the presence of an interfacial gold nanofilm does not impede IT for model ions such as tetramethylammonium cations (TMA^+).[20] Further strategies may be explored that combine the demonstrated ability to achieve electrocatalysis at gold nanofilms with the plasmonic enhancement at the hot-spots between the AuNPs. For example, the redox-active dye Nile Blue is a very popular probe in EC-SERS studies as its oxidized form undergoes resonant excitation at 633 nm, giving a strong SERS signal, but its reduced form is nonresonant, leading to a weak SERS signal.[255] Thus, the oxidized and reduced forms of this species are readily distinguishable by SERS. As a proof-of-concept, the analogous EC-SERS@ITIES experiment may involve the reduction of the oxidized form of Nile Blue in the aqueous

DOI: 10.1021/acs.chemrev.7b00595
Chem. Rev. 2018, 118, 3722−3751

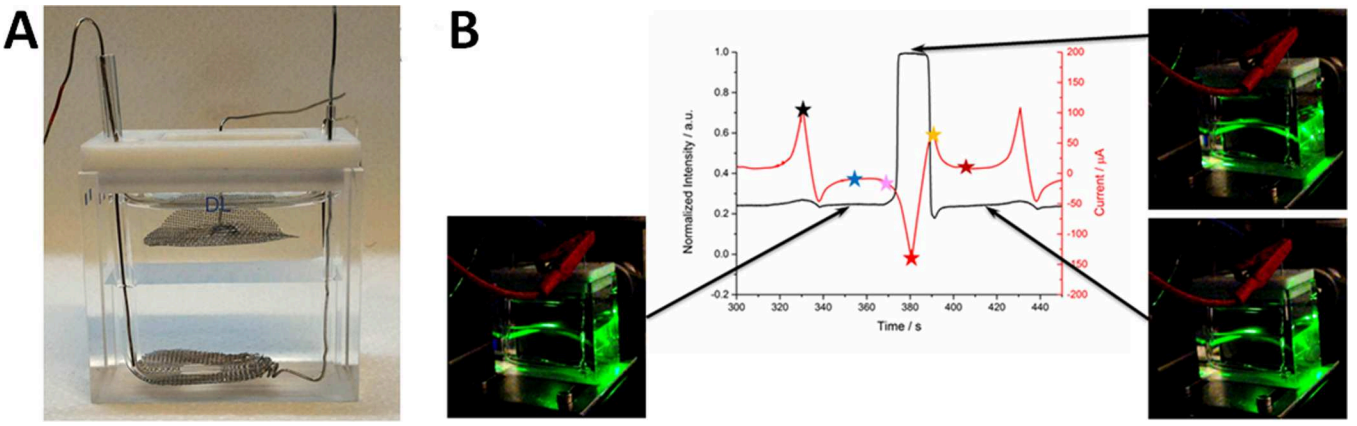

Figure 15. Electrovariable Marangoni shutters with floating gold nanofilms at the ITIES. (A) Silanized four-electrode electrochemical cell in a quartz rectangular cuvette with large Pt-mesh aqueous and organic CEs, and an extremely flat and smooth water−TFT interface (critical for reflectance measurements). (B) Monitoring the intensity of light reflected from the center of a water−TFT interface (black line) as a function of $\Delta_o^w\phi$, varied by cyclic voltammetry (CV; red line). The light was incident on the water−TFT interface at 66°, i.e., below the critical angle for total internal reflection (TIR). The black star on the CV represents a positive $\Delta_o^w\phi$, with the current increasing at this point positively due to the transfer of residual metal cations to the oil phase. After this point $\Delta_o^w\phi$ was scanned to more negative values, immediately causing a dip in the current negatively as metal cations transferred back from the oil into the water phase. The blue and pink stars represent two progressively more negative potentials in the middle of the PPW as $\Delta_o^w\phi$ was scanned negatively. At very positive $\Delta_o^w\phi$ and at $\Delta_o^w\phi$ values spanning the center of the PPW (i.e., the region between the black and pink stars), the AuNPs were seen to be distributed around the perimeter of the quartz cuvette. Thus, a low reflectance was measured in this potential range (also seen by eye in a video snapshot, bottom-left image). Once $\Delta_o^w\phi$ was scanned to a very negative value (red star), the anionic surfactant SDS transferred from the water to oil phase, leading to a large negative increase in current. Immediately, AuNPs were seen to migrate to the center of the water−oil interface, rapidly accumulating and causing a huge increase in reflectance (seen by eye in top-right image). Once more, after this point $\Delta_o^w\phi$ was switched in the positive direction, causing the SDS to move back from the oil to the water phase, producing a positive current. The increased reflectance was maintained until all SDS ions were transferred back into the water phase (yellow star). Finally, as $\Delta_o^w\phi$ was scanned positively to $\Delta_o^w\phi$ values once more in the center of the PPW (dark red star), the system returned to its initial state with the AuNPs again crowded around the periphery of the quartz cuvette and the reflectance greatly diminished (seen by eye in bottom-right image). Adapted from ref 17 with permission from The Royal Society of Chemistry. Copyright 2017.

phase via AuNP-mediated IET from an electron-donor species in the oil phase (such as DMFc). The thermodynamics of IET would be controlled by external application of $\Delta_o^w\phi$ by the potentiostat and the disappearance of the oxidized dye signal monitored in situ by SERS.

6.2. Electrovariable Optics

As noted in section 3.3, to date, only one study has been published that demonstrates clearly the experimental observation of reversible adsorption/desorption of gold nanofilms composed of relatively large AuNPs (e.g., in the size range of 10−60 nm) by tuning $\Delta_o^w\phi$.[22] However, there are several examples of the reversible stimuli-induced self-assembly of NPs on 2D interfaces. Sashuk et al. reported the dynamic self-assembly of amphiphilic and uncharged NPs dispersed at an air−water interface in response to changes in the gradient of $\gamma_{w/o}$.[277] The gradient was changed by either adding or removing organic solvent on the fluid interface, causing the NPs to compress into local dense spots. Once the gradient of $\gamma_{w/o}$ dissipated, the compressed AuNPs disassembled.[277] Ding et al. dynamically tuned the distance between the AuNPs in a floating gold nanofilm (and hence the nanofilm's optical properties) by rapid, repeatable expansion and contraction of PNIPAM nanocoatings on the AuNPs at different temperatures.[86] Meanwhile, as discussed, Bera et al. have definitively shown that the dynamic lateral movement of AuNPs at the interface is possible by tuning $\Delta_o^w\phi$,[18] a much more convenient external stimulus to employ in possible electrovariable optical devices than the introduction/removal of solvent or varying temperature.

Recently, Gschwend et al. have created so-called "electrovariable Marangoni shutters".[17] The concept harnesses known changes in $\gamma_{w/o}$ that can be reversibly induced at the liquid−liquid interface as a function of $\Delta_o^w\phi$ in the presence of an anionic surfactant (sodium dodecyl sulfate (SDS)) that undergoes IT. The interplay of adsorption−desorption and IT as a function of $\Delta_o^w\phi$ causes instabilities or Marangoni-type movements (i.e., mass transfer along an interface between two fluids due to a surface-tension gradient).[278−280] The AuNPs in the gold nanofilm are swept up in these Marangoni-type movements, always moving to regions of higher $\gamma_{w/o}$. Indeed, the AuNPs may be induced to either reversibly crowd around the periphery of the interface (leading to the shutter being off with the majority of the interface nonreflective) or spread uniformly across the interface (leading to the shutter being on and the interface being highly reflective) as a function of $\Delta_o^w\phi$;[17] see Figure 15. The distribution of the electric field at the ITIES is critically dependent on the shape and position of the Pt CEs on either side of the liquid−liquid interface. As a result, by manipulating the latter, further enhanced control over the spatial regions on the interface where the Marangoni effects are felt strongest, and thus where the AuNPs can be induced to assemble more densely, will be possible.

A major factor when designing electrovariable optics based on dynamic self-assembly of NPs will be response time to the external stimulus (i.e., the applied electric field especially, but also perhaps temperature or light).[134] With regard to the reversible adsorption and desorption of gold nanofilms from the ITIES, the response time will be limited by the rate of diffusion of AuNPs in the bulk liquid toward the interface and back off again. Thus, the time constant for observable on/off behavior could be tens of minutes depending on the concentration and diffusion coefficient of the AuNPs in the

DOI: 10.1021/acs.chemrev.7b00595
Chem. Rev. 2018, 118, 3722−3751

bulk phase and their size.[134] Such response times may be suitable for niche applications, e.g., windows in large buildings that gradually become more or less reflective to help equalize the temperature at a desired level as the intensity of sunlight rises and drops during the day. Realistically, however, for more general applications the time constant for observable on/off behavior needs to be reduced to second, or ideally millisecond, regimes. In this regard, the near instantaneous on/off behavior observed by Gschwend et al.[17] for lateral movement of the AuNPs across the fluidic interface is hugely encouraging. Thus, building on this initial premise of combining interfacial gold nanofilms and charged surfactant at an ITIES, rapid-response electrovariable optics for mirror and filters applications will be within reach in the short term.

A more traditional approach has been to deposit a nanofilm on a solid transparent conductive electrode to obtain a mirror and then strip the metal to obtain a window.[281] In this case, 100 s was required to obtain 90% of the maximum reflectance for an optimized system.[282] Another approach for decreasing the time constant for electrotunable reflecting nanoshutters was recently proposed by Kornyshev et al.,[134] who showed theoretically that fast switching within subsecond time scales from mirror to window could be obtained by electrically induced rotation of 2D arrays of nanocuboids tethered to a transparent conductive electrode.

7. CONCLUSIONS AND OUTLOOK

To conclude, the practical utility of floating gold nanofilms is already being realized in the analytical chemistry community for SERS sensor applications. However, approaches to date have broadly been limited in scope to using liquid−liquid interfaces for bottom-up self-assembly purposes only. Major advances in SERS and SPR sensors can be made by simultaneously harnessing the aspects of AuNP self-assembly and controllably applying electric fields at the gold nanofilm-functionalized ITIES. In this way, for example, the electrocatalytic properties of AuNPs can be utilized in conjunction with their nanoplasmonic properties to create truly unique sensors in a new branch of SERS we call EC-SERS@ITIES. Immediate applications of floating gold nanofilms in rapid-response electrovariable optic devices are now within reach thanks to pioneering simulation studies and recent experimental breakthroughs.

To fully realize the potential of functionalizing ITIES with nanomaterials, some fundamental scientific questions and practical considerations remain to be addressed.[283] For example, precisely where at the water−oil interface is the potential drop located? To describe the electrovariable assembly of nanomaterials at the ITIES, can we develop a combined theory of the interplay of forces on nanomaterials at the ITIES as a function of the strength and polarity of an applied electric field?[283] Currently, experimental observations of electrovariable NP assembly/disassembly at the ITIES are primarily described with empirical rules and formulas. The realization of such a combined theory would have major implications for the development of smart window technology in particular. Can we develop new techniques to probe the three-phase contact angles of interfacial adsorbed NPs <100 nm in size in situ at the ITIES? Although several techniques are now available in this regard, as described in section 4.2, greater resolution of the three-phase contact angle in situ at the ITIES remains a challenge. The relative influences of the plasmonic and electrocatalytic properties of gold nanofilms at the ITIES on photoinduced electron-transfer events remains an open question, as described in section 5.4. If fully understood, can the plasmonic features of gold nanofilms be harnessed to develop efficient solar-energy conversion devices based on the interaction of AuNP nanofilms at the ITIES and light-absorbing species such as porphyrins?

Finally, while this Review is limited to discussing mainly simple round-shaped AuNPs, the potential utility and impact of ITIES functionalized with gold (or any other metal) nanorods, nanotriangles, nanocubes, core−shell NPs, Janus NPs, carbon-supported NPs, semiconductors, etc. for electrocatalytic, nanoplasmonic, and electrovariable optic applications has barely been scratched and represents an exciting research avenue for the future.

AUTHOR INFORMATION

Corresponding Authors

*E-mail: micheal.scanlon@ul.ie.
*E-mail: pekka.peljo@epfl.ch.

ORCID

Micheál D. Scanlon: 0000-0001-7951-7085
Evgeny Smirnov: 0000-0001-7930-7758
Pekka Peljo: 0000-0002-1229-2261

Notes

The authors declare no competing financial interest.

Biographies

Micheál D. Scanlon completed his Ph.D. studies under the supervision of Prof. Damien W. M. Arrigan at the Tyndall National Institute in Cork, Ireland, in 2009. He was a postdoctoral researcher in the group of Prof. Edmond Magner at the University of Limerick (UL), Ireland, from 2009 to 2011 and in the group of Prof. Hubert H. Girault at Ecole Polytechnique Fédérale de Lausanne (EPFL), Switzerland, from 2011 to 2014. He returned to Ireland in 2014 to begin his independent research career by establishing the Scanlon Electrochemistry Group at University College Cork (UCC) through a Science Foundation Ireland (SFI) Starting Investigator Research Grant. He was awarded a European Research Council (ERC) Starting Grant in 2016, and in 2017 he moved his research group to the Bernal Institute at UL in Ireland, where he is a lecturer in the Department of Chemical Sciences. Dr Scanlon's research interests involve electrochemistry, photochemistry, and spectro-electrochemistry at functionalized liquid−liquid interfaces for solar energy conversion and storage, sensor development, and electro-optical applications.

Evgeny Smirnov was born in Tver, Russia. He received his M.Sc. degree from Lomonosov Moscow State University, Russia, with emphasis on materials chemistry in 2011. He did his doctoral studies devoted to self-assembly of nanoparticles at liquid−liquid interfaces in Laboratory of Physical and Analytical Electrochemistry at EPFL, Switzerland, and successfully defended his Ph.D. degree in 2017. His scientific interests are mainly focused on the topic of settling gold nanoparticles at various liquid−liquid interfaces, investigating the properties of such nanoparticle assemblies, and implementing them for redox catalysis at interfaces as well as for biphasic analyte detection in Raman spectroscopy.

T. Jane Stockmann received her Ph.D. in 2013 under Pr. Zhifeng Ding at Western University in Canada. She then moved to Switzerland to the group of Pr. Hubert Girault at EPFL as a postdoctoral fellow and performed numerical evaluations of O_2 reduction at soft interfaces. She is currently in France in the group of Drs. Fred Kanoufi and Catherine Combellas as a postdoctoral fellow, where she has been working to

DOI: 10.1021/acs.chemrev.7b00595
Chem. Rev. 2018, 118, 3722−3751

characterize oscillating reactions using SECM, ensemble nanoparticle detection for biosensor applications, and single nanoparticle detection at soft interfaces, as well as develop novel nanocomposite materials through a Horizon 2020 Marie-Skłodowska Curie Action.

Dr. Pekka Peljo is a group leader and SNSF Ambizione Energy grant holder at the Laboratoire d'Electrochimie Physique et Analytique (LEPA), EPFL, Switzerland, since 2016. He received his D.Sc. (Tech.) in 2013 from Aalto University, Finland, under supervision of Prof. Kyösti Kontturi, and has worked as a postdoctoral researcher at LEPA (2013−2016). His research interests currently include nonaqueous redox flow batteries, electrochemistry at soft interfaces, and understanding of fundamental theoretical electrochemistry based on thermodynamics.

ACKNOWLEDGMENTS

This publication has emanated from research by M.D.S. supported by the European Research Council through a Starting Grant (Agreement no. 716792) and in part by a research grant from Science Foundation Ireland (SFI) under Grant no. 13/SIRG/2137. T.J.S. is grateful to the European Commission for a H2020-MSCA-IF grant, Project no. nanoOIPC-DLV-708814. P.P. acknowledges the financial support from the Swiss National Science Foundation under Grant Ambizione Energy 160553.

ABBREVIATIONS

AFM = atomic force microscopy
Ag/AgCl = silver/silver chloride
AgNP = silver nanoparticle
AuNP = gold nanoparticle
AVS = absolute vacuum scale
BA^+ = bis(triphenylphosphoranylidene)ammonium cations
BATB = bis(triphenylphosphoranylidene)ammonium tetrakis(pentafluorophenyl)borate
$BiVO_4$ = bismuth vanadate
CE = counter electrode
CNT = carbon nanotube
DCB = 1,2-dichlorobenzene
DCE = 1,2-dichloroethane
DDT = 1-dodecanethiol
DMFc = decamethylferrocene
DTBE = 2,2′-dithiobis[1-(2-bromo-2-methyl-propionyloxy)-ethane]
ε = relative permittivity
EC-SERS = electrochemical surface-enhanced Raman spectroscopy
EC-SERS@ITIES = electrochemical surface-enhanced Raman spectroscopy in situ at the interface between two immiscible electrolyte solutions
E_F^{NP} = Fermi level of the electrons in a single gold nanoparticle within a gold nanofilm
EP = epinephrine
ET-IT = electron transfer−ion transfer
Fc = ferrocene
$[Fe^{III}(CN)_6]^{3-}/[Fe^{II}(CN)_6]^{4-}$ = ferri-/ferrocyanide
FIT = facilitated ion transfer
FreSCa cryo-SEM = freeze-fracture shadow casting cryogenic scanning electron microscopy
FTDT = finite-difference time domain
$\gamma_{w/o}$ = interfacial energy of the water−organic solvent interface
$\gamma_{NP/w}$ = interfacial energy of the NP−aqueous phase interface
$\gamma_{NP/o}$ = interfacial energy of the NP−organic solvent interface
GIXRD = grazing-incidence X-ray diffraction
GISAXS = grazing-incidence small-angle X-ray scattering
HER = hydrogen evolution reaction
IET = interfacial electron transfer
IT = ion transfer
ITIES = interface between two immiscible electrolyte solutions
k^0_{app} = apparent standard ion transfer constant
LC-TEM = liquid cell transmission electron microscopy
LSPR = localized surface plasmon resonance
MD = molecular dynamics
MDDA = 12-mercaptododecanoic acid
MPC = monolayer protected cluster
NP = nanoparticle
ORR = oxygen reduction reaction
PAL = polyaromatic ligand
PC = propylene carbonate
PDMS = polydimethylsiloxane
PIET = photoinduced interfacial electron transfer
PNIPAM = poly-*N*-isopropylacrylamide
PPW = polarizable potential window
$\Delta^w_o\phi$ = interfacial Galvani potential difference
$\Delta^w_o\phi^{0\prime}$ = formal ion-transfer potential
QELS = quasi-elastic light scattering
RE = reference electrode
σ = surface charge density
SAXS = small-angle X-ray scattering
SDS = sodium dodecyl sulfate
SECM = scanning electrochemical microscopy
SERS = surface-enhanced Raman spectroscopy
SERRS = surface-enhanced resonance Raman spectroscopy
SEM = scanning electron microscopy
SHE = standard hydrogen electrode
SPC = surface plasmon coupling
SPM = scanning probe microscopy
SPR = surface plasmon resonance
SSHG = surface second harmonic generation
STM = scanning tunneling micrscopy
θ = surface coverage
θ_0 = three-phase contact angle of the nanoparticle at the water−oil interface
θ_{SPR} = surface plasmon resonance angle
TB^- = tetrakis(pentafluorophenyl)borate anions
TBA^+ = tetrabutylammonium cations
TBATPB = tetrabutylammonium tetraphenylborate
TEM = transmission electron microscopy
TFT = α,α,α-trifluorotoluene
TIR = total internal reflection
TMA^+ = tetramethylammonium cations
TPB^- = tetraphenylborate anions
TR-SSHG = time-resolved surface second harmonic generation
UV−vis-NIR = ultraviolet−visible−near-infrared
W_{cap} = capillary forces
W_{line} = line tension
W_{solv} = solvation energy
W_{sum} = overall energy profile
WOR = water oxidation reaction
Z_{AuNP} = excess of charge on the gold nanoparticle

DOI: 10.1021/acs.chemrev.7b00595
Chem. Rev. 2018, 118, 3722−3751

REFERENCES

(1) Edel, J. B.; Kornyshev, A. A.; Kucernak, A. R.; Urbakh, M. Fundamentals and Applications of Self-Assembled Plasmonic Nanoparticles at Interfaces. *Chem. Soc. Rev.* **2016**, *45*, 1581−1596.

(2) Konrad, M. P.; Doherty, A. P.; Bell, S. E. J. Stable and Uniform SERS Signals from Self-Assembled Two-Dimensional Interfacial Arrays of Optically Coupled Ag Nanoparticles. *Anal. Chem.* **2013**, *85*, 6783−6789.

(3) Hu, L.; Chen, M.; Fang, X.; Wu, L. Oil−Water Interfacial Self-Assembly: A Novel Strategy for Nanofilm and Nanodevice Fabrication. *Chem. Soc. Rev.* **2012**, *41*, 1350−1362.

(4) Ciesa, F.; Plech, A. Gold Nanoparticle Membranes as Large-Area Surface Monolayers. *J. Colloid Interface Sci.* **2010**, *346*, 1−7.

(5) Park, Y. K.; Yoo, S. H.; Park, S. Assembly of Highly Ordered Nanoparticle Monolayers at a Water/ Hexane Interface. *Langmuir* **2007**, *23*, 10505−10510.

(6) Park, Y.-K.; Park, S. Directing Close-Packing of Midnanosized Gold Nanoparticles at a Water/Hexane Interface. *Chem. Mater.* **2008**, *20*, 2388−2393.

(7) Smirnov, E.; Peljo, P.; Scanlon, M. D.; Gumy, F.; Girault, H. H. Self-Healing Gold Mirrors and Filters at Liquid−liquid Interfaces. *Nanoscale* **2016**, *8*, 7723−7737.

(8) Ramsden, W. Separation of Solids in the Surface-Layers of Solutions and "Suspensions" (Observations on Surface-Membranes, Bubbles, Emulsions, and Mechanical Coagulation). – Preliminary Account. *Proc. R. Soc. London* **1903**, *72*, 156−164.

(9) Pickering, S. U. CXCVI. -Emulsions. *J. Chem. Soc., Trans.* **1907**, *91*, 2001−2021.

(10) Bormashenko, E. Liquid Marbles: Properties and Applications. *Curr. Opin. Colloid Interface Sci.* **2011**, *16*, 266−271.

(11) Bresme, F.; Oettel, M. Nanoparticles at Fluid Interfaces. *J. Phys.: Condens. Matter* **2007**, *19*, 413101.

(12) Binks, B. P. Particles as Surfactants—Similarities and Differences. *Curr. Opin. Colloid Interface Sci.* **2002**, *7*, 21−41.

(13) Binder, W. H. Supramolecular Assembly of Nanoparticles at Liquid−Liquid Interfaces. *Angew. Chem., Int. Ed.* **2005**, *44*, 5172−5175.

(14) Wang, D.; Duan, H.; Möhwald, H. The Water/Oil Interface: The Emerging Horizon for Self-Assembly of Nanoparticles. *Soft Matter* **2005**, *1*, 412−416.

(15) Böker, A.; He, J.; Emrick, T.; Russell, T. P. Self-Assembly of Nanoparticles at Interfaces. *Soft Matter* **2007**, *3*, 1231−1248.

(16) Binks, B. P. Colloidal Particles at a Range of Fluid−Fluid Interfaces. *Langmuir* **2017**, *33*, 6947−6963.

(17) Gschwend, G. C.; Smirnov, E.; Peljo, P.; Girault, H. H. Electrovariable Gold Nanoparticle Films at Liquid−liquid Interfaces: From Redox Electrocatalysis to Marangoni-Shutters. *Faraday Discuss.* **2017**, *199*, 565−583.

(18) Bera, M. K.; Chan, H.; Moyano, D. F.; Yu, H.; Tatur, S.; Amoanu, D.; Bu, W.; Rotello, V. M.; Meron, M.; Král, P.; et al. Interfacial Localization and Voltage-Tunable Arrays of Charged Nanoparticles. *Nano Lett.* **2014**, *14*, 6816−6822.

(19) Smirnov, E.; Peljo, P.; Scanlon, M. D.; Girault, H. H. H. Gold Nanofilm Redox Catalysis for Oxygen Reduction at Soft Interfaces. *Electrochim. Acta* **2016**, *197*, 362−373.

(20) Smirnov, E.; Peljo, P.; Scanlon, M. D.; Girault, H. H. Interfacial Redox Catalysis on Gold Nanofilms at Soft Interfaces. *ACS Nano* **2015**, *9*, 6565−6575.

(21) Gründer, Y.; Fabian, M. D.; Booth, S. G.; Plana, D.; Fermín, D. J.; Hill, P. I.; Dryfe, R. A. W. Solids at the Liquid-Liquid Interface: Electrocatalysis with Pre-Formed Nanoparticles. *Electrochim. Acta* **2013**, *110*, 809−815.

(22) Montelongo, Y.; Sikdar, D.; Ma, Y.; McIntosh, A. J. S.; Velleman, L.; Kucernak, A. R.; Edel, J. B.; Kornyshev, A. A. Electrotunable Nanoplasmonic Liquid Mirror. *Nat. Mater.* **2017**, *16*, 1127−1135.

(23) Peljo, P.; Girault, H. H. Liquid/Liquid Interfaces, Electrochemistry at. In *Encyclopedia of Analytical Chemistry*; John Wiley & Sons, Ltd.: Chichester, U.K., 2012.

(24) Samec, Z. Electrochemistry at the Interface between Two Immiscible Electrolyte Solutions (IUPAC Technical Report). *Pure Appl. Chem.* **2004**, *76*, 2147−2180.

(25) Samec, Z.; Langmaier, J.; Kakiuchi, T. Charge-Transfer Processes at the Interface between Hydrophobic Ionic Liquid and Water. *Pure Appl. Chem.* **2009**, *81*, 1473−1488.

(26) Cousens, N. E. A.; Kucernak, A. R. Electrochemistry of the Ionic Liquidloil Interface: A New Water-Free Interface between Two Immiscible Electrolyte Solutions. *Electrochem. Commun.* **2013**, *31*, 63−66.

(27) *Nanoparticle Assemblies and Superstructures.*; Kotov, N. A., Ed.; CRC Press: 2005.

(28) Lin, X. M.; Sorensen, C. M.; Klabunde, K. J. Digestive Ripening, Nanophase Segregation and Superlattice Formation in Gold Nanocrystal Colloids. *J. Nanopart. Res.* **2000**, *2*, 157−164.

(29) Prasad, B. L. V.; Sorensen, C. M.; Klabunde, K. J. Gold Nanoparticle Superlattices. *Chem. Soc. Rev.* **2008**, *37*, 1871−1883.

(30) Pileni, M. P. 2D Superlattices and 3D Supracrystals of Metal Nanocrystals: A New Scientific Adventure. *J. Mater. Chem.* **2011**, *21*, 16748−16758.

(31) Ma, H.; Hao, J. Ordered Patterns and Structures via Interfacial Self-Assembly: Superlattices, Honeycomb Structures and Coffee Rings. *Chem. Soc. Rev.* **2011**, *40*, 5457−5471.

(32) Xu, L.; Ma, W.; Wang, L.; Xu, C.; Kuang, H.; Kotov, N. A. Nanoparticle Assemblies: Dimensional Transformation of Nanomaterials and Scalability. *Chem. Soc. Rev.* **2013**, *42*, 3114−3126.

(33) Boles, M. A.; Engel, M.; Talapin, D. V. Self-Assembly of Colloidal Nanocrystals: From Intricate Structures to Functional Materials. *Chem. Rev.* **2016**, *116*, 11220−11289.

(34) Gwo, S.; Chen, H.-Y.; Lin, M.-H.; Sun, L.; Li, X. Nanomanipulation and Controlled Self-Assembly of Metal Nanoparticles and Nanocrystals for Plasmonics. *Chem. Soc. Rev.* **2016**, *45*, 5672−5716.

(35) Si, K. J.; Chen, Y.; Shi, Q.; Cheng, W. Nanoparticle Superlattices: The Roles of Soft Ligands. *Adv. Sci.* **2017**, 1700179.

(36) Kumar, S. K.; Kumaraswamy, G.; Prasad, B. L. V.; Bandyopadhyaya, R.; Granick, S.; Gang, O.; Manoharan, V. N.; Frenkel, D.; Kotov, N. A. Nanoparticle Assembly: A Perspective and Some Unanswered Questions. *Curr. Sci.* **2017**, *112*, 1635−1641.

(37) Michael, D.; Benjamin, I. Molecular Dynamics Simulation of the Waterlnitrobenzene Interface. *J. Electroanal. Chem.* **1998**, *450*, 335−345.

(38) Trojánek, A.; Langmaier, J.; Kvapilová, H.; Záliš, S.; Samec, Z. Inhibitory Effect of Water on the Oxygen Reduction Catalyzed by Cobalt(II) Tetraphenylporphyrin. *J. Phys. Chem. A* **2014**, *118*, 2018−2028.

(39) Stockmann, T. J.; Guterman, R.; Ragogna, P. J.; Ding, Z. Trends in Hydrophilicity/Lipophilicity of Phosphonium Ionic Liquids As Determined by Ion-Transfer Electrochemistry. *Langmuir* **2016**, *32*, 12966−12974.

(40) Stockmann, T. J.; Montgomery, A.-M.; Ding, Z. Determination of Alkali Metal Ion Transfers at Liquidlliquid Interfaces Stabilized by a Micropipette. *J. Electroanal. Chem.* **2012**, *684*, 6−12.

(41) Olaya, A. J.; Méndez, M. A.; Cortes-Salazar, F.; Girault, H. H. Voltammetric Determination of Extreme Standard Gibbs Ion Transfer Energy. *J. Electroanal. Chem.* **2010**, *644*, 60−66.

(42) Hundhammer, B.; Müller, C.; Solomon, T.; Alemu, H.; Hassen, H. Ion Transfer across the Water-O-Dichlorobenzene Interface. *J. Electroanal. Chem. Interfacial Electrochem.* **1991**, *319*, 125−135.

(43) Peljo, P.; Qiao, L.; Murtomäki, L.; Johans, C.; Girault, H. H.; Kontturi, K. Electrochemically Controlled Proton-Transfer-Catalyzed Reactions at Liquid-Liquid Interfaces: Nucleophilic Substitution on Ferrocene Methanol. *ChemPhysChem* **2013**, *14*, 311−314.

(44) Olaya, A. J.; Ge, P.; Girault, H. H. Ion Transfer across the Waterltrifluorotoluene Interface. *Electrochem. Commun.* **2012**, *19*, 101−104.

(45) *CRC Handbook of Chemistry & Physics*, 95th ed.; Haynes, W. M., Ed.; CRC Press, Taylor & Francis Group: 2014.

DOI: 10.1021/acs.chemrev.7b00595
Chem. Rev. 2018, 118, 3722−3751

(46) Stockmann, T. J.; Noël, J. M.; Abou-Hassan, A.; Combellas, C.; Kanoufi, F. Facilitated Lewis Acid Transfer by Phospholipids at a (Water|$CHCl_3$) Liquid|Liquid Interface toward Biomimetic and Energy Applications. *J. Phys. Chem. C* **2016**, *120*, 11977−11983.
(47) Ohde, H.; Uehara, A.; Yoshida, Y.; Maeda, K.; Kihara, S. Some Factors in the Voltammetric Measurement of Ion Transfer at the Micro Aqueous|organic Solution Interface. *J. Electroanal. Chem.* **2001**, *496*, 110−117.
(48) Kasuno, M.; Matsuyama, Y.; Iijima, M. Voltammetry of Ion Transfer at a Water-Toluene Micro- Interface. *ChemElectroChem* **2016**, *3*, 694−697.
(49) Samec, Z.; Mareček, V.; Weber, J. Charge Transfer between Two Immiscible Electrolyte Solutions: Part IV. Electron Transfer between hexacyanoferrate(III) in Water and Ferrocene in Nitrobenzene Investigated by Cyclic Voltammetry with Four-Electrode System. *J. Electroanal. Chem. Interfacial Electrochem.* **1979**, *103*, 11−18.
(50) Watkins, J. D.; Amemiya, F.; Atobe, M.; Bulman-Page, P. C.; Marken, F. Liquid |Liquid Biphasic Electrochemistry in Ultra-Turrax Dispersed Acetonitrile |Aqueous Electrolyte Systems. *Electrochim. Acta* **2010**, *55*, 8808−8814.
(51) Hidalgo-Acosta, J. C.; Méndez, M. A.; Scanlon, M. D.; Vrubel, H.; Amstutz, V.; Adamiak, W.; Opallo, M.; Girault, H. H. Catalysis of Water Oxidation in Acetonitrile by Iridium Oxide Nanoparticles. *Chem. Sci.* **2015**, *6*, 1761−1769.
(52) Smirnov, E.; Peljo, P.; Girault, H. H. Self-Assembly and Redox Induced Phase Transfer of Gold Nanoparticles at a Water−propylene Carbonate Interface. *Chem. Commun.* **2017**, *53*, 4108−4111.
(53) Strutwolf, J.; Barker, A. L.; Gonsalves, M.; Caruana, D. J.; Unwin, P. R.; Williams, D. E.; Webster, J. R. P. Probing Liquid|liquid Interfaces Using Neutron Reflection Measurements and Scanning Electrochemical Microscopy. *J. Electroanal. Chem.* **2000**, *483*, 163−173.
(54) Benjamin, I. Theoretical Study of the water/1,2-Dichloroethane Interface: Structure, Dynamics, and Conformational Equilibria at the Liquid−liquid Interface. *J. Chem. Phys.* **1992**, *97*, 1432−1445.
(55) Benjamin, I. Dynamics of Ion Transfer Across a Liquid-Liquid Interface - a Comparison between Molecular-Dynamics and a Diffusion-Model. *J. Chem. Phys.* **1992**, *96*, 577−585.
(56) Michael, D.; Benjamin, I. Solute Orientational Dynamics and Surface Roughness of Water/Hydrocarbon Interfaces. *J. Phys. Chem.* **1995**, *99*, 1530−1536.
(57) Hou, B.; Laanait, N.; Yu, H.; Bu, W.; Yoon, J.; Lin, B.; Meron, M.; Luo, G.; Vanysek, P.; Schlossman, M. L. Ion Distributions at the water/1,2-Dichloroethane Interface: Potential of Mean Force Approach to Analyzing X-Ray Reflectivity and Interfacial Tension Measurements. *J. Phys. Chem. B* **2013**, *117*, 5365−5378.
(58) Yu, H.; Yzeiri, I.; Hou, B.; Chen, C.-H.; Bu, W.; Vanysek, P.; Chen, Y.; Lin, B.; Král, P.; Schlossman, M. L. Electric Field Effect on Phospholipid Monolayers at an Aqueous−Organic Liquid−Liquid Interface. *J. Phys. Chem. B* **2015**, *119*, 9319−9334.
(59) Ding, Z.; Fermín, D. J.; Brevet, P.-F.; Girault, H. H. Spectroelectrochemical Approaches to Heterogeneous Electron Transfer Reactions at the Polarised water|1,2-Dichloroethane Interfaces. *J. Electroanal. Chem.* **1998**, *458*, 139−148.
(60) Zhou, M.; Gan, S.; Zhong, L.; Dong, X.; Niu, L. Which Mechanism Operates in the Electron-Transfer Process at Liquid/liquid Interfaces? *Phys. Chem. Chem. Phys.* **2011**, *13*, 2774−2779.
(61) Schmickler, W. Electron-Transfer Reactions across Liquid|liquid Interfaces. *J. Electroanal. Chem.* **1997**, *428*, 123−127.
(62) Samec, Z. Dynamic Electrochemistry at the Interface between Two Immiscible Electrolytes. *Electrochim. Acta* **2012**, *84*, 21−28.
(63) Dryfe, R. A. W. The Electrified Liquid−Liquid Interface. In *Advances in Chemical Physics*; Rice, S. A., Ed.; John Wiley & Sons, Inc.: Hoboken, NJ, 2009; Vol. *141*, pp 153−215.
(64) Samec, Z. Dynamic Electrochemistry at the Interface between Two Immiscible Electrolytes. *Electrochim. Acta* **2012**, *84*, 21−28.
(65) Arrigan, D. W. M.; Herzog, G. Theory of Electrochemistry at Miniaturised Interfaces between Two Immiscible Electrolyte Solutions. *Curr. Opin. Electrochem.* **2017**, *1*, 66−72.
(66) Arrigan, D. W. M.; Liu, Y. Electroanalytical Ventures at Nanoscale Interfaces Between Immiscible Liquids. *Annu. Rev. Anal. Chem.* **2016**, *9*, 145−161.
(67) Mareček, V.; Samec, Z. Ion Transfer Kinetics at the Interface between Two Immiscible Electrolyte Solutions Supported on a Thick-Wall Micro-Capillary. A Mini Review. *Curr. Opin. Electrochem.* **2017**, *1*, 133−139.
(68) Arrigan, D. W. M.; Alvarez de Eulate, E.; Liu, Y. Electroanalytical Opportunities Derived from Ion Transfer at Interfaces between Immiscible Electrolyte Solutions. *Aust. J. Chem.* **2016**, *69*, 1016−1032.
(69) Booth, S. G.; Dryfe, R. A. W. Assembly of Nanoscale Objects at the Liquid/Liquid Interface. *J. Phys. Chem. C* **2015**, *119*, 23295−23309.
(70) Dryfe, R. A. W.; Uehara, A.; Booth, S. G. Metal Deposition at the Liquid-Liquid Interface. *Chem. Rec.* **2014**, *14*, 1013−1023.
(71) Poltorak, L.; Gamero-Quijano, A.; Herzog, G.; Walcarius, A. Decorating Soft Electrified Interfaces: From Molecular Assemblies to Nano-Objects. *Appl. Mater. Today* **2017**, *9*, 533−550.
(72) Lee, H. K.; Lee, Y. H.; Phan-Quang, G. C.; Han, X.; Koh, C. S. L.; Ling, X. Y. Constructing Soft Substrate-Less Platforms Using Particle-Assembled Fluid−Fluid Interfaces and Their Prospects in Multiphasic Applications. *Chem. Mater.* **2017**, *29*, 6563−6577.
(73) Aussillous, P.; Quéré, D. Liquid Marbles. *Nature* **2001**, *411*, 924−927.
(74) Dinsmore, A. D.; Hsu, M. F.; Nikolaides, M. G.; Marquez, M.; Bausch, A. R.; Weitz, D. A. Colloidosomes: Selectively Permeable Capsules Composed of Colloidal Particles. *Science* **2002**, *298*, 1006−1009.
(75) Niederberger, M. Multiscale Nanoparticle Assembly: From Particulate Precise Manufacturing to Colloidal Processing. *Adv. Funct. Mater.* **2017**, *27*, 1703647.
(76) Fontana, J.; Naciri, J.; Rendell, R.; Ratna, B. R. Macroscopic Self-Assembly and Optical Characterization of Nanoparticle-Ligand Metamaterials. *Adv. Opt. Mater.* **2013**, *1*, 100−106.
(77) Reincke, F.; Hickey, S. G.; Kegel, W. K.; Vanmaekelbergh, D. Spontaneous Assembly of a Monolayer of Charged Gold Nanocrystals at the Water/Oil Interface. *Angew. Chem., Int. Ed.* **2004**, *43*, 458−462.
(78) Duan, H.; Wang, D.; Kurth, D. G.; Möhwald, H. Directing Self-Assembly of Nanoparticles at Water/oil Interfaces. *Angew. Chem., Int. Ed.* **2004**, *43*, 5639−5642.
(79) Reincke, F.; Kegel, W. K.; Zhang, H.; Nolte, M.; Wang, D.; Vanmaekelbergh, D.; Möhwald, H. Understanding the Self-Assembly of Charged Nanoparticles at the Water/Oil Interface. *Phys. Chem. Chem. Phys.* **2006**, *8*, 3828−3835.
(80) Flatté, M. E.; Kornyshev, A. A.; Urbakh, M. Understanding Voltage-Induced Localization of Nanoparticles at a Liquid−liquid Interface. *J. Phys.: Condens. Matter* **2008**, *20*, 073102.
(81) Smirnov, E.; Scanlon, M. D.; Momotenko, D.; Vrubel, H.; Méndez, M. A.; Brevet, P.-F.; Girault, H. H.; et al. Gold Metal Liquid-Like Droplets. *ACS Nano* **2014**, *8*, 9471−9481.
(82) Xu, Y.; Konrad, M. P.; Lee, W. W. Y.; Ye, Z.; Bell, S. E. J. A Method for Promoting Assembly of Metallic and Nonmetallic Nanoparticles into Interfacial Monolayer Films. *Nano Lett.* **2016**, *16*, 5255−5260.
(83) Xu, Y.; Konrad, M. P.; Trotter, J. L.; McCoy, C. P.; Bell, S. E. J. Rapid One-Pot Preparation of Large Freestanding Nanoparticle-Polymer Films. *Small* **2017**, *13*, 1602163.
(84) Turek, V. A.; Cecchini, M. P.; Paget, J.; Kucernak, A. R.; Kornyshev, A. A.; Edel, J. B. Plasmonic Ruler at the Liquid−Liquid Interface. *ACS Nano* **2012**, *6*, 7789−7799.
(85) Luo, M.; Olivier, G. K.; Frechette, J. Electrostatic Interactions to Modulate the Reflective Assembly of Nanoparticles at the Oil−Water Interface. *Soft Matter* **2012**, *8*, 11923−11932.
(86) Ding, T.; Rudrum, A. W.; Herrmann, L. O.; Turek, V.; Baumberg, J. J. Polymer-Assisted Self-Assembly of Gold Nanoparticle Monolayers and Their Dynamical Switching. *Nanoscale* **2016**, *8*, 15864−15869.

DOI: 10.1021/acs.chemrev.7b00595
Chem. Rev. 2018, 118, 3722−3751

(87) Li, Y.-J.; Huang, W.-J.; Sun, S.-G. A Universal Approach for the Self-Assembly of Hydrophilic Nanoparticles into Ordered Monolayer Films at a Toluene/Water Interface. *Angew. Chem., Int. Ed.* **2006**, *45*, 2537−2539.
(88) Younan, N.; Hojeij, M.; Ribeaucourt, L.; Girault, H. H. Electrochemical Properties of Gold Nanoparticles Assembly at Polarised Liquid|Liquid Interfaces. *Electrochem. Commun.* **2010**, *12*, 912−915.
(89) Hojeij, M.; Younan, N.; Ribeaucourt, L.; Girault, H. H. Surface Plasmon Resonance of Gold Nanoparticles Assemblies at Liquid | Liquid Interfaces. *Nanoscale* **2010**, *2*, 1665−1669.
(90) Fang, P.; Chen, S.; Deng, H.; Scanlon, M. D.; Gumy, F.; Lee, H. J.; Momotenko, D.; Amstutz, V.; Cortés-Salazar, F.; Pereira, C. M.; et al. Conductive Gold Nanoparticle Mirrors at Liquid/Liquid Interfaces. *ACS Nano* **2013**, *7*, 9241−9248.
(91) Schaming, D.; Hojeij, M.; Younan, N.; Nagatani, H.; Lee, H. J.; Girault, H. H. Photocurrents at Polarized Liquid|liquid Interfaces Enhanced by a Gold Nanoparticle Film. *Phys. Chem. Chem. Phys.* **2011**, *13*, 17704−17711.
(92) Vazquez, G.; Alvarez, E.; Navaza, J. M. Surface Tension of Alcohol Water + Water from 20 to 50 °C. *J. Chem. Eng. Data* **1995**, *40*, 611−614.
(93) Luo, M.; Song, Y.; Dai, L. L. Effects of Methanol on Nanoparticle Self-Assembly at Liquid−Liquid Interfaces: A Molecular Dynamics Approach. *J. Chem. Phys.* **2009**, *131*, 194703.
(94) Xia, H.; Wang, D. Fabrication of Macroscopic Freestanding Films of Metallic Nanoparticle Monolayers by Interfacial Self-Assembly. *Adv. Mater.* **2008**, *20*, 4253−4256.
(95) Smirnov, E. *Assemblies of Gold Nanoparticles at Liquid-Liquid Interfaces: From Liquid Optics to Electrocatalysis*; Ecole Polytechnique Fédérale de Lausanne: 2017.
(96) Reichhelm, A.; Haubold, D.; Eychmüller, A. Ligand Versatility in Supercrystal Formation. *Adv. Funct. Mater.* **2017**, *27*, 1700361.
(97) Shimpi, J. R.; Sidhaye, D. S.; Prasad, B. L. V. Digestive Ripening: A Fine Chemical Machining Process on the Nanoscale. *Langmuir* **2017**, *33*, 9491−9507.
(98) Manzanares, J. A.; Peljo, P.; Girault, H. H. Understanding Digestive Ripening of Ligand-Stabilized, Charged Metal Nanoparticles. *J. Phys. Chem. C* **2017**, *121*, 13405−13411.
(99) Murray, C. B.; Kagan, C. R.; Bawendi, M. G. Self-Organization of CdSe Nanocrystallites into Three-Dimensional Quantum Dot Superlattices. *Science* **1995**, *270*, 1335−1338.
(100) Paik, T.; Diroll, B. T.; Kagan, C. R.; Murray, C. B. Binary and Ternary Superlattices Self-Assembled from Colloidal Nanodisks and Nanorods. *J. Am. Chem. Soc.* **2015**, *137*, 6662−6669.
(101) Ye, X.; Zhu, C.; Ercius, P.; Raja, S. N.; He, B.; Jones, M. R.; Hauwiller, M. R.; Liu, Y.; Xu, T.; Alivisatos, A. P. Structural Diversity in Binary Superlattices Self-Assembled from Polymer-Grafted Nanocrystals. *Nat. Commun.* **2015**, *6*, 10052.
(102) Alder, B. J.; Wainwright, T. E. Phase Transition in Elastic Disks. *Phys. Rev.* **1962**, *127*, 359−361.
(103) Kirkwood, J. G.; Maun, E. K.; Alder, B. J. Radial Distribution Functions and the Equation of State of a Fluid Composed of Rigid Spherical Molecules. *J. Chem. Phys.* **1950**, *18*, 1040−1047.
(104) Alder, B. J.; Hoover, W. G.; Young, D. A. Studies in Molecular Dynamics. V. High-Density Equation of State and Entropy for Hard Disks and Spheres. *J. Chem. Phys.* **1968**, *49*, 3688−3696.
(105) Lee, B.; Podsiadlo, P.; Rupich, S.; Talapin, D. V.; Rajh, T.; Shevchenko, E. V. Comparison of Structural Behavior of Nanocrystals in Randomly Packed Films and Long-Range Ordered Superlattices by Time-Resolved Small Angle X-Ray Scattering. *J. Am. Chem. Soc.* **2009**, *131*, 16386−16388.
(106) Ryan, K. M.; Mastroianni, A.; Stancil, K. A.; Liu, H.; Alivisatos, A. P. Electric-Field-Assisted Assembly of Perpendicularly Oriented Nanorod Superlattices. *Nano Lett.* **2006**, *6*, 1479−1482.
(107) Zhang, Y.; Sun, L.; Fu, Y.; Huang, Z. C.; Bai, X. J.; Zhai, Y.; Du, J.; Zhai, H. R. The Shape Anisotropy in the Magnetic Field-Assisted Self-Assembly Chain-like Structure of Magnetite. *J. Phys. Chem. C* **2009**, *113*, 8152−8157.
(108) Ryan, K. M.; Singh, S.; Liu, P.; Singh, A. Assembly of Binary, Ternary and Quaternary Compound Semiconductor Nanorods: From Local to Device Scale Ordering Influenced by Surface Charge. *CrystEngComm* **2014**, *16*, 9446−9454.
(109) Yu, Y.; Yu, D.; Orme, C. A. Reversible, Tunable, Electric-Field Driven Assembly of Silver Nanocrystal Superlattices. *Nano Lett.* **2017**, *17*, 3862−3869.
(110) Yang, G.; Hu, L.; Keiper, T. D.; Xiong, P.; Hallinan, D. T. Gold Nanoparticle Monolayers with Tunable Optical and Electrical Properties. *Langmuir* **2016**, *32*, 4022−4033.
(111) Yang, G.; Hallinan, D. T. Self-Assembly of Large-Scale Crack-Free Gold Nanoparticle Films Using a "drain-to-Deposit" Strategy. *Nanotechnology* **2016**, *27*, 225604.
(112) Wen, T.; Majetich, S. A. Ultra-Large-Area Self-Assembled Monolayers of Nanoparticles. *ACS Nano* **2011**, *5*, 8868−8876.
(113) Yang, G.; Nanda, J.; Wang, B.; Chen, G.; Hallinan, D. T. Self-Assembly of Large Gold Nanoparticles for Surface-Enhanced Raman Spectroscopy. *ACS Appl. Mater. Interfaces* **2017**, *9*, 13457−13470.
(114) Yu, Y.; Guillaussier, A.; Voggu, V. R.; Houck, D. W.; Smilgies, D.-M.; Korgel, B. A. Bubble Assemblies of Nanocrystals: Superlattices without a Substrate. *J. Phys. Chem. Lett.* **2017**, *8*, 4865−4871.
(115) Su, B.; Abid, J.-P.; Fermín, D. J.; Girault, H. H.; Hoffmannová, H.; Krtil, P.; Samec, Z. Reversible Voltage-Induced Assembly of Au Nanoparticles at Liquid|Liquid Interfaces. *J. Am. Chem. Soc.* **2004**, *126*, 915−919.
(116) Abid, J. P.; Abid, M.; Bauer, C.; Girault, H. H.; Brevet, P. F. Controlled Reversible Adsorption of Core-Shell Metallic Nanoparticles at the Polarized Water/1,2-Dichloroethane Interface Investigated by Optical Second-Harmonic Generation. *J. Phys. Chem. C* **2007**, *111*, 8849−8855.
(117) Kim, J.-Y.; Kotov, N. A. Charge Transport Dilemma of Solution-Processed Nanomaterials. *Chem. Mater.* **2014**, *26*, 134−152.
(118) Wuelfing, W. P.; Green, S. J.; Pietron, J. J.; Cliffel, D. E.; Murray, R. W.; et al. Electronic Conductivity of Solid-State, Mixed-Valent, Monolayer-Protected Au Clusters. *J. Am. Chem. Soc.* **2000**, *122*, 11465−11472.
(119) Rodgers, A. N. J.; Dryfe, R. A. W. Oxygen Reduction at the Liquid-Liquid Interface: Bipolar Electrochemistry through Adsorbed Graphene Layers. *ChemElectroChem* **2016**, *3*, 472−479.
(120) Toth, P. S.; Ramasse, Q. M.; Velický, M.; Dryfe, R. A. W. Functionalization of Graphene at the Organic/water Interface. *Chem. Sci.* **2015**, *6*, 1316−1323.
(121) Toth, P. S.; Rodgers, A. N. J.; Rabiu, A. K.; Dryfe, R. A. W. Electrochemical Activity and Metal Deposition Using Few-Layer Graphene and Carbon Nanotubes Assembled at the Liquid−Liquid Interface. *Electrochem. Commun.* **2015**, *50*, 6−10.
(122) Rastgar, S.; Deng, H.; Cortés-Salazar, F.; Scanlon, M. D.; Pribil, M.; Amstutz, V.; Karyakin, A. A.; Shahrokhian, S.; Girault, H. H. Oxygen Reduction at Soft Interfaces Catalyzed by In Situ-Generated Reduced Graphene Oxide. *ChemElectroChem* **2014**, *1*, 59−63.
(123) Ge, P.; Scanlon, M. D.; Peljo, P.; Bian, X.; Vubrel, H.; O'Neill, A.; Coleman, J. N.; Cantoni, M.; Hu, X.; Kontturi, K.; et al. Hydrogen Evolution across Nano-Schottky Junctions at Carbon Supported MoS_2 Catalysts in Biphasic Liquid Systems. *Chem. Commun.* **2012**, *48*, 6484−6486.
(124) Bian, X.; Scanlon, M. D.; Wang, S.; Liao, L.; Tang, Y.; Liu, B.; Girault, H. H. Floating Conductive Catalytic Nano-Rafts at Soft Interfaces for Hydrogen Evolution. *Chem. Sci.* **2013**, *4*, 3432−3441.
(125) Peljo, P.; Scanlon, M. D.; Olaya, A. J.; Rivier, L.; Smirnov, E.; Girault, H. H. Redox Electrocatalysis of Floating Nanoparticles: Determining Electrocatalytic Properties without the Influence of Solid Supports. *J. Phys. Chem. Lett.* **2017**, *8*, 3564−3575.
(126) Ghosh, S. K.; Pal, T. Interparticle Coupling Effect on the Surface Plasmon Resonance of Gold Nanoparticles: From Theory to Applications. *Chem. Rev.* **2007**, *107*, 4797−4862.
(127) Jain, P. K.; El-Sayed, M. A. Noble Metal Nanoparticle Pairs: Effect of Medium for Enhanced Nanosensing. *Nano Lett.* **2008**, *8*, 4347−4352.

DOI: 10.1021/acs.chemrev.7b00595
Chem. Rev. 2018, 118, 3722−3751

(128) Jain, P. K.; El-Sayed, M. A. Plasmonic Coupling in Noble Metal Nanostructures. *Chem. Phys. Lett.* **2010**, *487*, 153−164.
(129) Flatté, M. E.; Kornyshev, A. A.; Urbakh, M. Nanoparticles at Electrified Liquid−Liquid Interfaces: New Options for Electro-Optics. *Faraday Discuss.* **2009**, *143*, 109−115.
(130) Flatté, M. E.; Kornyshev, A. A.; Urbakh, M. Electrovariable Nanoplasmonics and Self-Assembling Smart Mirrors. *J. Phys. Chem. C* **2010**, *114*, 1735−1747.
(131) Kornyshev, A. A.; Marinescu, M.; Paget, J.; Urbakh, M. Reflection of Light by Metal Nanoparticles at Electrodes. *Phys. Chem. Chem. Phys.* **2012**, *14*, 1850−1859.
(132) Paget, J.; Walpole, V.; Blancafort Jorquera, M.; Edel, J. B.; Urbakh, M.; Kornyshev, A. A.; Demetriadou, A. Optical Properties of Ordered Self-Assembled Nanoparticle Arrays at Interfaces. *J. Phys. Chem. C* **2014**, *118*, 23264−23273.
(133) Sikdar, D.; Kornyshev, A. A. Theory of Tailorable Optical Response of Two-Dimensional Arrays of Plasmonic Nanoparticles at Dielectric Interfaces. *Sci. Rep.* **2016**, *6*, 33712.
(134) Sikdar, D.; Bucher, A.; Zagar, C.; Kornyshev, A. A. Electrochemical Plasmonic Metamaterials: Towards Fast Electro-Tuneable Reflecting Nanoshutters. *Faraday Discuss.* **2017**, *199*, 585−602.
(135) Velleman, L.; Sikdar, D.; Turek, V. A.; Kucernak, A. R.; Roser, S. J.; Kornyshev, A. A.; Edel, J. B. Tuneable 2D Self-Assembly of Plasmonic Nanoparticles at Liquid|Liquid Interfaces. *Nanoscale* **2016**, *8*, 19229−19241.
(136) Girault, H. H.; Schiffrin, D. J.; Smith, B. D. V. Drop Image Processing for Surface and Interfacial Tension Measurements. *J. Electroanal. Chem. Interfacial Electrochem.* **1982**, *137*, 207−217.
(137) Girault, H. H. J.; Schiffrin, D. J.; Smith, B. D. V. The Measurement of Interfacial Tension of Pendant Drops Using a Video Image Profile Digitizer. *J. Colloid Interface Sci.* **1984**, *101*, 257−266.
(138) Martins, M. C.; Pereira, C. M.; Girault, H. H.; Silva, F. Specific Adsorption of Tetraalkylammonium Cations on the 1,2-Dicloroethane/Water Interface. *Electrochim. Acta* **2004**, *50*, 135−139.
(139) Fernandez-Rodriguez, M. A.; Song, Y.; Rodríguez-Valverde, M. Á.; Chen, S.; Cabrerizo-Vilchez, M. A.; Hidalgo-Alvarez, R. Comparison of the Interfacial Activity between Homogeneous and Janus Gold Nanoparticles by Pendant Drop Tensiometry. *Langmuir* **2014**, *30*, 1799−1804.
(140) Fernández-Rodríguez, M. A.; Percebom, A. M.; Giner-Casares, J. J.; Rodríguez-Valverde, M. A.; Cabrerizo-Vílchez, M. A.; Liz-Marzán, L. M.; Hidalgo-Álvarez, R. Interfacial Activity of Gold Nanoparticles Coated with a Polymeric Patchy Shell and the Role of Spreading Agents. *ACS Omega* **2016**, *1*, 311−317.
(141) Fernandez-Rodriguez, M. A.; Ramos, J.; Isa, L.; Rodriguez-Valverde, M. A.; Cabrerizo-Vilchez, M. A.; Hidalgo-Alvarez, R. Interfacial Activity and Contact Angle of Homogeneous, Functionalized, and Janus Nanoparticles at the Water/Decane Interface. *Langmuir* **2015**, *31*, 8818−8823.
(142) Hua, X.; Bevan, M. A.; Frechette, J. Reversible Partitioning of Nanoparticles at an Oil−Water Interface. *Langmuir* **2016**, *32*, 11341−11352.
(143) Marinescu, M.; Urbakh, M.; Kornyshev, A. A. Voltage-Dependent Capacitance of Metallic Nanoparticles at a Liquid/liquid Interface. *Phys. Chem. Chem. Phys.* **2012**, *14*, 1371−1380.
(144) Olaya, A. J.; Brevet, P.-F.; Smirnov, E. A.; Girault, H. H. Ultrafast Population Dynamics of Surface-Active Dyes during Electrochemically Controlled Ion Transfer across a Liquid|Liquid Interface. *J. Phys. Chem. C* **2014**, *118*, 25027−25031.
(145) Galletto, P.; Girault, H. H.; Gomis-Bas, C.; Schiffrin, D. J.; Antoine, R.; Broyer, M.; Brevet, P. F. Second Harmonic Generation Response by Gold Nanoparticles at the Polarized Water/2-Octanone Interface: From Dispersed to Aggregated Particles. *J. Phys.: Condens. Matter* **2007**, *19*, 375108.
(146) Zanini, M.; Isa, L. Particle Contact Angles at Fluid Interfaces: Pushing the Boundary Bayond Hard Uniform Spherical Colloids. *J. Phys.: Condens. Matter* **2016**, *28*, 313002.
(147) Maestro, A.; Guzmán, E.; Ortega, F.; Rubio, R. G. Contact Angle of Micro- and Nanoparticles at Fluid Interfaces. *Curr. Opin. Colloid Interface Sci.* **2014**, *19*, 355−367.
(148) Snoeyink, C.; Barman, S.; Christopher, G. F. Contact Angle Distribution of Particles at Fluid Interfaces. *Langmuir* **2015**, *31*, 891−897.
(149) Isa, L. Freeze-Fracture Shadow-Casting (FreSCa) Cryo-SEM as a Tool to Investigate the Wetting of Micro- and Nanoparticles at Liquid−Liquid Interfaces. *Chimia* **2013**, *67*, 231−235.
(150) Isa, L.; Lucas, F.; Wepf, R.; Reimhult, E. Measuring Single-Nanoparticle Wetting Properties by Freeze-Fracture Shadow-Casting Cryo-Scanning Electron Microscopy. *Nat. Commun.* **2011**, *2*, 438.
(151) Cayre, O. J.; Paunov, V. N. Contact Angles of Colloid Silica and Gold Particles at Air−Water and Oil−Water Interfaces Determined with the Gel Trapping Technique. *Langmuir* **2004**, *20*, 9594−9599.
(152) Costa, L.; Li-Destri, G.; Thomson, N. H.; Konovalov, O.; Pontoni, D. Real Space Imaging of Nanoparticle Assembly at Liquid−Liquid Interfaces with Nanoscale Resolution. *Nano Lett.* **2016**, *16*, 5463−5468.
(153) Kubowicz, S.; Hartmann, M. a; Daillant, J.; Sanyal, M. K.; Agrawal, V. V.; Blot, C.; Konovalov, O.; Möhwald, H. Gold Nanoparticles at the Liquid−Liquid Interface: X-Ray Study and Monte Carlo Simulation. *Langmuir* **2009**, *25*, 952−958.
(154) Sanyal, M. K.; Agrawal, V. V.; Bera, M. K.; Kalyanikutty, K. P.; Daillant, J.; Blot, C.; Kubowicz, S.; Konovalov, O.; Rao, C. N. R. Formation and Ordering of Gold Nanoparticles at the Toluene−Water Interface. *J. Phys. Chem. C* **2008**, *112*, 1739−1743.
(155) Laanait, N.; Mihaylov, M.; Hou, B.; Yu, H.; Vanýsek, P.; Meron, M.; Lin, B.; Benjamin, I.; Schlossman, M. L. Tuning Ion Correlations at an Electrified Soft Interface. *Proc. Natl. Acad. Sci. U. S. A.* **2012**, *109*, 20326−20331.
(156) Cohanoschi, I.; Thibert, A.; Toro, C.; Zou, S.; Hernández, F. E. Surface Plasmon Enhancement at a Liquid−Metal−Liquid Interface. *Plasmonics* **2007**, *2*, 89−94.
(157) Velleman, L.; Scarabelli, L.; Sikdar, D.; Kornyshev, A. A.; Liz-Marzán, L. M.; Edel, J. B. Monitoring Plasmon Coupling and SERS Enhancement through In Situ Nanoparticle Spacing Modulation. *Faraday Discuss.* **2017**, *205*, 67−83.
(158) Rastgar, S.; Pilarski, M.; Wittstock, G. Polarized Liquid−Liquid Interface Meets Visible Light-Driven Catalytic Water Oxidation. *Chem. Commun.* **2016**, *52*, 11382−11385.
(159) Amatore, C.; Savéant, J. M.; Tessier, D. Charge Transfer at Partially Blocked Surfaces: A Model for the Case of Microscopic Active and Inactive Sites. *J. Electroanal. Chem. Interfacial Electrochem.* **1983**, *147*, 39−51.
(160) Bard, A. J.; Faulkner, L. R. Electroactive Layers and Modified Electrodes. In *Electrochemical methods: Fundamentals and applications*; John Wiley & Sons, Inc.: 2001; pp 580−631.
(161) Chow, E.; Raguse, B.; Müller, K. H.; Wieczorek, L.; Bendavid, A.; Cooper, J. S.; Hubble, L. J.; Webster, M. S. Influence of Gold Nanoparticle Film Porosity on the Chemiresistive Sensing Performance. *Electroanalysis* **2013**, *25*, 2313−2320.
(162) Wokaun, A.; Bergman, J. G.; Heritage, J. P.; Glass, A. M.; Liao, P. F.; Olson, D. H. Surface Second-Harmonic Generation from Metal Island Films and Microlithographic Structures. *Phys. Rev. B: Condens. Matter Mater. Phys.* **1981**, *24*, 849−856.
(163) Shen, S.; Meng, L.; Zhang, Y.; Han, J.; Ma, Z.; Hu, S.; He, Y.; Li, J.; Ren, B.; Shih, T. M.; et al. Plasmon-Enhanced Second-Harmonic Generation Nanorulers with Ultrahigh Sensitivities. *Nano Lett.* **2015**, *15*, 6716−6721.
(164) Tan, S. F.; Chee, S. W.; Lin, G.; Mirsaidov, U. Direct Observation of Interactions between Nanoparticles and Nanoparticle Self-Assembly in Solution. *Acc. Chem. Res.* **2017**, *50*, 1303−1312.
(165) Diroll, B. T.; Doan-Nguyen, V. V. T.; Cargnello, M.; Gaulding, E. A.; Kagan, C. R.; Murray, C. B. X-Ray Mapping of Nanoparticle Superlattice Thin Films. *ACS Nano* **2014**, *8*, 12843−12850.
(166) Li, T.; Senesi, A. J.; Lee, B. Small Angle X-Ray Scattering for Nanoparticle Research. *Chem. Rev.* **2016**, *116*, 11128−11180.

DOI: 10.1021/acs.chemrev.7b00595
Chem. Rev. 2018, 118, 3722−3751

(167) Olichwer, N.; Meyer, A.; Yesilmen, M.; Vossmeyer, T. Gold Nanoparticle Superlattices: Correlating Chemiresistive Responses with Analyte Sorption and Swelling. *J. Mater. Chem. C* **2016**, *4*, 8214−8225.
(168) Stamenkovic, V. R.; Strmcnik, D.; Lopes, P. P.; Markovic, N. M. Energy and Fuels from Electrochemical Interfaces. *Nat. Mater.* **2017**, *16*, 57−69.
(169) Ostojic, N.; Crooks, R. M. Electrocatalytic Reduction of Oxygen on Platinum Nanoparticles in the Presence and Absence of Interactions with the Electrode Surface. *Langmuir* **2016**, *32*, 9727−9735.
(170) Herranz, J.; Durst, J.; Fabbri, E.; Patru, A.; Cheng, X.; Permyakova, A. A.; Schmidt, T. J. Interfacial Effects on the Catalysis of the Hydrogen Evolution, Oxygen Evolution and CO_2-Reduction Reactions for (Co-)Electrolyzer Development. *Nano Energy* **2016**, *29*, 4−28.
(171) Hayden, B. E. Particle Size and Support Effects in Electrocatalysis. *Acc. Chem. Res.* **2013**, *46*, 1858−1866.
(172) Cunnane, V. J.; Murtomäki, L. Electrocatalysis and Electrolysis. In *Liquid−liquid interfaces: Theory and methods*; Volkov, A. G., Deamer, D. W., Eds.; CRC Press: 1996; pp 401−416.
(173) Scanlon, M. D.; Peljo, P.; Méndez, M. A.; Smirnov, E.; Girault, H. H. Charging and Discharging at the Nanoscale: Fermi Level Equilibration of Metallic Nanoparticles. *Chem. Sci.* **2015**, *6*, 2705−2720.
(174) Peljo, P.; Scanlon, M. D.; Stockmann, T. J. Simulations Employing Finite Element Method at Liquid|liquid Interfaces. *Curr. Opin. Electrochem.* **2017**, DOI: 10.1016/j.coelec.2017.09.011.
(175) Peljo, P.; Smirnov, E.; Girault, H. H. Heterogeneous versus Homogeneous Electron Transfer Reactions at Liquid−liquid Interfaces: The Wrong Question? *J. Electroanal. Chem.* **2016**, *779*, 187−198.
(176) Stockmann, T. J.; Angelé, L.; Brasiliense, V.; Combellas, C.; Kanoufi, F. Platinum Nanoparticle Impacts at a Liquid|Liquid Interface. *Angew. Chem., Int. Ed.* **2017**, *56*, 13493−13497.
(177) Trojánek, A.; Mareček, V.; Jänchenová, H.; Samec, Z. Molecular Electrocatalysis of the Oxygen Reduction at a Polarised Interface between Two Immiscible Electrolyte Solutions by Co(II) Tetraphenylporphyrin. *Electrochem. Commun.* **2007**, *9*, 2185−2190.
(178) Su, B.; Nia, R. P.; Li, F.; Hojeij, M.; Prudent, M.; Corminboeuf, C.; Samec, Z.; Girault, H. H. H_2O_2 Generation by Decamethylferrocene at a Liquid|liquid Interface. *Angew. Chem., Int. Ed.* **2008**, *47*, 4675−4678.
(179) Hatay, I.; Su, B.; Li, F.; Méndez, M. A.; Khoury, T.; Gros, C. P.; Barbe, J. M.; Ersoz, M.; Samec, Z.; Girault, H. H. Proton-Coupled Oxygen Reduction at Liquid−Liquid Interfaces Catalyzed by Cobalt Porphine. *J. Am. Chem. Soc.* **2009**, *131*, 13453−13459.
(180) Hatay, I.; Su, B.; Méndez, M. A.; Corminboeuf, C.; Khoury, T.; Gros, C. P.; Bourdillon, M.; Meyer, M.; Barbe, J.-M.; Ersoz, M.; et al. Oxygen Reduction Catalyzed by a Fluorinated Tetraphenylporphyrin Free Base at Liquid/Liquid Interfaces. *J. Am. Chem. Soc.* **2010**, *132*, 13733−13741.
(181) Su, B.; Hatay, I.; Ge, P. Y.; Mendez, M.; Corminboeuf, C.; Samec, Z.; Ersoz, M.; Girault, H. H. Oxygen and Proton Reduction by Decamethylferrocene in Non-Aqueous Acidic Media. *Chem. Commun.* **2010**, *46*, 2918−2919.
(182) Méndez, M. a; Partovi-Nia, R.; Hatay, I.; Su, B.; Ge, P.; Olaya, A.; Younan, N.; Hojeij, M.; Girault, H. H. Molecular Electrocatalysis at Soft Interfaces. *Phys. Chem. Chem. Phys.* **2010**, *12*, 15163−15171.
(183) Su, B.; Hatay, I.; Trojánek, A.; Samec, Z.; Khoury, T.; Gros, C. P.; Barbe, J.-M.; Daina, A.; Carrupt, P.-A.; Girault, H. H. Molecular Electrocatalysis for Oxygen Reduction by Cobalt Porphyrins Adsorbed at Liquid/Liquid Interfaces. *J. Am. Chem. Soc.* **2010**, *132*, 2655−2662.
(184) Su, B.; Hatay, I.; Li, F.; Partovi-Nia, R.; Méndez, M. A.; Samec, Z.; Ersoz, M.; Girault, H. H. Oxygen Reduction by Decamethylferrocene at Liquid/Liquid Interfaces Catalyzed by Dodecylaniline. *J. Electroanal. Chem.* **2010**, *639*, 102−108.
(185) Nieminen, J. J.; Hatay, I.; Ge, P.; Méndez, M. A.; Murtomäki, L.; Girault, H. H. Hydrogen Evolution Catalyzed by Electrodeposited Nanoparticles at the Liquid/liquid Interface. *Chem. Commun.* **2011**, *47*, 5548−5550.
(186) Olaya, A. J.; Ge, P.; Gonthier, J. F.; Pechy, P.; Corminboeuf, C.; Girault, H. H. Four-Electron Oxygen Reduction by Tetrathiafulvalene. *J. Am. Chem. Soc.* **2011**, *133*, 12115−12123.
(187) Hatay Patir, I. Oxygen Reduction Catalyzed by Aniline Derivatives at Liquid/Liquid Interfaces. *J. Electroanal. Chem.* **2012**, *685*, 28−32.
(188) Olaya, A. J.; Schaming, D.; Brevet, P. F.; Nagatani, H.; Xu, H. J.; Meyer, M.; Girault, H. H. Interfacial Self-Assembly of Water-Soluble Cationic Porphyrins for the Reduction of Oxygen to Water. *Angew. Chem., Int. Ed.* **2012**, *51*, 6447−6451.
(189) Olaya, A. J.; Schaming, D.; Brevet, P. F.; Nagatani, H.; Zimmermann, T.; Vanicek, J.; Xu, H. J.; Gros, C. P.; Barbe, J. M.; Girault, H. H. Self-Assembled Molecular Rafts at Liquid|Liquid Interfaces for Four-Electron Oxygen Reduction. *J. Am. Chem. Soc.* **2012**, *134*, 498−506.
(190) Peljo, P.; Murtomäki, L.; Kallio, T.; Xu, H. J.; Meyer, M.; Gros, C. P.; Barbe, J. M.; Girault, H. H.; Laasonen, K.; Kontturi, K. Biomimetic Oxygen Reduction by Cofacial Porphyrins at a Liquid−Liquid Interface. *J. Am. Chem. Soc.* **2012**, *134*, 5974−5984.
(191) Trojánek, A.; Langmaier, J.; Samec, Z. Thermodynamic Driving Force Effects in the Oxygen Reduction Catalyzed by a Metal-Free Porphyrin. *Electrochim. Acta* **2012**, *82*, 457−462.
(192) Wu, S.; Su, B. Metal-Free-Porphyrin-Catalyzed Oxygen Reduction at Liquid−Liquid Interfaces. *Chem. - Eur. J.* **2012**, *18*, 3169−3173.
(193) Patir, I. H. Fluorinated-Cobalt Phthalocyanine Catalyzed Oxygen Reduction at Liquid/Liquid Interfaces. *Electrochim. Acta* **2013**, *87*, 788−793.
(194) Jedraszko, J.; Nogala, W.; Adamiak, W.; Rozniecka, E.; Lubarska-Radziejewska, I.; Girault, H. H.; Opallo, M. Hydrogen Peroxide Generation at Liquid|Liquid Interface under Conditions Unfavorable for Proton Transfer from Aqueous to Organic Phase. *J. Phys. Chem. C* **2013**, *117*, 20681−20688.
(195) Liu, X.; Wu, S.; Su, B. Oxygen Reduction with Tetrathiafulvalene at Liquid/Liquid Interfaces Catalyzed by 5,10,15,20-Tetraphenylporphyrin. *J. Electroanal. Chem.* **2013**, *709*, 26−30.
(196) Deng, H.; Peljo, P.; Stockmann, T. J.; Qiao, L.; Vainikka, T.; Kontturi, K.; Opallo, M.; Girault, H. H. Surprising Acidity of Hydrated Lithium Cations in Organic Solvents. *Chem. Commun.* **2014**, *50*, 5554−5557.
(197) Deng, H.; Stockmann, T. J.; Peljo, P.; Opallo, M.; Girault, H. H. Electrochemical Oxygen Reduction at Soft Interfaces Catalyzed by the Transfer of Hydrated Lithium Cations. *J. Electroanal. Chem.* **2014**, *731*, 28−35.
(198) Deng, H.; Peljo, P.; Momotenko, D.; Cortés-Salazar, F.; Jane Stockmann, T.; Kontturi, K.; Opallo, M.; Girault, H. H. Kinetic Differentiation of Bulk/interfacial Oxygen Reduction Mechanisms at/near Liquid/Liquid Interfaces Using Scanning Electrochemical Microscopy. *J. Electroanal. Chem.* **2014**, *732*, 101−109.
(199) Rastgar, S.; Deng, H.; Cortés-Salazar, F.; Scanlon, M. D.; Pribil, M.; Amstutz, V.; Karyakin, A. A.; Shahrokhian, S.; Girault, H. H. Oxygen Reduction at Soft Interfaces Catalyzed by In Situ-Generated Reduced Graphene Oxide. *ChemElectroChem* **2014**, *1*, 59−63.
(200) Jane Stockmann, T.; Deng, H.; Peljo, P.; Kontturi, K.; Opallo, M.; Girault, H. H. Mechanism of Oxygen Reduction by Metallocenes near Liquid|Liquid Interfaces. *J. Electroanal. Chem.* **2014**, *729*, 43−52.
(201) Adamiak, W.; Jedraszko, J.; Krysiak, O.; Nogala, W.; Hidalgo-acosta, J. C.; Girault, H. H.; Opallo, M. Hydrogen and Hydrogen Peroxide Formation in Tri Fluorotoluene−Water Biphasic Systems. *J. Phys. Chem. C* **2014**, *118*, 23154−23161.
(202) Adamiak, W.; Jedraszko, J.; Nogala, W.; Jönsson-Niedziolka, M.; Dongmo, S.; Wittstock, G.; Girault, H. H.; Opallo, M. A Simple Liquid−Liquid Biphasic System for Hydrogen Peroxide Generation. *J. Phys. Chem. C* **2015**, *119*, 20011−20015.
(203) Xuan, Y.; Huang, X.; Su, B. Biomimetic Oxygen Reduction Reaction Catalyzed by Microperoxidase-11 at Liquid/Liquid Interfaces. *J. Phys. Chem. C* **2015**, *119*, 11685−11693.

DOI: 10.1021/acs.chemrev.7b00595
Chem. Rev. 2018, 118, 3722−3751

(204) Xuan, Y.; Xie, L.; Huang, X.; Su, B. Molecular Electrocatalysis of Oxygen Reduction by Iron(II) Phthalocyanine at the Liquid/liquid Interface. *J. Electroanal. Chem.* **2016**, *766*, 37−43.
(205) Liu, S.-J.; Yu, Z.-W.; Qiao, L.; Liu, B.-H. Electrochemistry-Mass Spectrometry for Mechanism Study of Oxygen Reduction at Water/Oil Interface. *Sci. Rep.* **2017**, *7*, 46669.
(206) Hatay, I.; Su, B.; Li, F.; Partovi-Nia, R.; Vrubel, H.; Hu, X.; Ersoz, M.; Girault, H. H. Hydrogen Evolution at Liquid−Liquid Interfaces. *Angew. Chem., Int. Ed.* **2009**, *48*, 5139−5142.
(207) Méndez, M. A.; Partovi-Nia, R.; Hatay, I.; Su, B.; Ge, P.; Olaya, A.; Younan, N.; Hojeij, M.; Girault, H. H. Molecular Electrocatalysis at Soft Interfaces. *Phys. Chem. Chem. Phys.* **2010**, *12*, 15163−15171.
(208) Hatay, I.; Ge, P. Y.; Vrubel, H.; Hu, X.; Girault, H. H. Hydrogen Evolution at Polarised Liquid/Liquid Interfaces Catalyzed by Molybdenum Disulfide. *Energy Environ. Sci.* **2011**, *4*, 4246−4251.
(209) Bian, X.; Scanlon, M. D. M. D.; Wang, S.; Liao, L.; Tang, Y.; Liu, B.; Girault, H. H. Floating Conductive Catalytic Nano-Rafts at Soft Interfaces for Hydrogen Evolution. *Chem. Sci.* **2013**, *4*, 3432−3441.
(210) Scanlon, M. D.; Bian, X.; Vrubel, H.; Amstutz, V.; Schenk, K.; Hu, X.; Liu, B.; Girault, H. H. Low-Cost Industrially Available Molybdenum Boride and Carbide As "Platinum-Like" Catalysts for the Hydrogen Evolution Reaction in Biphasic Liquid Systems. *Phys. Chem. Chem. Phys.* **2013**, *15*, 2847−2857.
(211) Jedraszko, J.; Nogala, W.; Adamiak, W.; Girault, H. H.; Opallo, M. Scanning Electrochemical Microscopy Determination of Hydrogen Flux at Liquid|Liquid Interface with Potentiometric Probe. *Electrochem. Commun.* **2014**, *43*, 22−24.
(212) Aslan, E.; Patir, I. H.; Ersoz, M. Cu Nanoparticles Electrodeposited at Liquid−Liquid Interfaces: A Highly Efficient Catalyst for the Hydrogen Evolution Reaction. *Chem. - Eur. J.* **2015**, *21*, 4585−4589.
(213) Ozel, F.; Yar, A.; Aslan, E.; Arkan, E.; Aljabour, A.; Can, M.; Patir, I. H.; Kus, M.; Ersoz, M. Earth-Abundant Cu_2CoSnS_4 Nanofibers for Highly Efficient H_2 Evolution at Soft Interfaces. *ChemNanoMat* **2015**, *1*, 477−481.
(214) Aslan, E.; Akin, I.; Patir, I. H. Highly Active Cobalt Sulfide/Carbon Nanotube Catalyst for Hydrogen Evolution at Soft Interfaces. *Chem. - Eur. J.* **2016**, *22*, 5342−5349.
(215) Aslan, E.; Akin, I.; Patir, I. H. Enhanced Hydrogen Evolution Catalysis Based on Cu Nanoparticles Deposited on Carbon Nanotubes at the Liquid/Liquid Interface. *ChemCatChem* **2016**, *8*, 719−723.
(216) Ozel, F.; Aslan, E.; Sarilmaz, A.; Hatay Patir, I. Hydrogen Evolution Catalyzed by Cu_2WS_4 at Liquid−Liquid Interfaces. *ACS Appl. Mater. Interfaces* **2016**, *8*, 25881−25887.
(217) Akin, I.; Aslan, E.; Hatay Patir, I. Enhanced Hydrogen Evolution Catalysis at the Liquid/Liquid Interface by Ni_xS_y and Ni_xS_y/Carbon Nanotube Catalysts. *Eur. J. Inorg. Chem.* **2017**, *2017*, 3961−3966.
(218) Henry, C. R. 2D-Arrays of Nanoparticles as Model Catalysts. *Catal. Lett.* **2015**, *145*, 731−749.
(219) Wang, C.; Yin, H.; Dai, S.; Sun, S. A General Approach to Noble Metal−Metal Oxide Dumbbell Nanoparticles and Their Catalytic Application for CO Oxidation. *Chem. Mater.* **2010**, *22*, 3277−3282.
(220) Holmberg, N.; Laasonen, K.; Peljo, P. Charge Distribution and Fermi Level in Bimetallic Nanoparticles. *Phys. Chem. Chem. Phys.* **2016**, *18*, 2924−2931.
(221) Peljo, P.; Manzanares, J. A.; Girault, H. H. Contact Potentials, Fermi Level Equilibration, and Surface Charging. *Langmuir* **2016**, *32*, 5765−5775.
(222) Binninger, T.; Schmidt, T. J.; Kramer, D. Capacitive Electronic Metal-Support Interactions: Outer Surface Charging of Supported Catalyst Particles. *Phys. Rev. B: Condens. Matter Mater. Phys.* **2017**, *96*, 165405.
(223) Kang, Y.; Ye, X.; Chen, J.; Qi, L.; Diaz, R. E.; Doan-Nguyen, V.; Xing, G.; Kagan, C. R.; Li, J.; Gorte, R. J.; et al. Engineering Catalytic Contacts and Thermal Stability: Gold/iron Oxide Binary Nanocrystal Superlattices for CO Oxidation. *J. Am. Chem. Soc.* **2013**, *135*, 1499−1505.
(224) Yamada, Y.; Tsung, C.-K.; Huang, W.; Huo, Z.; Habas, S. E.; Soejima, T.; Aliaga, C. E.; Somorjai, G. A.; Yang, P. Nanocrystal Bilayer for Tandem Catalysis. *Nat. Chem.* **2011**, *3*, 372−376.
(225) Kleijn, S. E. F.; Lai, S. C. S.; Koper, M. T. M.; Unwin, P. R. Electrochemistry of Nanoparticles. *Angew. Chem., Int. Ed.* **2014**, *53*, 3558−3586.
(226) Kang, Y.; Ye, X.; Chen, J.; Cai, Y.; Diaz, R. E.; Adzic, R. R.; Stach, E. A.; Murray, C. B. Design of Pt−Pd Binary Superlattices Exploiting Shape Effects and Synergistic Effects for Oxygen Reduction Reactions. *J. Am. Chem. Soc.* **2013**, *135*, 42−45.
(227) Tian, L.; Qian, K.; Qi, J.; Liu, Q.; Yao, C.; Song, W.; Wang, Y. Gold Nanoparticles Superlattices Assembly for Electrochemical Biosensor Detection of microRNA-21. *Biosens. Bioelectron.* **2018**, *99*, 564−570.
(228) Yu, A.; Liang, Z.; Cho, J.; Caruso, F. Nanostructured Electrochemical Sensor Based on Dense Gold Nanoparticle Films. *Nano Lett.* **2003**, *3*, 1203−1207.
(229) Hidalgo-Acosta, J. C.; Scanlon, M. D.; Méndez, M. A.; Amstutz, V.; Vrubel, H.; Opallo, M.; Girault, H. H. Boosting Water Oxidation Layer-by-Layer. *Phys. Chem. Chem. Phys.* **2016**, *18*, 9295−9304.
(230) Hidalgo-Acosta, J. C.; Scanlon, M. D.; Méndez, M. A.; Peljo, P.; Opallo, M.; Girault, H. H. Enhanced Reactivity of Water Clusters towards Oxidation in Water/Acetonitrile Mixtures. *ChemElectroChem* **2016**, *3*, 2003−2007.
(231) Potyrailo, R. A. Toward High Value Sensing: Monolayer-Protected Metal Nanoparticles in Multivariable Gas and Vapor Sensors. *Chem. Soc. Rev.* **2017**, *46*, 5311−5346.
(232) Yang, Z.; Chen, S.; Fang, P.; Ren, B.; Girault, H. H.; Tian, Z. LSPR Properties of Metal Nanoparticles Adsorbed at a Liquid−liquid Interface. *Phys. Chem. Chem. Phys.* **2013**, *15*, 5374−5378.
(233) Kadkhodazadeh, S.; Christensen, T.; Beleggia, M.; Mortensen, N. A.; Wagner, J. B. The Substrate Effect in Electron Energy-Loss Spectroscopy of Localized Surface Plasmons in Gold and Silver Nanoparticles. *ACS Photonics* **2017**, *4*, 251−261.
(234) Mahmoud, M. A.; El-Sayed, M. A. Substrate Effect on the Plasmonic Sensing Ability of Hollow Nanoparticles of Different Shapes. *J. Phys. Chem. B* **2013**, *117*, 4468−4477.
(235) Mahmoud, M. A.; Chamanzar, M.; Adibi, A.; El-Sayed, M. A. Effect of the Dielectric Constant of the Surrounding Medium and the Substrate on the Surface Plasmon Resonance Spectrum and Sensitivity Factors of Highly Symmetric Systems: Silver Nanocubes. *J. Am. Chem. Soc.* **2012**, *134*, 6434−6442.
(236) Knight, M. W.; Wu, Y.; Lassiter, J. B.; Nordlander, P.; Halas, N. J. Substrates Matter: Influence of an Adjacent Dielectric on an Individual Plasmonic Nanoparticle. *Nano Lett.* **2009**, *9*, 2188−2192.
(237) Ringe, E.; McMahon, J. M.; Sohn, K.; Cobley, C.; Xia, Y.; Huang, J.; Schatz, G. C.; Marks, L. D.; Van Duyne, R. P. Unraveling the Effects of Size, Composition, and Substrate on the Localized Surface Plasmon Resonance Frequencies of Gold and Silver Nanocubes: A Systematic Single-Particle Approach. *J. Phys. Chem. C* **2010**, *114*, 12511−12516.
(238) Hanske, C.; González-Rubio, G.; Hamon, C.; Formentín, P.; Modin, E.; Chuvilin, A.; Guerrero-Martínez, A.; Marsal, L. F.; Liz-Marzán, L. M. Large-Scale Plasmonic Pyramidal Supercrystals via Templated Self-Assembly of Monodisperse Gold Nanospheres. *J. Phys. Chem. C* **2017**, *121*, 10899−10906.
(239) Halas, N. J.; Lal, S.; Chang, W. S.; Link, S.; Nordlander, P. Plasmons in Strongly Coupled Metallic Nanostructures. *Chem. Rev.* **2011**, *111*, 3913−3961.
(240) Pazos-Perez, N.; Garcia De Abajo, F. J.; Fery, A.; Alvarez-Puebla, R. A. From Nano to Micro: Synthesis and Optical Properties of Homogeneous Spheroidal Gold Particles and Their Superlattices. *Langmuir* **2012**, *28*, 8909−8914.
(241) Tang, L.; Li, J. Plasmon-Based Colorimetric Nanosensors for Ultrasensitive Molecular Diagnostics. *ACS Sensors* **2017**, *2*, 857−875.

DOI: 10.1021/acs.chemrev.7b00595
Chem. Rev. 2018, 118, 3722−3751

(242) Stiles, P. L.; Dieringer, J. A.; Shah, N. C.; Van Duyne, R. P. Surface-Enhanced Raman Spectroscopy. *Annu. Rev. Anal. Chem.* **2008**, *1*, 601−626.
(243) Mayer, K.; Hafner, J. Localized Surface Plasmon Resonance Sensors. *Chem. Rev.* **2011**, *111*, 3828−3857.
(244) Kedem, O.; Vaskevich, A.; Rubinstein, I. Improved Sensitivity of Localized Surface Plasmon Resonance Transducers Using Reflection Measurements. *J. Phys. Chem. Lett.* **2011**, *2*, 1223−1226.
(245) Wu, L.; Wang, Z.; Shen, B. Large-Scale Gold Nanoparticle Superlattice and Its SERS Properties for the Quantitative Detection of Toxic Carbaryl. *Nanoscale* **2013**, *5*, 5274−5278.
(246) Nagatani, H.; Tonari, S.; Shibata, T.; Sagara, T. Gold Nanoparticles-Enhanced Photocurrent at a Dye-Sensitized Liquid|liquid Interface. *Electrochem. Commun.* **2011**, *13*, 985−988.
(247) Schaming, D.; Hatay, I.; Cortez, F.; Olaya, A.; Méndez, M. A.; Ge, P. Y.; Deng, H.; Voyame, P.; Nazemi, Z.; Girault, H. Artificial Photosynthesis at Soft Interfaces. *Chimia* **2011**, *65*, 356−359.
(248) Lahtinen, R.; Fermín, D. J.; Kontturi, K.; Girault, H. H. Artificial Photosynthesis at Liquid|Liquid Interfaces: Photoreduction of Benzoquinone by Water Soluble Porphyrin Species. *J. Electroanal. Chem.* **2000**, *483*, 81−87.
(249) Zheng, P.; Cushing, S. K.; Suri, S.; Wu, N. Tailoring Plasmonic Properties of Gold Nanohole Arrays for Surface-Enhanced Raman Scattering. *Phys. Chem. Chem. Phys.* **2015**, *17*, 21211−21219.
(250) Bartlett, P. N.; Baumberg, J. J.; Coyle, S.; Abdelsalam, M. E. Optical Properties of Nanostructured Metal Films. *Faraday Discuss.* **2004**, *125*, 117−132.
(251) Hulteen, J. C.; Van Duyne, R. P. Nanosphere Lithography: A Materials General Fabrication Process for Periodic Particle Array Surfaces. *J. Vac. Sci. Technol., A* **1995**, *13*, 1553−1558.
(252) Zhang, X.; Hicks, E. M.; Zhao, J.; Schatz, G. C.; Van Duyne, R. P. Electrochemical Tuning of Silver Nanoparticles Fabricated by Nanosphere Lithography. *Nano Lett.* **2005**, *5*, 1503−1507.
(253) Fang, P.-P.; Li, J.-F.; Yang, Z.-L.; Li, L.-M.; Ren, B.; Tian, Z.-Q. Optimization of SERS Activities of Gold Nanoparticles and Gold-Core−Palladium-Shell Nanoparticles by Controlling Size and Shell Thickness. *J. Raman Spectrosc.* **2008**, *39*, 1679−1687.
(254) Wilson, A. J.; Willets, K. A. Visualizing Site-Specific Redox Potentials on the Surface of Plasmonic Nanoparticle Aggregates with Superlocalization SERS Microscopy. *Nano Lett.* **2014**, *14*, 939−945.
(255) Wain, A. J.; O'Connell, M. A. Advances in Surface-Enhanced Vibrational Spectroscopy at Electrochemical Interfaces. *Adv. Phys. X* **2017**, *2*, 188−209.
(256) Wu, D.-Y.; Li, J.-F.; Ren, B.; Tian, Z.-Q. Electrochemical Surface-Enhanced Raman Spectroscopy of Nanostructures. *Chem. Soc. Rev.* **2008**, *37*, 1025−1041.
(257) Zaleski, S.; Wilson, A. J.; Mattei, M.; Chen, X.; Goubert, G.; Cardinal, M. F.; Willets, K. A.; Van Duyne, R. P. Investigating Nanoscale Electrochemistry with Surface- and Tip-Enhanced Raman Spectroscopy. *Acc. Chem. Res.* **2016**, *49*, 2023−2030.
(258) Wilson, A. J.; Molina, N. Y.; Willets, K. A. Modification of the Electrochemical Properties of Nile Blue through Covalent Attachment to Gold As Revealed by Electrochemistry and SERS. *J. Phys. Chem. C* **2016**, *120*, 21091−21098.
(259) Wilson, A. J.; Willets, K. A. Unforeseen Distance-Dependent SERS Spectroelectrochemistry from Surface-Tethered Nile Blue: The Role of Molecular Orientation. *Analyst* **2016**, *141*, 5144−5151.
(260) Zong, C.; Chen, C. J.; Zhang, M.; Wu, D. Y.; Ren, B. Transient Electrochemical Surface-Enhanced Raman Spectroscopy: A Millisecond Time-Resolved Study of an Electrochemical Redox Process. *J. Am. Chem. Soc.* **2015**, *137*, 11768−11774.
(261) Millyard, M. G.; Min Huang, F.; White, R.; Spigone, E.; Kivioja, J.; Baumberg, J. J. Stretch-Induced Plasmonic Anisotropy of Self-Assembled Gold Nanoparticle Mats. *Appl. Phys. Lett.* **2012**, *100*, 073101.
(262) Guo, P.; Sikdar, D.; Huang, X.; Si, K. J.; Su, B.; Chen, Y.; Xiong, W.; Yap, L. W.; Premaratne, M.; Cheng, W. Large-Scale Self-Assembly and Stretch-Induced Plasmonic Properties of Core−Shell Metal Nanoparticle Superlattice Sheets. *J. Phys. Chem. C* **2014**, *118*, 26816−26824.
(263) Guo, P.; Huang, X.; Li, L.; Zhao, S. Interfacial Self-Assembly Approach of Plasmonic Nanostructures for Efficient SERS and Recyclable Catalysts Applications. *Chem. Res. Chin. Univ.* **2017**, *33*, 135−142.
(264) Zhou, B.; Li, X.; Tang, X.; Li, P.; Yang, L.; Liu, J. Highly Selective and Repeatable Surface-Enhanced Resonance Raman Scattering Detection for Epinephrine in Serum Based on Interface Self-Assembled 2D Nanoparticles Arrays. *ACS Appl. Mater. Interfaces* **2017**, *9*, 7772−7779.
(265) Yan, L.; Zhang, K.; Xu, H.; Ji, J.; Wang, Y.; Liu, B.; Yang, P. Target Induced Interfacial Self-Assembly of Nanoparticles: A New Platform for Reproducible Quantification of Copper Ions. *Talanta* **2016**, *158*, 254−261.
(266) Yin, X.; Peretz, Y.; Oppenheimer, P. G.; Zeiri, L.; Masarwa, A.; Froumin, N.; Jelinek, R. Conductive and SERS-Active Colloidal Gold Films Spontaneously Formed at a Liquid/Liquid Interface. *RSC Adv.* **2016**, *6*, 33326−33331.
(267) Lin, X.; Hasi, W.-L.-J.; Han, S.-Q.-G.-W.; Lou, X.-T.; Lin, D.-Y.; Lu, Z.-W. Fabrication of Transparent SERS Platform via Interface Self-Assembly of Gold Nanorods and Gel Trapping Technique for on-Site Real Time Detection. *Phys. Chem. Chem. Phys.* **2015**, *17*, 31324−31331.
(268) Zhang, K.; Zhao, J.; Xu, H.; Li, Y.; Ji, J.; Liu, B. Multifunctional Paper Strip Based on Self-Assembled Interfacial Plasmonic Nanoparticle Arrays for Sensitive SERS Detection. *ACS Appl. Mater. Interfaces* **2015**, *7*, 16767−16774.
(269) Zhang, K.; Zhao, J.; Ji, J.; Li, Y.; Liu, B. Quantitative Label-Free and Real-Time Surface-Enhanced Raman Scattering Monitoring of Reaction Kinetics Using Self-Assembled Bifunctional Nanoparticle Arrays. *Anal. Chem.* **2015**, *87*, 8702−8708.
(270) Zhang, K.; Ji, J.; Li, Y.; Liu, B. Interfacial Self-Assembled Functional Nanoparticle Array: A Facile Surface-Enhanced Raman Scattering Sensor for Specific Detection of Trace Analytes. *Anal. Chem.* **2014**, *86*, 6660−6665.
(271) Yamamoto, S.; Watarai, H. Surface-Enhanced Raman Spectroscopy of Dodecanethiol-Bound Silver Nanoparticles at the Liquid/Liquid Interface. *Langmuir* **2006**, *22*, 6562−6569.
(272) Cecchini, M. P.; Turek, V. A.; Paget, J.; Kornyshev, A. A.; Edel, J. B. Self-Assembled Nanoparticle Arrays for Multiphase Trace Analyte Detection. *Nat. Mater.* **2013**, *12*, 165−171.
(273) Kim, K.; Han, H. S.; Choi, I.; Lee, C.; Hong, S.; Suh, S.-H.; Lee, L. P.; Kang, T. Interfacial Liquid-State Surface-Enhanced Raman Spectroscopy. *Nat. Commun.* **2013**, *4*, 2182.
(274) Cecchini, M. P.; Turek, V. A.; Demetriadou, A.; Britovsek, G.; Welton, T.; Kornyshev, A. A.; Wilton-Ely, J. D. E. T.; Edel, J. B. Heavy Metal Sensing Using Self-Assembled Nanoparticles at a Liquid−Liquid Interface. *Adv. Opt. Mater.* **2014**, *2*, 966−977.
(275) Wang, M.; Zhang, Z.; He, J. A SERS Study on the Assembly Behavior of Gold Nanoparticles at the Oil/Water Interface. *Langmuir* **2015**, *31*, 12911−12919.
(276) Booth, S. G.; Cowcher, D. P.; Goodacre, R.; Dryfe, R. A. W. Electrochemical Modulation of SERS at the Liquid/liquid Interface. *Chem. Commun.* **2014**, *50*, 4482−4484.
(277) Sashuk, V.; Winkler, K.; Żywociński, A.; Wojciechowski, T.; Górecka, E.; Fiałkowski, M. Nanoparticles in a Capillary Trap: Dynamic Self-Assembly at Fluid Interfaces. *ACS Nano* **2013**, *7*, 8833−8839.
(278) Kakiuchi, T. Electrochemical Instability of the Liquid|Liquid Interface in the Presence of Ionic Surfactant Adsorption. *J. Electroanal. Chem.* **2002**, *536*, 63−69.
(279) Zhang, L.; Kitazumi, Y.; Kakiuchi, T. Potential-Dependent Adsorption and Transfer of Poly(diallyldialkylammonium) Ions at the Nitrobenzene|Water Interface. *Langmuir* **2011**, *27*, 13037−13042.
(280) Kitazumi, Y.; Kakiuchi, T. Imaging of the Liquid−Liquid Interface under Electrochemical Instability Using Confocal Fluorescence Microscopy. *Langmuir* **2009**, *25*, 10829−10833.

DOI: 10.1021/acs.chemrev.7b00595
Chem. Rev. 2018, 118, 3722−3751

(281) Park, C.; Seo, S.; Shin, H.; Sarwade, B. D.; Na, J.; Kim, E. Switchable Silver Mirrors with Long Memory Effects. *Chem. Sci.* **2015**, *6*, 596−602.
(282) Park, C.; Na, J.; Han, M.; Kim, E. Transparent Electrochemical Gratings from a Patterned Bistable Silver Mirror. *ACS Nano* **2017**, *11*, 6977−6984.
(283) Bazant, M.; Bennewitz, R.; Booth, S.; Dryfe, R.; Girault, H.; Hillman, R.; Kornyshev, A. A.; Lee, A.; Lemay, S.; Mount, A.; et al. Electrovariable Nanoplasmonics: General Discussion. *Faraday Discuss.* **2017**, *199*, 603−613.

DOI: 10.1021/acs.chemrev.7b00595
Chem. Rev. 2018, 118, 3722−3751